Titre: Title:	Development of Pet/Kaolin Nanocomposites with Improved Mechanical Properties
Auteur: Author:	Khalil Shahverdi-Shahraki
Date:	2014
Type:	Mémoire ou thèse / Dissertation or Thesis
Référence: Citation:	Shahverdi-Shahraki, K. (2014). Development of Pet/Kaolin Nanocomposites with Improved Mechanical Properties [Thèse de doctorat, École Polytechnique de Montréal]. PolyPublie. https://publications.polymtl.ca/1407/

UNIVERSITÉ DE MONTRÉAL

DEVELOPMENT OF PET/KAOLIN NANOCOMPOSITES WITH IMPROVED MECHANICAL PROPERTIES

KHALIL SHAHVERDI-SHAHRAKI

DÉPARTEMENT DE GÉNIE CHIMIQUE

ÉCOLE POLYTECHNIQUE DE MONTRÉAL

THÉSE PRÉSENTÉE EN VUE DE L'OBTENTION

DU DIPLÔME DE PHILOSOPHIAE DOCTOR

(GÉNIE CHIMIQUE)

AVRIL 2014

UNIVERSITÉ DE MONTRÉAL

ÉCOLE POLYTECHNIQUE DE MONTRÉAL

Cette thèse intitulée:

DEVELOPMENT OF PET/KAOLIN NANOCOMPOSITES WITH IMPROVED MECHANICAL PROPERTIES

présentée par: SHAHVERDI-SHAHRAKI Khalil

en vue de l'obtention du diplôme de: Philosophiae Doctor

a été dûment acceptée par le jury d'examen constitué de:

M. BERTRAND François, Ph.D., président

M. AJJI Abdellah, Ph.D., membre et directeur de recherche

M. CARREAU Pierre, Ph.D., membre et codirecteur de recherche

M. TAVARES Jason-Robert, Ph.D., membre

M. SUNDARARAJ Uttandaraman, Ph.D., membre

DEDICATION

In memory of my father Abbasali Shahverdi-Shahraki,

To

My mother, a truly caring and loving soul,

My sisters who have never left my side,

My wife, for her love and constant support.

ACKNOWLEDGMENTS

I would first like to thank my supervisor, Prof. Abdellah Ajji, for the trust he placed in me. This thesis would not have been possible without his help, support and patience on both an academic and a personal level. The good advice and support of my second supervisor, Prof. Pierre J. Carreau, has been invaluable, for which I am extremely grateful.

I would like to acknowledge the financial and technical support of PepsiCo, particularly Dr. Tamal Ghosh and Dr. Kamal Mahajan who provided the necessary financial support for this research.

I want to thank the many individuals from all sectors of École Polytechnique de Montreal; particularly Ms. Melina Hamdine, Ms. Claire Cerclé, and Mr. Guillaume Lessard.

I would like to thank Mounia Arkoun for her warm and quick response to my request for translating the abstract of this thesis to French.

An especial thank to my friend Erfan Meshkati for his kindness and generosity that I will never forget.

I would like to extend my gratitude to my friends in Montreal, Tehran, Isfahan and elsewhere for their support and encouragement; very special thanks to Ramin Yousofzadeh, Navid Najafi, Ahmad rezaei, Abbas Ghanbari, Amir Saffar, Maryam Dini and Maryam Fereydoun for all friendly discussions we had together.

I thank my old and best friends: Jaber Shabanian, Laleh Dashtban, Majid Talebi, Amirhossein Maani, and Hesamoddin Tabatabaei. No matter when or where, they are always there for me when I need them. I will never forget the wonderful moments we have had together.

Finally, my very special acknowledgement goes to my beloved wife, Sara, for her love, patience and continuous encouragement at all times. There are no words to convey how much I love her.

My mother and sisters have given me their unending love and support in everything for which my mere expression of thanks likewise does not suffice. If this work has sometimes prevented us from sharing important moments of life, know that I never stopped thinking of you.

RÉSUMÉ

Le polyéthylène téréphtalate (PET) est un polymère essentiel utilisé dans plusieurs industries dont le textile et l'emballage. En ce qui concerne l'impact économique et environnemental des matériaux polymères d'emballage, il y a une grande demande pour le développement des systèmes d'emballage de poids réduits. D'un autre côté, les faibles propriétés mécaniques et barrières sont les principaux inconvénients de ces systèmes d'emballage. En dépit des nombreuses études menées sur les performances barrières et mécaniques des composites PET-argile, peu d'améliorations ont été apportées. Dans cette étude, l'influence de l'ajout de kaolin comme un autre type de matériau argileux sur la performance du PET sera étudiée.

La première partie de ce travail porte sur le traitement chimique des particules de kaolin hydraté. Compte tenu de la structure chimique spécifique du kaolin, les agents de modification conventionnels tels que les alkyles d'aluminium qui sont largement employés, tels que dans des argiles de type smectite, ne sont pas applicables dans le cas du kaolin. Comme le nanocomposite final PET-kaolin est censé être en contact direct avec l'aliment, la toxicité des agents de modification est un autre défi à prendre en considération. L'agent de modification doit également être thermiquement stable à la température de traitement du PET. Éventuellement, l'acétate de potassium (KAc) et le diméthylsulfoxyde (DMSO) ont été choisis pour le traitement chimique des particules et leur influence sur la structure et les propriétés physicochimiques des particules a été étudiée.

Dans la deuxième partie, un procédé de déplacement a été appliqué. Le précurseur produit dans la première partie a été mélangé avec du poly(éthylène oxyde) (PEO) dans un mélangeur interne pour donner un mélange-maître PEO-kaolin hautement concentré. Ce dernier a été dilué avec du PET dans une extrudeuse bi-vis pour produire les nanocomposites finaux.

Les résultats de la diffraction des rayons-X ont montré que la structure en couches du kaolin est altérée de façon significative en raison du traitement chimique. Lors de l'intercalation des molécules KAc dans la structure du kaolin, l'intensité du pic caractéristique du kaolin est remarquablement réduite et de nouveaux pics apparaissent à des angles inférieurs; ces pics finissent par disparaître lorsque le kaolin est mélangé avec le PET. Les images MÉB (microscopie électronique à balayage) confirment que le traitement au KAc et l'ajout de PEO ont un effet significatif sur la dispersion des particules. À partir des images MÉT (microscopie électronique en transmission), la taille des particules dans le nanocomposite est estimée de 100 à 200 nm de longueur, tandis que l'épaisseur varie de manière générale entre 10 et 50 nm. Par rapport aux particules telle que reçues, la dispersion du kaolin traité chimiquement dans la matrice de PET est remarquablement améliorée. Toutefois, les études rhéologiques ont montré que la dégradation du PET au cours de l'étape de mélange à l'état fondu entraîne une diminution de la viscosité à l'état fondu et une réduction considérable du poids moléculaire.

Dans la troisième partie, la possibilité de préparer des nanoparticules de kaolin calciné par broyage humide et de les utiliser comme une nano-charge dans la matrice PET a été étudiée. Les images MÉB et MÉT ont montré que les particules broyées ayant une taille entre 50 et 250 nanomètres sont distribuées uniformément dans la matrice de PET. Il a été montré que le module et les propriétés barrière du PET sont améliorés après incorporation des particules broyées, cependant, l'allongement à la rupture est significativement inférieur à celui du PET seul. La présence des nanoparticules altère légèrement les propriétés optiques des échantillons.

La dernière partie a été consacrée à l'étude de l'effet des processus secondaires (tels que l'étirage à chaud) sur les propriétés finales des matériaux composites PET/kaolin-calciné. L'incorporation des particules de kaolin calciné améliore les propriétés finales de la matrice de PET et cette

amélioration s'est révélée être plus prononcée après étirement uniaxial au-dessus de la température de transition vitreuse. Cependant, l'addition de particules a été associée à une certaine opacité dans les composites et le processus d'étirement favorise cet effet qui a été attribué à la cristallinité et au décollement des particules de la matrice.

ABSTRACT

Polyethylene terephthalate (PET) is a major polymer used in industries such as textile and packaging. Regarding the economic and environmental effect of polymeric packaging materials, there is a large demand for the development of reduced weight packaging systems. But on the other hand, low barrier and mechanical properties are the main drawbacks of such packaging systems. In spite of numerous studies conducted on the barrier and mechanical performance of PET-clay composites, little improvement has been reported. In this work, the influence of adding kaolin as a different type of clay material on the performance of PET will be investigated.

The first part of this work focused on the chemical treatment of hydrous kaolin particles. Considering the specific chemical structure of kaolin, conventional modifiers such as alkyl aluminum which are widely used for smectite type clays are not applicable in case of kaolin. Since the final PET-kaolin nanocomposite was supposed to be in direct contact with foods, toxicity of the modifiers was another challenge to be considered. The modifier also needed to be thermally stable at processing temperature of PET. Eventually, potassium acetate (KAc) and dimethyl sulfoxide (DMSO) were chosen for chemical treatment of particles and their influences on the structure and physicochemical properties of the particles were investigated.

In the second part, a displacement method, in which one element is replaced by another in a compound, was applied; the precursor produced in the first part was blended with poly(ethylene oxide) (PEO) in an internal mixer to give a high concentrated PEO-Kaolin masterbatch, and this masterbatch was diluted with neat PET in a twin screw extruder to produce the final nanocomposites.

X-Ray diffraction results showed that the layered structure of kaolin was significantly altered due to the chemical treatment. Upon the intercalation of KAc molecules into the kaolin structure, the

intensity of a kaolin characteristic peak was remarkably decreased and new peaks appeared at lower angles; these peaks eventually disappeared after blending with PET. SEM (scanning electron microscopy) images confirmed that the KAc treatment and blending with PEO had a significant effect on dispersion of the particles. From TEM (transmission electron microscopy) images, the particles in the nanocomposite were estimated to be 100-200 nm in length while their thickness was generally in the range of 10 to 50 nm. Compared to the as-received particles, the dispersion of the chemically treated kaolin in the PET matrix was remarkably improved. However, rheological studies showed that degradation of PET during the melt mixing step led to reduced melt viscosity and a considerable loss in molecular weight.

In the third part, the possibility of preparing calcined kaolin nanoparticles via wet-grinding and using them as a nanofiller in a PET matrix was investigated. SEM and TEM images showed that the ground particles with sizes between 50 and 250 nanometers were uniformly distributed in the PET matrix. It was shown that the modulus and barrier properties of PET were improved after incorporation of ground particles; however, the elongation at break was significantly smaller than that of neat PET. The presence of nanoparticles slightly impaired the optical properties of the samples as well.

The last part was dedicated to studying the effect of secondary processes (such as hot-stretching) on the final properties of the PET/calcined-kaolin composites. Incorporation of calcined kaolin particles enhanced the final properties of PET matrix and this enhancement was shown to be more pronounced after uniaxial stretching above the glass transition temperature. However, the addition of particles was associated with haziness in the composites and the stretching process promoted this effect, which was assigned to crystallinity and debonding between the particles and the matrix.

TABLE OF CONTENTS

LIST OF TABLES

LIST OF FIGURES

NOMENCLATURES

English letters

d_{001}	Clay interlayer spacing
d_L	Distance between two adjacent layers along the z axis
G	Elastic modulus
G'	Storage modulus
G'_{com}	Storage modulus of composites
G'_{PET}	Storage modulus of neat PET
H	Heat flow
ΔH_m	Melting enthalpy
ΔH_0	Melting heat of 100% crystalline PET
M_w	Weight averaged molecular weight
M_n	Number averaged molecular weight
n	Avrami index
t	Time
$t_{1/2}$	Crystallization half-life
T	Temperature
$T_{c,m}$	Crystallization temperature
$T_{c,max}$	Temperature of maximum crystallization rate
$T_{c,o}$	Onset temperatures of crystallization
$T_{d,max}$	Temperature of maximum decomposition rate
T_g	Glass transition temperature

T_m	Melting point temperature
T_{max}	Temperature at which the maximum mass loss occurs
$T_{m,o}$	Onset temperatures of melting
T_{onset}	Onset temperatures of decomposition
T_∞	End temperatures of crystallization
W_f	Filler weight fractions
W_p	PEO weight fractions
X_c	Degree of crystallinity
$X(t)$	Relative crystallinity at time t
Z_c	Nonisothermal crystallization kinetic rate constant
Z_t	Kinetic crystallization rate

Greek letters

δ	Phase angle
η^*	Complex viscosity
θ	Angle between incident ray and scattering planes in XRD
λ	Wavelength of incident wave
υ	Band assignment in FT-IR
φ	Heating / cooling rate
ω	Angular frequency

LIST OF ABBREVIATIONS

AHA	6-aminohexanoic acid
BHET	Bis-hydroxyethyl terephthalate
ch	Chain extender
CKao	Calcined kaolin
D90	Diameter at which 90% of a sample's mass is comprised of smaller particles
DMA	Dynamic mechanical analysis
DMSO	Dimethyl sulfoxide
DMT	Dimethyl terephthalate
DSC	Differential scanning calorimetry
EG	Ethylene glycol
FDA	Food and Drug Administration
FT-IR	Fourier transform infrared spectroscopy
gUlt	Ground calcined kaolin
HNO_3	Nitric acid
IPA	Isophthalic acid
KAc	Potassium acetate
kao	Kaolin (hydrous)
MMT	Montmorillonite clay
NaOH	Sodium hydroxide

OTR	Oxygen transmission rate
PEO	Poly(ethylene oxide)
PET	Polyethylene terephthalate
PKHA	Phenoxy resin (polyhydroxyether)
PSD	Particle size distribution
SEM	Scanning electron microscopy
SHMP	Sodium hexametaphosphate
SiE	3-(Glycidoxy-propyl) trimethoxysilane
TEM	Transmission electron microscopy
TGA	Thermal gravimetric analysis
WAXD	Wide angle X-ray diffraction
XRD	X-ray Diffraction

CHAPTER 1: INTRODUCTION

Polyethylene terephthalate (PET) is an industrialized aromatic polyester representing about 18 % of world polymer production, which makes it the third most produced polymer, behind polyethylene and polypropylene (Wikipedia, 2013). PET has been widely used in the fields of fibers, packaging and specifically for the production of soft drink bottles due to high transparency and good barrier properties. However, the shelf life of a beverage in PET is usually shorter than in glass bottles.

The preparation of PET nanocomposites by melt compounding in order to improve the mechanical properties was the main objective of this study, while higher barrier properties were also favorable. Since PET is a stable and non-degradable compound in environment, it has been always a big challenge to reduce the economic and environmental impacts of PET-based products. The development of light packaging systems could be one solution for this problem, in other words, it would be favorable to use less material for the production of a packaging system without losing the main properties. To do so, the material must have higher mechanical properties in order to retain the shape stability and the properties required by end users. The addition of fillers to a polymer matrix will improve many properties of the composite material while it may have a destructive effect on a few other properties such as optical properties. Therefore, it is of a great importance to have a balance between different properties.

So much effort has been made to improve the barrier and mechanical properties of PET through blending with other polymers (Motta *et al.*, 1996; Prattipati *et al.*, 2005), coating (Barker *et al.*, 1995; Schmachtenberg *et al.*, 2006), and developing multi-layer structures; however, these methods are usually non-economic and give rise to more recycling issues. Dispersing layered materials in a polymeric matrix in order to develop polymer-based nanocomposites has received

great attention in recent years. According to the literature, it seems that nanocomposites offer tremendous improvements in thermo-mechanical and barrier properties (even with low filler loading) when compared to conventional composite materials (Ghanbari *et al.*, 2013; Priolo *et al.*, 2010). In comparison to solution and in-situ polymerization, melt-compounding is environmentally and economically the most preferred technique for compounding and preparation of polymer composites due to the absence of solvents and monomers.

Among the materials with a layered structure, which are capable of being dispersed in polymeric matrix, smectite-type clays, such as hectorite, montmorillonite and synthetic mica are the most investigated ones. However, no study on the effect of other clay minerals such as kaolinite and talc on properties of polymers (and specifically PET) has been conducted. The unique structure and properties of kaolin compared to other clays results in some difficulties in dispersing the particles in polymeric matrices. However, intercalation of a variety of small molecules and few polymers such as poly(vinyl alcohol) (Jia *et al.*, 2008), polystyrene (Elbokl & Detellier, 2006), and poly(vinyl chloride) (Turhan *et al.*, 2010) into the lamellar spacing of kaolinite have been reported. They mainly investigated the morphology of resulting composites while the effect of the filler on different properties of polymers has not been discussed in detail.

Based on the information provided in the literature, a combination of chemical and mechanical treatment (grinding) was applied to improve the dispersion of particles in the polymer matrix; however, their simultaneous effect on the structure, morphology, and properties of kaolin particles was not clear. Therefore, the first part of this work was done to investigate the influence of chemical / mechanical treatments on hydrous kaolin particles. In the second part of this project, PET-kaolin composites were prepared by blending the intercalated particles with neat PET and their morphology and thermal properties were studied. Considering the massive degradation in PET

matrix due to blending with hydrous kaolin, in the third part of this work, calcined (dehydroxylated) kaolin was substituted to the hydrous grade. The calcined kaolin particles were ground prior to mixing with PET; morphology, mechanical, thermal, and optical properties of the final nanocomposites were investigated. The last phase of the thesis looks at the influence of secondary processing (uniaxial hot-stretching) on different properties of the composites.

This dissertation is based on four articles that have been submitted to scientific journals and comprises nine chapters:

Chapter 2 provides a literature review including a discussion on the topics of interest.

Chapter 3 introduces the objectives of this work.

Chapter 4 explains the organization of the articles.

Chapters 5, 6, 7, and 8 report the four articles containing the main results of this study.

Chapter 9 presents a general discussion with regard to the results obtained in this work.

Chapter 10 summarizes the conclusions and outlines of the thesis followed by some recommendations for future work.

CHAPTER 2: LITTERATURE REVIEW

2.1 Clay Minerals

Clay minerals are naturally occurring minerals with a platelet morphology which are categorized as aluminum phyllosilicates. They are very abundant in nature, about 16 % of the Earth's crust is composed of clay minerals. Clay minerals are generally made of tetrahedral silicate and octahedral hydroxide sheets arranged in a layered format in which the layers are stacked upon one another. The way these layers join and arrange in the structure leads to the formation of different types of clay minerals with different compositions and chemical properties. Based on the type and number of layers they may be categorized as 1:1 or 2:1. A 1:1 clay, such as kaolinite, is composed of one tetrahedral sheet and one octahedral sheet. However, most of clay minerals including montmorillonite, vermiculite and talc belong to the 2:1 group in which the octahedral sheet is sandwiched between two tetrahedral sheets. Figure 2-1 displays the 1:1 and 2:1 structures.

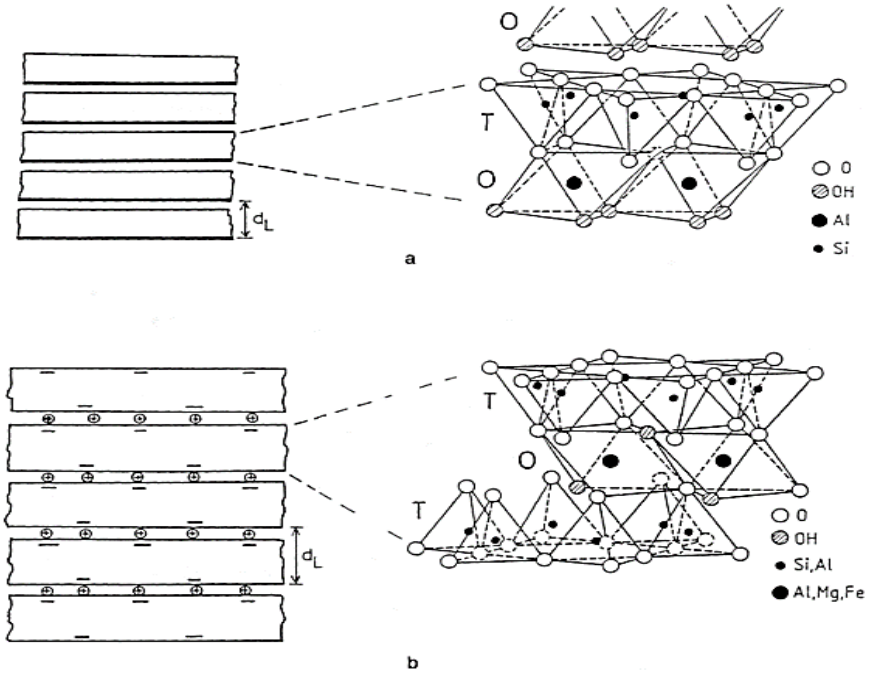

Figure 2-1 Structure of (a) 1:1 and (b) 2:1 clay mineral layer. T= tetrahedral sheet, O= octahedral sheet. d_L = basal spacing of the crystal (Jasmund & Lagaly, 1993).

Table 2-1 Structural and physical properties of common clay minerals (Black, 2009).

Clay mineral group	Kaolin	Illite	Smectite	Vermiculite
Structure	1 : 1 Non-expanding	2 : 1 Non-expanding	2 : 1 High expansion	2 : 1 : 1 Non-expanding
swelling capacity	Almost none	Low	High	Very low
layer thickness	0.7 nm	1.0 nm	1.0 – 2.0 nm	1.4 nm
Interlayer bonding	Strong	Strong	Very weak	Moderate to Strong
CEC [meq/100g]	3 – 15	10 - 40	80 – 150	10 - 40
Surface area [m2/g]	5 - 20	50 - 100	700 - 800	< 80

There are four main groups of clay minerals:

- Kaolinite group: including kaolinite, dickite, nacrite, and halloysite.
- Illite group: including hydrous micas, phengite, brammalite, celadonite, and glauconite.
- Smectite group: including montmorillonite, bentonite, nontronite, hectorite, saponite and sauconite.
- Vermiculite.

The structural and physical properties of these groups are summarized in Table 2-1.

2.2 Kaolin

Kaolin is a soft, earthy, usually white powder consisting principally of the mineral kaolinite and small amounts of other minerals such as quartz and feldspar. Kaolinite is one of the most common minerals in nature and is produced by the chemical weathering of aluminum silicate minerals such as feldspar.

The pulp and paper industry is the main consumer of kaolin and uses approximately 40 percent of total annual production. It employs kaolin to improve color, opacity, and printability of paper. Kaolin is also used extensively in the ceramic and rubber industries and has found minor

applications in ink, organic plastics, and cosmetics. Table 2-2 lists the major producers of kaolin in the world.

Table 2-2 Major Producers of Kaolin in World (Data in thousand metric tons) [Source: USGS: Mineral Commodity Summaries 2013].

	2011	2012 (estimated)
United States	5770	5900
Brazil	2200	2250
Czech Republic	3610	3600
Germany	4900	4500
Italy	640	640
Mexico	120	120
Spain	49	50
Turkey	700	1000
Ukraine	1100	1300
United Kingdom	900	900
Uzbekistan	5500	5500
Other Countries	8410	8300
World Total	33900	34000

2.2.1 Structural features

Mineral kaolinite with a general composition of $Al_2Si_2O_5(OH)_4$ (or written in terms of oxides: $Al_2O_3\ 2SiO_2\ 2H_2O$) is the main component of kaolin (>98%) and typically occurs in platelet forms. The chemical structure of kaolinite is displayed in Figure 2-2. Kaolinite mineral is composed of consecutive alumina octahedral and silica tetrahedral sheets, which sandwich a common plane of oxygen atoms. Aluminum atoms form the octahedral sheets with a structure similar to γ-$Al(OH)_3$

or gibbsite. Combination of the sheets forms the layers, which are hydrogen bonded together (Bear, 1955).

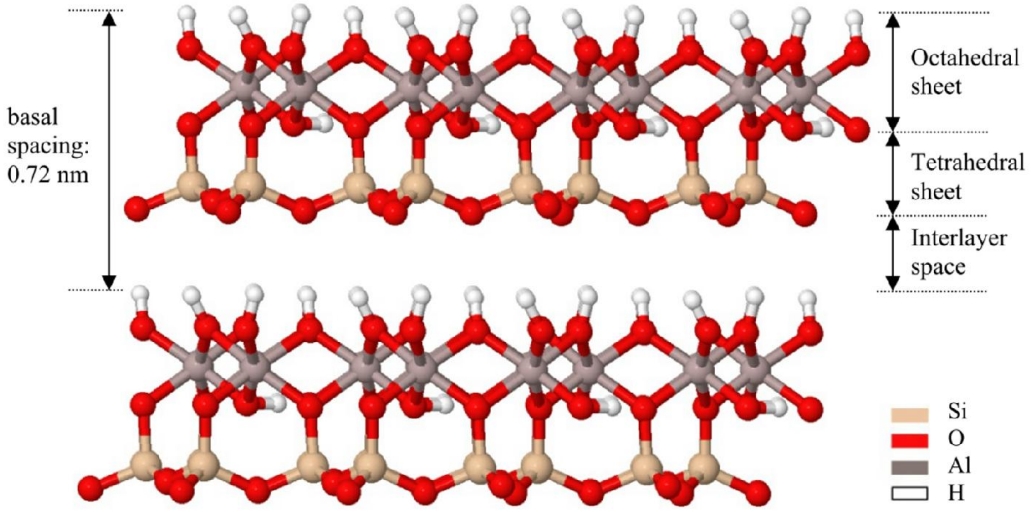

Figure 2-2 Structure of kaolinite [image reproduced from the Virtual Museum of Minerals and Molecules (http://virtual-museum.soils.wisc.edu/displays.html), Accessed October 2013].

From a crystallographic point of view, kaolinite layers can be considered as XY planes stacked along the Z axis forming a triclinic unit cell. The cell parameters are displayed in Table 2-3.

Table 2-3 Crystallographic data for the kaolin group minerals (Jasmund & Lagaly, 1993).

a_0 (Å)	b_0 (Å)	c_0 (Å)	α (°)	β (°)	γ (°)
5.16	8.94	7.40	91.7	104.9	89.8

Where a_0, b_0, and c_0 are the unit cell axes dimensions and α, β, and γ are the inclination angles of the axes in the unit cell. The *d*-spacing (d_L), which is defined as the distance between two adjacent layers along the z axis, can be calculated by the following equation:

$$d_{001} = c_0(1 - cos^2\alpha - cos^2\beta)^{1/2} = d_L = 7.16\ \text{Å} \qquad \text{Eq. 1}$$

In well-crystallized kaolinite, there is a regular stacking of the layers with respect to the Y axis, as displayed in Figure 2-3. The interlayer basal planes are considered as cleavage planes, but due to the ordered stacking and the hydrogen-bonds between two adjacent layers, the separation of layers is very difficult.

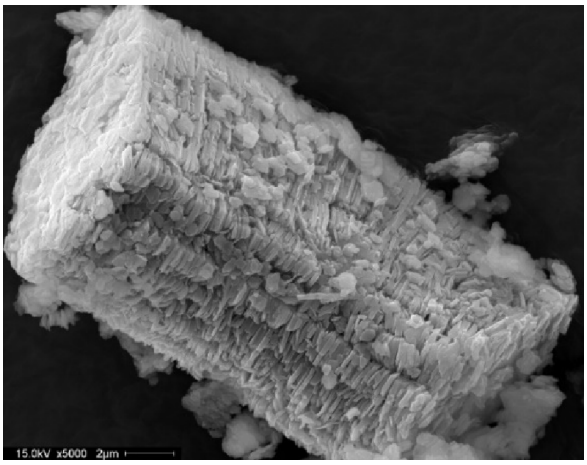

Figure 2-3 Large kaolinite stack [image reproduced from the 'Images of Clay Archive' of the Mineralogical Society of Great Britain & Ireland and The Clay Minerals Society (www.minersoc.org/gallery.php?id=2), Accessed December 2013].

Well-crystallized kaolinite comprise crystallites with a typical hexagonal morphology. These particles with a thickness much smaller than its other dimensions are highly anisometric (Santos, 1989) and range from 0.2 to 4 µm in diameter. Figure 2-4a displays a SEM image of typical kaolinite particles in which the hexagonal morphology is well observed. Stacked kaolinite layers, due to the high tendency for aggregation, are recognized as booklets or tactoids. The aggregates may also form a vermicular morphology with very long and accordion-like booklets, as seen in Figure 2-4b.

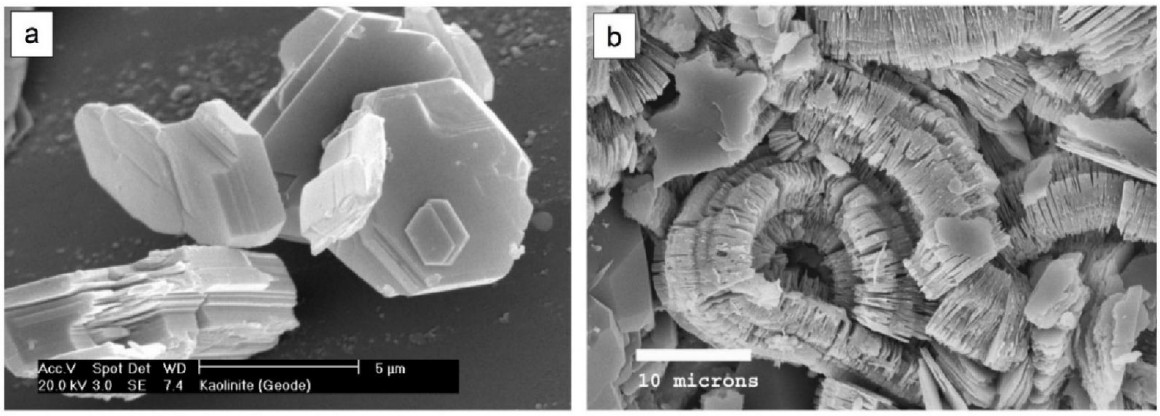

Figure 2-4 SEM image of (a) typical platelet kaolinite particles and (b) vermicular kaolinite particles [Image reproduced from the 'Images of Clay Archive' of the Mineralogical Society of Great Britain & Ireland and The Clay Minerals Society (www.minersoc.org/gallery.php?id=2) , Accessed December 2013].

2.2.2 Cation Exchange Capacity

Cation-exchange capacity (CEC) is defined as the maximum quantity of total exchangeable cations that a mineral clay is capable of holding in its structure. These cations are adsorbed onto surfaces in order to balance the negatively charged sites (unsatisfied valences) at the broken edges or on the flat external surfaces of layers. Due to the predominance of Al^{3+} in the octahedral sheet and lack of substitutions by other cations such as Fe^{3+} or Mg^{2+}, the CEC value of kaolinite is very low compared to that of smectite (Table 2-1) (Brigatti *et al.*, 2006). The cation exchange capacity of the 1:1 type minerals (kaolin) is mainly attributed to the broken edges of the layers, whereas, that of expanding 2:1 type clays (smectite) comes from ionic substitution within the central octahedral sheet of the molecular layer.

Table 2-4 Surface modifications of kaolinite.

Reacting molecule	To form	Reference
phenylbenzene & benzylbenzene	phenylphenoxy- & benzylphenoxy-kaolinite	(Kukharskaya & Fedoseev, 1963)
ethylpolysiloxane,	ethylpolysiloxyl kaolinite	(Kukharskaya & Fedoseev, 1963)
diazomethane	methyl kaolinite	(Santos, 1989)
carboxylic acid chlorides	acetyl and benzoyl kaolinite	(Santos, 1989)
thionyl Chloride	kaolinite chloride	(Kukharskaya & Fedoseev, 1963; Santos, 1989)
benzene-AlCl3	phenyl kaolinite (Friedel-Kraft reaction)	(Santos, 1989)
phenyl-magnesium bromide	phenyl kaolinite	(Kukharskaya & Fedoseev, 1963; Santos, 1989)
chorosilanes	(Si-O)-Si-R3 or (Al-O)-Si-R3 bonds	(Braggs, Fornasiero, Ralston, Smart, & others, 1994; Santos, 1989)

2.2.3 Surface modification reactions of kaolinite

The chemical modification of clay minerals may be divided into two general categories: (i) the reactions occurring on the external surfaces of particles and (ii) the reactions in which the inter-layer surfaces are involved. Ionic exchange reactions with polyatomic cations, which form ionic bonds between the clay surface and the cation, are an example of the first category. The silanol or

aluminol groups located at the edges and basal surfaces of the layers have a great potential as functional groups to react with some other chemical species and form covalent bonds between the particle surface and the reacting molecules. The silanol and aluminol groups at the edges of the particles seem to be more reactive than those of the octahedral basal surfaces (Brady *et al.*, 1996). Table 2-4 summarizes some of the surface modifications of kaolinite.

The improvement of mechanical properties of polymer composites containing silane-modified kaolinite has been reported in the literature (Buggy *et al.*, 2005; Domka *et al.*, 2003; Domka *et al.*, 2002).

2.2.4 Intercalation of kaolin minerals

Kaolinite is generally known as a non-expandable clay mineral, which roots in its unique structure, and with a strong binding energy between the layers. Three different components are involved in the bonding energy of kaolinite:

- Van der Waals' forces
- Hydrogen bonding between hydroxyls and basal oxygen groups.
- Electrostatic interactions, which is a result of dipolar nature of kaolinite.

Among these cohesion forces, hydrogen bonding is known to be the major factor. As shown in Figure 2-2, there are two types of hydroxyl groups in the structure. Inner-surface hydroxyls located on the interlayer basal surfaces and inner hydroxyls located inside the layers, between the octahedral and tetrahedral sheets. The hydrogen ions of the inner-surface hydroxyls in the octahedral sheet tend to form hydrogen bonds with positively charged oxygen atoms in the tetrahedral sheet. This gives rise to high cohesive forces between the layers and keep them tightly stacked on top of each other. However, for 2:1 clay minerals, due to lack of basal inner-surface

hydroxyl, no hydrogen bonds are formed and only weak Van-der-Waals forces bond the layers together. The strength of hydrogen bonds depends on the position and orientation of hydroxyls in the interlamellar spaces. Based on molecular modeling, the bonding energy between individual layers of kaolinite was calculated to be in the range of 200-300 kJ per $Al_2Si_2O_5(OH)_4$ unit (Giese, 1978; Wieckowski & Wiewióra, 1976).

A small specific surface area, as a result of cohesion between the layers, and a very low cation exchange capacity of kaolinite give rise to a low adsorption capacity of organic modifiers. Although the modification of kaolinite by intercalation or grafting of small molecules is much more troublesome than that of smectites, there are some molecules capable of direct reaction with the inter-layer surfaces of kaolinite and intercalation of the structure. These molecules can be classified into four major types (Jasmund & Lagaly, 1993; Rausell-Colom *et al.*, 1987; Thompson *et al.*, 1993):

- Molecules with donor and acceptor groups for hydrogen bonds in different atoms, which are capable of forming strong hydrogen bonds such as urea, formamide, hydrazine, etc.
- Polar molecules with a large dipole moment such as dimethyl sulfoxide, pyridine N-oxide, etc.
- Alkali and ammonium salts of low molecular weight carboxylic acids such as ammonium acetate, potassium propionate, etc.
- Alkali halides such as sodium chloride, potassium iodide, etc.

Many other molecules can be intercalated in kaolin by use of pre-intercalated precursor via displacement method (indirect intercalation). Once the kaolinite layers are partially separated, the

intercalated molecules may be substituted by new chemical groups that do not react directly with the pristine mineral. Indirect intercalation compounds have been prepared by displacement reactions with a very large variety of substances. The organics and polymers, which cannot directly penetrate into the layers, may be incorporated through substitution reactions or active molecules.

Imidazolium derivatives were inserted within kaolinite layers via a melt reaction strategy (Letaief & Detellier, 2007). Letaief and Detellier (2009) revealed a new chemical method for delamination of kaolinite in which a set of displacement reactions sequentially took place to obtain a delaminated structure. Letaief and Detellier (2008) grafted glycidol(2,3-epoxy-1-propanol) on kaolinite surface using kaolinite-DMSO, they believed that presence of glycidol in the interlamellar spaces leads to more available hydroxyl groups for further reactions. Zhang and Xu (2007) utilized microwave radiations to promote intercalation of DMSO molecules into interlamellar spaces of kaolinite. It was revealed that microwave radiations markedly reduced the process time required for intercalation.

Fernando et al. (2000) reported intercalation of benzamide (Figure 2-5) into the interlayer spaces of kaolinite. At first, they expanded the interlayer space by intercalation of dimethyl sulfoxide (DMSO) and subsequently intercalated benzamide into the structure.

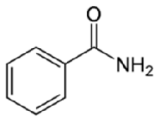

Figure 2-5 Benzamide.

Komori et al. (2000) modified the interlayer surface of kaolinite with methoxy group at room temperature. They mentioned that this material could be an intermediate for intercalating various species. Murakami (2004) prepared a kaolinite modified by butanediols. They reported that using this modifier increased basal spacing of kaolinite from 0.72 to 1.18 nm, which is more than other

modifiers such as methoxy groups (1.11 nm). Letaief *et al.* (2006) prepared ethyl pyridinium chloride-kaolinite (Figure 2-6). To do so, they intercalated urea into the kaolinite interlamellar space. Then replaced urea groups with 1-ethyl pyridinium chloride. The urea acted as a starting material for achieving the final nanostructure. XRD and FTIR proved the intercalation of pyridinium chloride into the galleries of kaolinite. This method was used earlier by applying DMSO-kaolinite as the starting material; however, the authors claimed that urea is more environmentally friendly than DMSO.

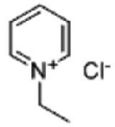

Figure 2-6 Ethylpyridinium chloride.

Komori and coworkers (1998) used kaolinite/N-methylformamide and kaolinite/formamide pre-intercalates in order to intercalate methanol into the structure of kaolinite, and further to displace the methanol with alkylamines of different carbon atoms in the alkyl chain. They managed to increase the basal spacing of kaolinite from 0.72 up to 4.2 nm.

2.3 Effect of grinding on clay minerals

Milling, sometimes also known as fine grinding, pulverizing or comminution, is the process of breaking a solid material into smaller pieces in order to obtain a powder of fine or very fine size in the low micron or even nano-size range. This process occurs under exposure of mechanical forces that split the structure by overcoming of the interior bonding forces. Generally speaking, grinding may serve two main purposes in engineering: (i) increase of the surface area of a solid and (ii) manufacturing of a solid with a desired grain size.

Grinding can be carried out in dry or wet operations using colliding grinding media such as stirred media mills. Many different types of grinding devices are available differing in their type, size,

design, and performance such as ball mills, attrition mills, and small media mills. Stirred media mill is generally a cylindrical drum inside which there are a series of rods, arms or perforated discs which are rotated on a central shaft. The drum is loaded with grinding media, such as metal balls, glass beads, etc. The grinding process takes place when the media and the charge are stirred together. The milling machine applies mechanical stresses to the individual particles in a powder mass to initiate fracture with a minimum of energy. Mechanical forces applied to particles simultaneously reduce the particle size and give rise to some structural changes near the surface region. During milling, four types of forces act on the material particles and result in size reduction (Prasher, 1987) :

- Impact: Sudden shock force acting on the particle, resulting in a very wide size distribution.
- Compression: Steady application of opposing normal forces resulting in a wide particle size distribution.
- Attrition: Removal of fine particles from the exterior of larger particles through particle-particle contacts.
- Abrasion: Size reduction of particles through shear forces from the medium.

The specific influence of grinding on a powder depends on the physical and mechanical properties of the powder itself, and the environment in which the operation is conducted (grinding media). Smaller size grinding media can provide larger surface area available to perform grinding and leads to a finer end particle size.

In most cases, the objective of milling is particle size reduction. However, grinding has a great effect on many other properties of a material such as enhancement of reactivity, alteration of the thermal decomposition behavior and phase transformation, decrease in the sintering temperatures,

etc. (Bégin-Colin *et al.*, 2000; MacKenzie *et al.*, 1999; Palaniandy & Azizli, 2009; Sánchez *et al.*, 2004; Welham & Llewellyn, 1998). Based on the amount of energy delivered by the grinding media to the materials, the grinding process may be classified into three categories including coarse grinding, fine grinding and mechanical activation (Boldyrev *et al.*, 1996; Tkáčová *et al.*, 1993; Tkáčová, 1989). The reduction of particle size can be achieved via coarse grinding, while mechanical activation may cause structural changes in the ground particles and increase their reactivity. Fine grinding is a combination of both coarse grinding and mechanical activation.

Fine grinding is normally performed in high intensity grinding mills such as planetary mill, attrition mill, oscillating mill and jet mill, which can transfer a remarkable amount of mechanical energy to the particles and break them up to produce much smaller particles. However, mechanochemical effects on crystallinity, crystallite size and lattice strain are inevitable during the fine grinding process when the power bulk density is more than 0.1 kWm^{-3} (Tkáčová, 1989).

During the grinding process mechanical energy is transferred to the particles and part of the energy is stored in the materials (Iguchi & Senna, 1985). However, for nonmetallic minerals, having low thermal conductivity, this energy cannot be absorbed as thermal energy and therefore cause bending or breaking of crystals instead, which is associated by loss of regularity in the crystalline structure (amorphization).

Formation of particles with increased surface energy is another important effect of the grinding process. The higher surface energy can promote the interaction between fine particles and facilitate the formation of larger ones, this effect is more pronounced for particles smaller than 10 μm. Adherence, aggregation and agglomeration are mentioned as the main three stages of interaction between the particles (Juhász *et al.*, 1990). At the first stage, particles tend to coat the surfaces of the grinding chamber and media. At the aggregation stage, the particles undergo a reversible

interaction due to the weak Van der Waals forces. And eventually during the agglomeration stage, an irreversible adhesion occurs between the particles which may involve the formation of chemical bonds. This phenomenon is totally unfavorable and therefore grinding aids or de-flocculants such as low-molecular-weight anionic polymers, that neutralize charges on suspended particles, are used to avoid the agglomeration during the grinding process (Frances *et al.*,1996; Godet-Morand *et al.*, 2002; Nair & Paramasivam, 1999).

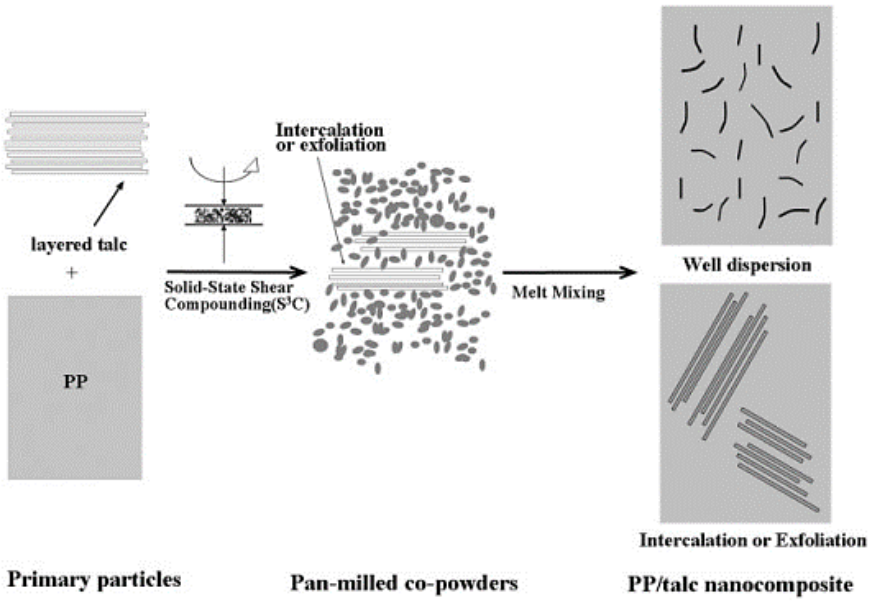

Figure 2-7 Dispersion and exfoliation mechanism of talc in PP matrix by solid state shear compounding using pan-mill (Shao *et al.*, 2005).

Many researchers believe that mechanical treatment can enhance the exfoliation process. It was observed that grinding as a mechano-chemical treatment led to changes in the structure of the kaolinite layers. Tsunematsu *et al.* (1999) ground urea-kaolinite intercalates in a mechanical mortar and observed that kaolinite was easily delaminated. Frost *et al.* (2001) investigated the effect of grinding on the structure and morphology of kaolinite. They found that after grinding (more than 6 hours) OH groups disappeared and were substituted by water molecules.

Shao *et al*. (2005) used a solid state shear compounding (SSSC) technique in a pan-mill equipment to achieve intercalation and/or exfoliation of talc in polypropylene (PP) matrix (Figure 2-7). They found that the characteristic peak of talc basal spacing disappeared after SSSC. TEM micrographs proved the formation of smaller aggregates and a better dispersion of particles.

2.4 Poly(ethylene terephthalate)

Poly(ethylene terephthalate) (PET) is a low cost engineering plastic with good chemical resistance, thermal, optical and mechanical properties. Having good properties and performance make PET a suitable material for many applications such as automotive and electronic parts, textile, soft beverage containers and packaging films.

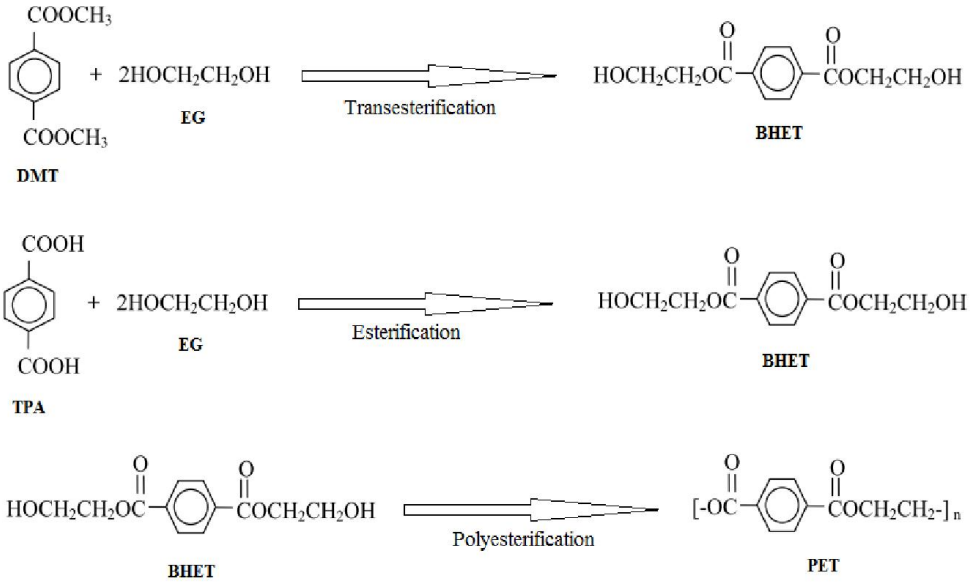

Scheme 2-1 Step-growth polymerization reactions for PET production.

2.4.1 Synthesis of PET

As shown in Scheme 2-1, synthesis of PET is performed in a step-growth polymerization by the reaction of bifunctional acids and alcohols catalyzed in presence of a metal catalyst (Rieckmann & Völker, 2004). The production of PET involves two steps: in the first step, trans-esterification of

dimethyl terephthalate (DMT) and ethylene glycol (EG) (temperature=150-220°C, pressure=100 kPa) or direct esterification reaction of terephthalic acid and ethylene glycol (temperature=240-260°C, pressure=300-500 kPa) yields bis-hydroxyethyl terephthalate (BHET). In the second step, a low molecular weight PET is produced by polycondensation reaction of BHET at a temperature in the range of 250-280°C and a pressure of 2-3 kPa. Higher molecular weight PET can be produced during a solid state polymerization. Depending on the final application, which requires a specific molecular weight of PET, solid state polymerization should be performed at different conditions:

- For fibers and sheets, a number-average molecular weight (M_n) of 15-20 kg/mol (intrinsic viscosity (IV) = 0.55-0.67 dL/g) is required; temperature=280–290°C, pressure = 50-100 kPa.
- For bottles and containers a M_n of 24 to 36 kg/mol (IV = 0.75 and 1.00 dL/g) is required; temperature = 210°C, under vacuum for 12h.

One of the main packaging applications of PET is blow-molded bottles for carbonated soft drinks (CSD), water and juice. In this case, the resin is a PET-copolymer rather than neat PET containing 2.3-3 wt% of a comonomer, such as isophthalic acid (IPA) or cyclohexane-dimethanol (CHDM). The addition of a comonomer can disorder polymer chains and decelerate crystallization during processing and eventually improve the clarity of the products (Rieckmann & Völker, 2004).

In spite of the fact that transparent PET products have a low crystallinity, they show good impact resistance, low permeability, good dimensional ability and high heat resistance which are assigned to molecular orientation of the PET chains (Lee, 1990). This molecular orientation may be achieved by the use of a stretching process above the glass transition temperature (T_g). The amorphous PET film is stretched in the machine direction at a temperature approximately 25°C above glass transition temperature (T_g) using ovens and rollers so the PET chains orient in the stretching

direction and subsequently is drawn in the transverse direction. To hinder the relaxation of chains during the cooling process, the oriented molecules should be frozen after being stretched. Stretched PET has a semicrystalline structure (strain-induced crystallization); however, the existence of crystals does not impair the clarity of the material. The alignment of stretched molecules induces the formation of many crystal nuclei, which grow rapidly and reach the boundary of the neighboring crystallite; therefore, they remain smaller than the wavelength of visible light (50-75Å) (Tekkanat, 2002).

Most beverage bottles are produced by stretching blow molding technique (also called biaxial orientation blow molding). T_g of PET is 82°C and the optimal stretching temperature is around 105°C. Blow-molded PET bottles having 25% crystallinity can be hot-filled up to 85°C. However, many hot-fill applications such as juices and sport drinks require heat resistance of 91-93°C. In these cases, the bottles are annealed at a temperature between T_g and T_m (heat-setting technique) in order to increases the crystallinity (39-42%) and promote the heat resistance to nearly 95°C (Tekkanat, 2002).

2.4.2 Thermal degradation of PET

There are contradictions in the literature about the proposed mechanisms for the primary thermal degradation reactions of polyesters. Since the presence of free radical trapping agents does not hinder the thermal degradation of PET, many researchers believe that degradation reactions should be heterolytic (Buxbaum, 1968; Montaudo *et al.*, 1993), whereas some others consider the formation of molecules such as carbon monoxide and carbon dioxide all over the temperature range of degradation and conclude that it involves a homolytic mechanism (Bounekhel & McNeill, 1995).

2.4.2.1 Heterolytic mechanism

It seems that the β-methylene groups in the structure of PET are the weak point from which the chain breaks down to form oligomers with olefin (vinyl ester) and carboxylic end groups. As it is shown in Scheme 2-2, in this process the C-H bonds and the alkoxy C-O bonds are partly broken, while the olefinic C=C bonds and the O-H bonds are partially formed. During the breakage of alkoxy bonds the α-carbon atoms show some carbonium-ion character in the transition state.

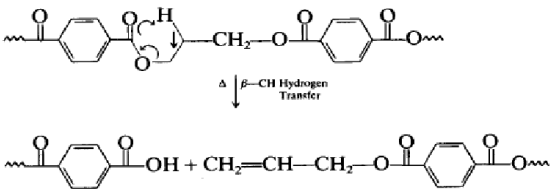

Scheme 2-2 Heterolytic degradation mechanism (Montaudo et al., 1993).

Another important thermal degradation reaction of polyesters is the intramolecular exchange process, which leads to the formation of cyclic oligomers (Scheme 2-3). Increasing the temperature will activate the ester exchange reaction (attack of hydroxyl end on the inner ester groups) with the consequent formation of cycles; actually there is a ring-chain equilibration, which can be shifted in favor of the rings at higher temperature.

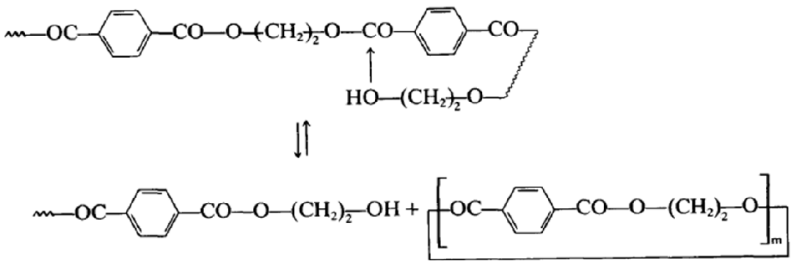

Scheme 2-3 Intramolecular exchange process to form cyclic oligomers (Montaudo et al., 1993).

The cyclic oligomers themselves will undergo a β-methylene hydrogen transfer reaction to form vinyl ester terminated oligomers (Scheme 2-4).

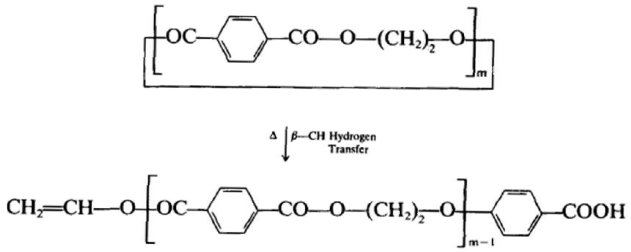

Scheme 2-4 Formation of vinyl ester terminated oligomers from cyclic oligomers (Montaudo et al., 1993).

Once the vinyl ester end-groups are formed they may undergo other reactions. These reactions are shown in Scheme 2-5.

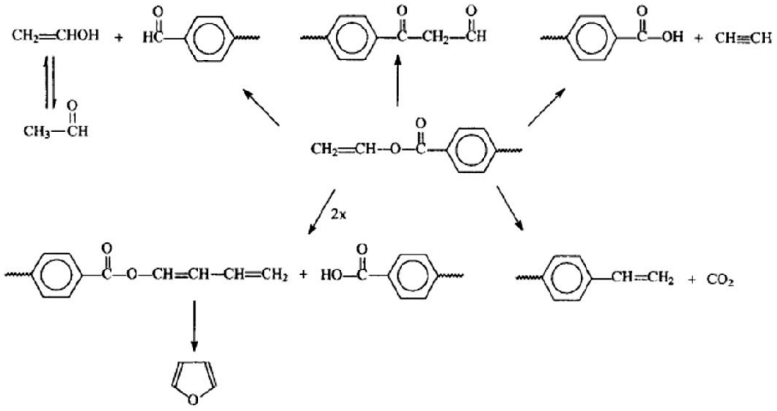

Scheme 2-5 Reactions of vinyl ester end-groups (Edge *et al.*, 1996).

The end-groups in PET are generally hydroxyl-esters, therefore vinyl ester terminated oligomers can undergo trans-esterification to produce vinyl alcohol (which may be converted to acetaldehyde) and regenerate PET chains; consequently, the average degree of polymerization will be maintained to some extent. This could be one reason why, after a considerable initial reduction in rheological and mechanical properties of the polymer, the properties become relatively stable (Edge *et al.*, 1996).

It is reported that recombination of vinyl-terminated end-groups and carboxylic acid-terminated units will lead to the formation of acetaldehyde (Scheme 2-6). This reaction involves the intra- or

intermolecular H shift to form vinyl alcohol, which subsequently isomerizes to yield acetaldehyde (Vijayakumar *et al.*, 1982).

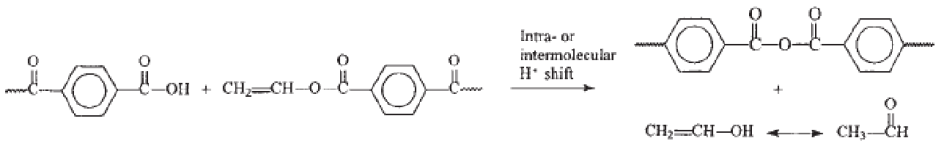

Scheme 2-6 Formation of acetaldehyde (Vijayakumar et al., 1982).

Ethylene is another specie, which evolves during the degradation process. It seems that the vinyl-terminated end groups and the PET units will be arranged in a cyclic transition state that decomposes and leads to the formation of ethylene and carboxylic acid-terminated units (Scheme 2-7).

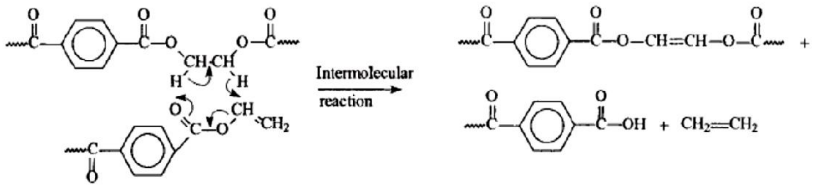

Scheme 2-7 Formation of ethylene and carboxylic acid-terminated units (Vijayakumar et al., 1982).

2.4.2.2 Homolytic mechanism

It is suggested that PET chain session can occur through a homolytic process (radical species). It has been suggested that initial degradation reactions can take place along two possible routes: (a) alkyl-oxygen, or (b) acyl-oxygen scission (Scheme 2-8). Homolytic reactions can explain the whole range of observed degradation products. The formation of CO and CO_2 throughout the main temperature range of decomposition supports the validity of this mechanism, because non-homolytic mechanisms predict the formation of such products only at higher degradation temperatures (up to 500 °C). The reason why radical-trapping agents are not able to stop the degradation process is the cage effect of chains. In other words, radical-trapping agents can hinder

a chain-reaction mechanism whereas homolytic reactions of PET degradation occur in a cage in which the pair of radicals then undergo disproportionation (Bounekhel & McNeill, 1995).

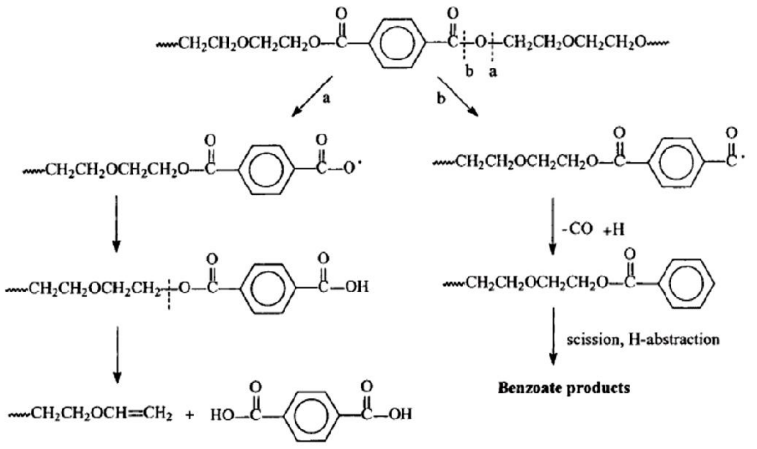

Scheme 2-8 Homolytic degradation reactions of PET (Bounekhel & McNeill, 1995).

2.5 Polymer nanocomposites

Dispersing particles (fillers) in a polymeric matrix has been a very common technique to produce composite materials with improved thermomechanical properties and reduced costs. Dispersion means reduction in the size of particles or agglomerates of the filler in the matrix. Based on the fact that polymers are usually hydrophobic, compounding them with common inorganic fillers with hydrophilic nature has been the main challenge in manufacturing of such composites.

Dispersion of agglomerates depends on three factors: cohesive energy between the particles and small fragments, flow field and forces acting on the particle and strength of the interactions between the matrix and particles. In other words, if the hydrodynamic force goes beyond the cohesive force between the particles or strong interactions between the matrix and particles are formed, dispersion will occur (Manas-Zloczower, 2009). Different mechanisms for dispersion phenomena have been reported in the literature. Among them rupture and erosion seem to be the main mechanisms. Rupture is a quick and large scale fragmentation of agglomerates in which agglomerates break up

into several large fragments, whereas in erosion mechanism, small fragments are separated continuously. Kao and Mason (1975) proposed a model based on the erosion mechanism:

$$\frac{d(R/R_0)}{dt} = -\hat{k}\frac{a}{R_0} \qquad \text{Equation 2-1}$$

where R is the radius of agglomerate, t is time, a is the radius of individual particles forming the agglomerate and $\hat{k}$ is a proportionality constant.

In the last two decades, nanomaterials have attracted a significant interest from both industrial and academic researchers. Nanomaterials comprise a new class of materials with at least one dimension of the order of 0.1–100 nanometers (nm). Many scientific articles have been published concerning the improvement of properties of different materials using nanoparticles in their structure (Beake & Leggett, 2002; Bizarria *et al.*, 2007; Choudalakis & Gotsis, 2009; Dini *et al.*, 2013; Ghanbari *et al.*, 2013a; Ghasemi *et al.*, 2011; Ghasemi *et al.*, 2012; Imai *et al.*, 2002; Kumar *et al.*, 2009; Liu *et al.*, 1997; Masoud & Alireza, 2009; Najafi *et al.*, 2012; Wang *et al.*, 2006; Wu & Ke, 2006). The major factor affecting the final properties of nanocomposites is the level of dispersion of filler particles.

Among the nanoparticles, which have been used as filler in nanocomposites, layered silicate (clay) and carbon nanotube have received the most attention because of good performance, availability and costs. The filler which is most commonly used as layer structure in preparation of polymer nanocomposites is the layered smectite clay silicates.

Most of the polymers are hydrophobic and inherently incompatible with hydrophilic silicates. Depending on the strength of interactions between the clay particles and polymeric matrix, nanocomposites are divided into three main groups (Figure 2-8):

i. Microcomposites: In this case, polymer molecules are not capable of penetrating into the gallery (interlayer space) of silicate layers so the basal spacing between layers does not change.

ii. Intercalated nanocomposites: for these materials, polymer molecules diffuse between silicate layers and increase the basal spacing to some extent.

iii. Exfoliated nanocomposites: in this case, the silicate layers are completely delaminated and the composite consists of individual silicate layers dispersed in the polymeric phase. The basal spacing between layers is significantly increased, which will lead to a maximum contact area between phases and the best composite properties (Liu *et al.*, 2006).

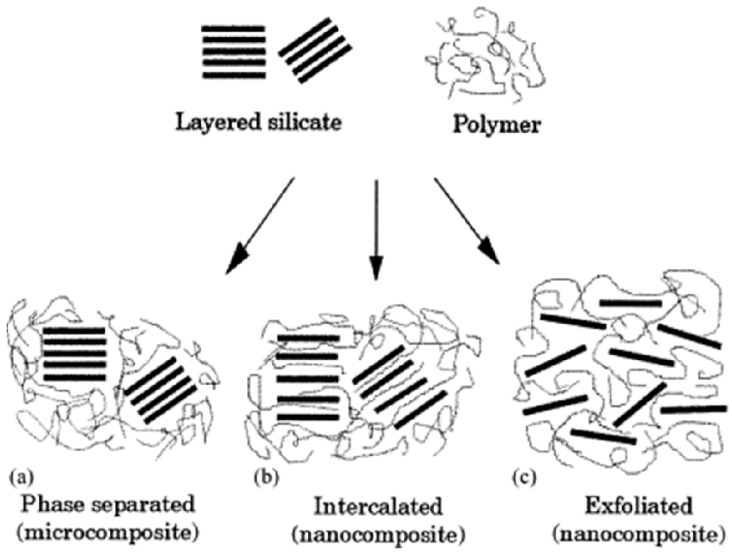

Figure 2-8 Schematic of three main types of polymer/layer structure composite morphologies: (a) Microcomposites, (b) intercalated nanocomposites, and (c) exfoliated nanocomposites (P., Alexandre, & Dubois, 2000).

Nanocomposites are usually prepared by three methods as below:

i. Solution method: in this method, the polymer and clay are dissolved in a same solvent, so polymer chains could diffuse between layers of the silicate and expand the interlamellar spaces. After evaporation of the solvent, the final composite structure will be achieved.

ii. *In situ* polymerization: in this method, layered silicates are swollen with a monomer or solution of the monomer. The monomer molecules can diffuse and settle in between the layers and then polymerization will occur to obtain an intercalated or exfoliated structure.

iii. Melt processing: in this method, nanofillers are incorporated in the molten state of the polymer. The process is usually done under high shear so polymeric chains can diffuse into the filler structure to form a nanocomposite material (Ray *et al.*, 2006).

In a melt-compounding process, big agglomerates of clay break into smaller tactoids under high shear applied by extruder or internal mixer. Diffusion of polymer chains and peeling effect of shear rate on tactoids separate the individual clay layers from the platelets to achieve an exfoliated structure. Figure 2-9 shows this mechanism schematically. Various researches *et al.*, 2008; Ghasemi *et al.*, 2011; Xu *et al.*, 2011) have revealed that many processing factors such as particle loading, screw configuration, feeding rate, processing temperature, etc. have an influence on the level of intercalation/exfoliation of particles. In spite of aforementioned factors, the affinity between polymer and clay seems to be the main parameter determining the final dispersion state of nanocomposite. This affinity mainly depends on the intrinsic characteristics of clay surface and polymer structure such as chemistry of clay and polymer, polarity, and cation exchange capacity (CEC), etc.

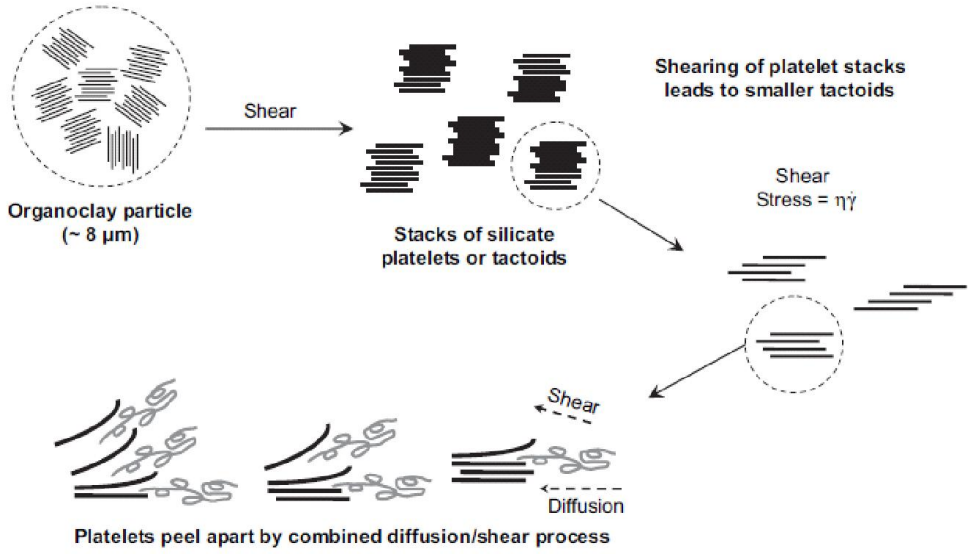

Figure 2-9 Mechanism of organoclay dispersion and exfoliation during melt processing (Paul & Robeson, 2008).

From a thermodynamic point of view, regarding the Helmholtz free energy ($\Delta F = \Delta U - T\Delta S$) one can say that entropic penalty for confinement of polymer chains between clay layers must be compensated by internal energy changes associated with the formation of new intermolecular interactions in order to have a good thermodynamic affinity between the phases so that intercalation can take place.

On the whole, since polymeric materials are usually hydrophobic, dispersing hydrophilic clay minerals in a polymer is a big challenge for manufacturing of such composites. To overcome this problem, modification of clay particles with chemical surfactants such as alkyl ammonium has been applied as an effective technique.

Many researchers have used different techniques to improve the structure and morphology of composites; among them applying different types of modifiers and changing the processing conditions have received the most attention. Jimenez *et al.* (1997) tried to develop a poly(ε-caprolactone)–clay nanocomposite. They modified montmorillonite clay by di-stearyl-dimethyl-ammonium chloride and blended this organo-modified clay with poly(ε-caprolactone) via the

solution method. Their study showed that neither intercalation nor exfoliation of clay particles took place.

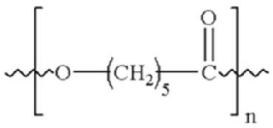

Figure 2-10 Poly (ε-caprolactone).

Vaia *et al*. (1997a) focused on the thermodynamic aspects of polymer melt intercalation in layered silicates; they considered both entropic and energetic factors in the system and developed the mean-field statistical lattice model to describe the polymer melt intercalation. They used this model for qualitative prediction of intercalation process and to obtain a guideline for selecting compatible polymer-layered silicate systems. They also investigated the effect of different parameters such as functionalization, annealing temperature, molecular weight of polymer, etc. on melt intercalation of styrene based polymers (Vaia & Giannelis, 1997).

Imai *et al*. (2002) used 10-[3,5-*bis*(methoxy carbonyl) phenoxy] decyl-triphenyl phosphonium bromide (IP10TP) as a reactive compatibilizer to prepare PET/Mica nanocomposite. Although they could not achieve an exfoliated structure, the flexural modulus of the nanocomposite was improved by 170%. They also investigated the structure and thermal properties of such nanocomposite elsewhere (Saujanya *et al.*, 2002) . According to their study, organo-modified nanoparticles remarkably increased the crystallization temperature (T_c). They believe that exfoliated nanolayers act as a nucleating agent, which leads to an increase in T_c. It was also observed that the glass transition temperature (T_g) of these nanocomposites decreased with an increase in the content of compatibilizer, they explained this effect as the result of restricted segmental motion of polymer chains near the interface of the matrix and filler.

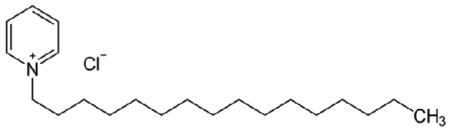

Figure 2-11 Cetylpyridinium chloride (a cationic quaternary ammonium compound).

Ou *et al.* (2004) prepared PET/MMT nanocomposite, modified with cetyl-pyridinium chloride, via a solution method. They reported that layers of clay were partially exfoliated but at higher contents of organoclay (>10%), some agglomerated particles appeared. T_c and the rate of crystallization were increased after increasing the amount of clay up to 10 wt% but, at higher contents, decreases were observed. According to this study, the melting point (T_m) was not affected by the presence of clay nanoparticles. They also observed that the thermal stability of nanocomposites increased to some extent.

Chang *et al.* (2004) applied dodecyl triphenyl phosphonium chloride to modify montmorillonite (MMT) nanoparticles and prepared PET nanocomposite by *in situ* polymerization in order to produce fibers. XRD graphs showed that using a chemical modifier did not lead to complete exfoliation but increasing the draw ratio of fibers improved the exfoliation process. They reported that introducing a low content of organoclay improved thermo-mechanical properties of the polymer. The addition of 1-3 wt% organoclay to the system increased tensile strength and modulus about two fold over that of pure PET. Thermal stability (degradation temperature) of the polymer was improved after addition of organoclay as well.

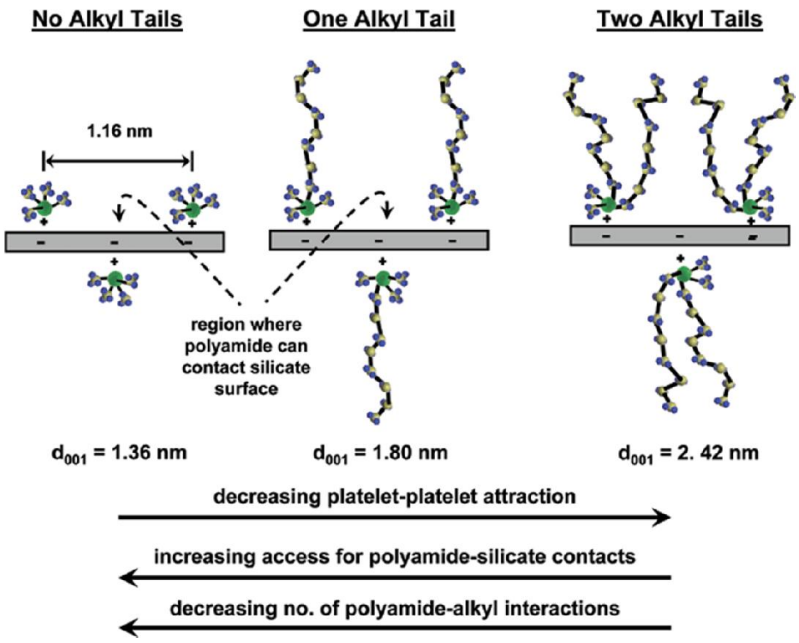

Figure 2-12 Illustration of the role of quaternary ammonium cations on the intercalation and exfoliation of organoclay by nylon-6 Illustration of the role of quaternary ammonium cations on the intercalation and exfoliation of organoclay by nylon-6 (Fornes, Hunter, & Paul, 2004).

Fornes *et al.* (2004) used alkyl ammonium modifiers with different numbers of long alkyl groups in polyamide/clay systems. They found that the modifier with one long group led to a more exfoliated structure than the two other ones. They believed that this effect may have two main reasons; the first one is that long chains limit the number of polyamide-silicate contacts by sterically blocking the surface and the second reason is that increasing the length of alkyl chains increase the amount of alkyl material that would have to mix with polyamide.

Shah *et al.* (2004) prepared Nylon 6-MMT nanocomposites by a melt mixing masterbatch process. Based on the fact that high molecular weight grades of Nylon 6 leads to higher levels of exfoliation, they prepared a high molecular weight Nylon 6-MMT masterbatch in a first step and then mixed it with low molecular Nylon 6 in a melt process. They believed that by this method, it will be possible to obtain a better exfoliation and lower viscosity (low viscosity resins are easier for processing). They reported that the properties of this nanocomposite were comprised between those of the corresponding composites prepared directly from HMW nylon-6 and LMW grade.

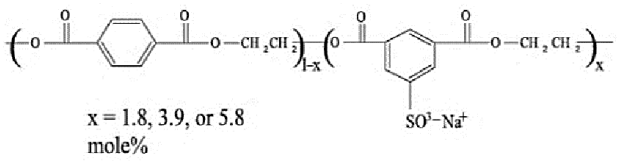

Figure 2-13 Structure of PET and PETI polymers used in this study. 'X' indicates the mole ratio of random incorporation of the ionic co-monomer (Barber, Calhoun, Moore, & R.B., 2005).

Barber *et al.* (2005) compared PET-clay with PETI (polyethylene terephthalate ionomer)-clay nanocomposites to see the effect of ionomer on the exfoliation and thermo-mechanical properties of composite. This study showed that a low content of ionomer led to better exfoliation and improved the mechanical properties; they believed that electrostatic interactions between the ionomer groups of the polymer and the edges of the clay platelets eased the insertion of chains segments attached to the ionic groups into the interlayer spaces of clay. It was also found that a better dispersion and better exfoliation led to lower rate of crystallization. The authors suggested two main reasons for this; the presence of interactive surfaces (tactoid sides) that are capable of immobilizing chains are decreased, and, better exfoliation and dispersion of particles which leads to higher viscosities (unfavorable for crystallization).

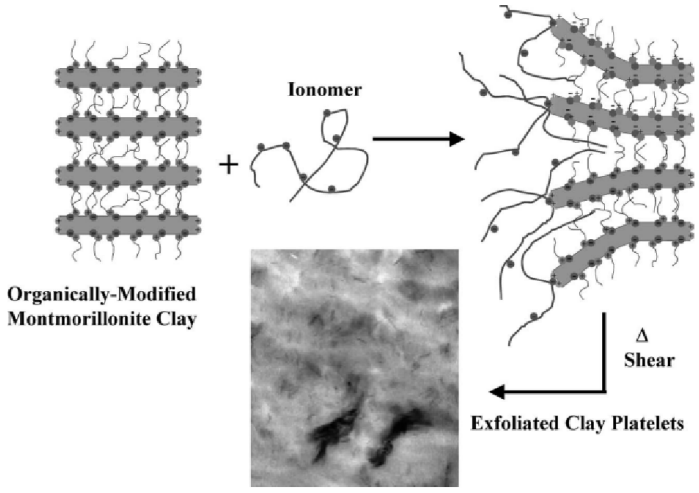

Figure 2-14 Schematic representation of the interaction between ionic groups in the polymer backbone and the edges of the clay platelets (Barber et al., 2005).

Lai *et al.* (2005) studied the effect of epoxy treatment of MMT on thermo-mechanical and transport properties of poly (ethylene terephthalate-co-ethylene naphthalate)/organomodified MMT nanocomposites. They treated the nanoparticles surface by an epoxy monomer to increase polar interactions between the polymer matrix and nanoclay. All thermo-mechanical properties and gas permeability of nanocomposites were improved by the addition of epoxy monomer to the system. They believed that the epoxy groups acted as a compatibilizer as well as a chain extender.

Lee *et al.* (2005) developed PET/Clay nanocomposites through ring-opening polymerization of cyclic oligomers. To do so, they polymerized ethylene terephthalate cyclic oligomer in the presence of organically modified clay. XRD, FTIR and NMR tests showed that the polymer chains had been completely intercalated into the layered silicate structure. They also studied the effect of polymerization reaction temperature on the thermal behavior of the nanocomposite. Based on this study, increasing reaction temperature increased the melting point and decreased the crystallization temperature of the resulting composite.

Qu *et al*. (2005) prepared PET/$BaSO_4$ nanocomposites via *in situ* polymerization. TEM micrographs showed a very good dispersion of particles in the matrix particularly at low concentrations. They reported that BaSO4 nanoparticles improved the crystallinity and thermal stability of the nanocomposites and the most efficient improvement was observed for samples with lower contents of particles (< 2.5 %).

Stretz *et al.* (2005) examined the effect of surfactants with different molecular weight and structure on the level of exfoliation and mechanical properties for SAN (Styrene Acrylonitrile)-MMT nanocomposites. They reported that surfactants with lower molecular weight head groups were more effective in expanding the clay gallery. They also found that the fewer the number of surfactant tails, the greater the change in the gallery spacing. For mechanical properties, they found

that the lowest molecular weight surfactant improved the modulus and tensile strength more than high molecular weight ones.

Wu *et al.* (2006) investigated water absorption and thermal behaviors of PET/SiO_2 nanocomposites. They prepared nanocomposites with different particle size distributions and concluded that decreasing the particle size of the filler would diminish water absorption. They also reported that increasing annealing time would decrease water absorption because of the more crystalline content in the nanocomposite. In this paper, it was mentioned that using nanoparticles improved the thermal stability of the nanocomposite.

Frounchi *et al.* (2006) achieved an intercalated structure using 3-5 % organo-modified MMT in PP/EPDM blend via solution casting. By increasing the clay content to 7%, the XRD peaks were similar to those of pure clay which means no intercalation took place. They also reported that the presence of organoclay led to a reduction in crystallinity and gas permeability of the nanocomposites.

Bizarria *et al.* (2007) studied the influence of clay nanoparticles (MMT) on the recycled PET. Although they did not observe complete delamination of the filler, but mechanical properties were improved. They also reported a great decrease in viscosity of the nanocomposite which was attributed to degradation during the process, opposite effect on viscosity has been reported by Chae *et al.* (2007). They observed an increase in viscosity after incorporation of ferrite nanoparticles.

Calgano *et al.* (2008) discussed the entropic and energetic aspects of interactions in the nanocomposites and concluded that polar modifiers would facilitate the intercalation (or exfoliation) process compared to apolar modifiers. Lai and coworkers (2008) compared the effect of two types of organomodifiers on the thermomechanical properties of PET/MMT nanocomposites and reported that applying (4-carboxy butyl)triphenyl phosphonium bromide

(Φ_3P^+-C_4) led to a better dispersion of particles in the matrix compared to hexadecyl trimethyl ammonium bromide. They believed that the organo-modification of clay had a great influence on the thermal behavior of nanocomposites, so they compared the effect of two different types of organomodifiers and concluded that (4-carboxybutyl) triphenyl phosphonium bromide exhibited a better dispersion in the matrix compared to hexadecyltrimethyl ammonium bromide. Ammala *et al.* (2008) reported that treatment of pristine flouromica with ionomers resulted in better exfoliation of layers compared to commercially available organomodifiers. They claimed that this method would improve thermal stability of nanocomposite, besides, the effectiveness of ionomer treatment is higher than clays modified with phosphonium or imidazolium.

In some papers, it is reported that the amount of clay added to the polymer can affect the level of exfoliation, for example Frounchi *et al.* (2009) observed that nanocomposites of PET-clay with lower contents of clay had exfoliated structure while raising the amount of organoclay led to an intercalated structure.

Ghasemi *et al.* (2011b) prepared PET nanocomposites with different types of modified MMT clay, including ammonium (C30B), phosphonium and imidazolium surfactants. Although better thermal stability was observed for phosphonium based nanocomposites, but they showed a lower degree of dispersion compared to ammonium and imidazolium-based nanocomposites.

Ghanbari *et al*. (2013a) prepared PET nanocomposites containing different types of modified MMT clay to investigate the effect of the screw geometry, clay concentration, and surfactant chemistry of the organoclays. The morphology and rheological behavior of nanocomposites were extensively studied; the highest level of exfoliation was achieved for the nanocomposites containing lower concentrations of C30B exhibited. In another study they prepared PET nanocomposites containing Closite 30B and Nanomer I.28E. In order to improve the dispersion of clay particles, a

sulfopolyester (PET-ionomer or PETi) was added to the nanocomposites. They compared the properties of two systems and concluded that incorporation of C30B in the absence of PETi resulted in better distribution of nanoclay and higher barrier properties. It was also reported that sulfopolyester (PETi) promoted the dispersion of clay particles. However, microscopy observations revealed that clay layers were localized into the PETi domains due to their greater affinity (Ghanbari et al., 2013a).

Dispersing clay particles in PET to improve its barrier and mechanical properties attracted a great deal of attempts, however, lack of compatibility between PET chains and clay particles obstruct the formation of highly dispersed systems. Although presence of oxygen atoms in the chemical structure of PET gives it some polarity, it is not enough to form strong interactions with polar surfaces of clay. There are some reports on the intercalation or partial exfoliation of clay in PET matrix but complete exfoliation (which happens for polar polymers such as polyamide) has not been achieved yet. Some additives such as pentaerythrytol and maleic anhydride have been utilized in the extrusion process to compatibilize PET with organoclay but results showed that complete exfoliation was not achieved.

Wang *et al.* (2006) prepared PET/organo-MMT nanocomposites. Although XRD and TEM graphs showed that an exfoliated structure was not achieved, when the content of MMT was up to 1%, the silicate layers were intercalated. When increasing the MMT content more than 1 wt%, no nanostructure was achieved. Based on DSC results, they observed that the introduction of nanoparticles to the system increased the rate of crystallization. The best results for tensile strength and flexural modulus were obtained at 1% MMT. By increasing the content of MMT, flexural strength increased but elongation at break and izod impact strength decreased.

Zhang *et al.* (2003) obtained PET/nanoclay composites with improved tensile strength. They claimed that samples with 10 wt % nanoclay were optically transparent.

Bandyopadhyay *et al*. (2007) investigated the thermomechanical properties of PET/MMT nanocomposites. They reported that thermal degradation started earlier in the nanocomposites compared to neat PET and attributed this effect to degradation of surfactants present in the organoclay. However, the average thermal stability increased. They found that, in contrast with neat PET, nanocomposites elastic and plastic behavior shifted to higher temperatures (higher values of E' and E'' at higher temperatures), which was attributed to the reinforcing effect of clay particles.

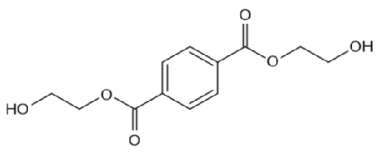

Figure 2-15 Bis(hydroxyethyl terephthalate).

Acierno *et al.* (2007) prepared a PBT-clay nanocomposite using BHET (bis(hydroxyethyl terephthalate)) as an organic modifier and compared the morphological and thermal properties of these nanocomposites with other PBT hybrid composites based on commercial organoclays. It was claimed that using BHET as a modifier improved the thermal properties of the nanocomposite.

It is obvious that thermal properties play an important role in the processing of polymers. In spite of excellent mechanical and optical properties, PET suffers from low crystallization rates and high melting temperatures, which have restricted its applications in high speed processes such as injection molding (Bizarria et al., 2007).

Nowadays it has been proved that the incorporation of nanoparticles could compensate for many drawbacks of polymeric materials. Kaolinite/poly(ethylene oxide) and kaolinite/poly(hydroxyl butyrate) intercalates show thermal stability up to 300 °C (Gardolinski .; Cantão,.; Wypych,. 2000). The same thermal stabilizing effect was observed in PET/ferrite nanocomposites (Chae & Kim,

2007). Yuan *et al.* (2008) investigated the thermal degradation of PET/Fibrous silicate nanocomposites. They modified the clay using water soluble PVP, which is thermally stable up to PET processing temperatures. It was disclosed that thermal stability of the nanocomposite decreased at slow heating rates whereas it increased at high heating rates. Some of the researchers have focused on the crystallization behavior of polymer/clay nanocomposites. It has been reported that nanoparticles acts as an external nucleating agent and raises the crystallization rate and crystallization temperature; PET-SiO_2/polystyrene composites showed accelerated crystallization compared to virgin PET (Wu and Ke 2007). Calcagno *et al.* (2007) believed that only polar modifiers increased the crystallization rate. There are some papers, which have indicated that clay nanoparticles do not have a remarkable influence on the thermal properties of nanocomposites. Villanueva *et al.* (2009) reported that the addition of nanoclay to the polymers did not affect the melting (T_m) and crystallization (T_c) temperatures of nanocomposites noticeably, while degradation temperatures were improved. Soon *et al.* (2009) obtained similar results for PET-mica nanocomposites: only a very slight decrease in T_c was reported as clay loading increased. They also observed that by the addition of mica nanoparticles, the glass transition temperature (T_g) declined. The authors ascribed this to the reduction of molecular weight of the polymer during processing. The same changes in T_g have been reported elsewhere (Bizarria et al., 2007). Guan *et al.* (2008) mentioned three phenomena which affect the crystallinity the most, including dispersion morphology of clay, surface modification and metallic derivatives released from clay. It is indicated that, although the presence of clay particles promote the crystallization process, surface modification and metallic derivatives influence it as well.

Ghasemi *et al.* (2012) reported a partially exfoliated/intercalated structure for PET-MMT (Closite 30B) nanocomposites. Incorporation of clay improved barrier properties and tensile modulus, but

the resistance to puncture and tear propagation was reduced. It was also claimed that nanocomposite films were hazier, but still in the acceptable range of transparency. In order to investigate the influence of processing conditions on properties of nanocomposite, Ghasemi *et al.* (2011a) prepared PET- Cloisite 30B nanocomposite films by cast extrusion in a twin screw extruder. They concluded from XRD and TEM analysis that increment of screw speed, reduction in feeding rate and increasing the number of mixing elements in the screw could improve the delamination of clay particles. Their results also showed that both higher screw speeds and longer residence times have a favorable effect on the barrier and mechanical properties.

Ghanbari *et al.* (2013) addressed the degradation of PET chains under processing which led to a remarkable molecular weight reduction. A multifunctional epoxy-based chain extender was added to the nanocomposite to compensate this effect and rebuild the molecular weight of PET. It was claimed that the addition of chain extender could improve the dispersion of particles and had a beneficial influence on the barrier and mechanical properties of nanocomposites, however, the destructive effect of chain extender on the optical properties of films was inevitable.

Dini *et al*. (2013) applied water-assisted melt-mixing process followed by SSP to produce partially exfoliated, PET-C30B nanocomposites. They reported that the mechanical and barrier properties of nanocomposites prepared by this novel technique were slightly enhanced compared to those of conventional nanocomposites; more interestingly the elongation at break of water assisted nanocomposites was significantly higher than that of conventional nanocomposites (180% compared to 6%).

2.5.1 Polymer-kaolinite nanocomposites

Tunney and coworker (1996) prepared poly (ethylene glycol)/kaolinite (Figure 2-16) intercalates using kaolin-dimethyl sulfoxide (Kao-DMSO). To do so, they prepared DMSO intercalate of

kaolinite first and then reacted it directly with poly(ethylene glycol) in the melt state. They reported an expansion in interlayer galleries of kaolinite using this method.

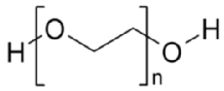

Figure 2-16 Poly(ethylene glycol).

Komori *et al.* (1998) directly intercalated poly(vinyl pyrrolidone) into kaolinite interlayer spaces at room temperature via a solution method. Itagaki *et al.* (2001) synthesized kaolinite/poly(β-alanine) via in situ polymerization. The resulting hybrid material showed improved thermal stability up to 340 °C.

Table 2-5 Mechanical properties of Nylon6/kaolinite composites (Itagaki et al. 2001).

	Clay content (wt%)	Tensile strength (MPa)	Tensile modulus (GPa)	Izod impact strength (with notch) (J m^{-1})
Nylon6	0	74.0	1.13	27.8
Nylon6 (blended)	0	72.7	1.16	34.5
Nylon6/kaolinite	1.42	79.2	1.29	27.7
Nylon6/kaolinite-AHA	1.48	77.0	1.25	21.6
Nylon6/kaolinite–nylon6	1.38	80.4	1.33	27.7
NCH	1.80	89.1	1.36	25.4

Itagaki et al. (2001) also prepared kaolinite-Nylon 6 composites. They melt mixed kaolinite-nylon 6 intercalated masterbatch (prepared by the polymerization of 6-aminohexanoic acid (AHA) in the interlayer space of kaolinite) and commercial Nylon 6 in a twin screw extruder. The basal spacing of kaolinite-nylon 6 was reduced after melt-mixing indicating that the exfoliation structure was not achieved. Their results indicated that mechanical properties had been improved by the addition of kaolinite; however, commercial grade Nylon6-clay hybrid (NCH) containing organically modified smectite exhibited higher mechanical properties (Table 2-5).

Liu Xuening and coworkers (2005) reported the intercalation of poly(styrene/maleic anhydride) into kaolinite via *in situ* polymerization using kaolinite-DMSO as a starting material. They achieved a complete exfoliated structure when the kaolinite content was in the range of 1-10 wt%.

Elbokl and Detellier (2006) prepared polystyrene-kaolinite nanocomposites via *in situ* polymerization. At first, they prepared kaolinite-DMSO and then polymerized styrene in its presence to form a nanohybrid material. X-ray and NMR tests showed that one layer of polystyrene had diffused completely into the interlamellar spaces of kaolinite.

Ammala *et al.* (2007) prepared nanocomposites of poly(m-xylene adipamide)-kaolinite and poly(m-xylene adipamide)-montmorillonite via melt blending technique. The findings from this research indicated that kaolinite and montmorillonite had the same effect on clarity and improvement of barrier properties. However, kaolinite led to higher degrees of crystallinity and was more difficult to exfoliate than MMT. Elbokl *et al.* (2009) achieved an intercalated kaolinite/methacrylamide compound via in situ polymerization using DMSO-kaolinite as a starting material.

Table 2-6 Mechanical and thermal properties of nanocomposites (Maria Pilar Cabedo; José Maria, Lagarón; Enrique, Giménez, 2009).

Sample	E (MPa)	σ_b (MPa)	T_c (°C)	T_m (°C)	ΔH_c (J/g)	ΔH_m (J/g)
PEMA	175 (±27)	[a]	99.3	119.7	−79.8	83.2
PEMA/K	300 (±31)	[a]	103.3	120.4	−81.5	89.1
PEMA/MMT	257 (±41)	[a]	102.9	120.0	−80.0	87.4
Ionomer	254 (±13)	15.4 (±0.9)	63.6	— 92.4	194.4 −40.6	— 48.9 4.2
Ionomer/K	393 (±24)	17.6 (±0.2)	70.3	146.3 92.0	194.0 −46.9	−3.3 51.4 1.9
Ionomer/MMT	319 (±30)	16.8 (±1.0)	69.3	162.6 92.7	189.0 −46.3	−2.2 53.3 1.2
EVA	63 (±4)	≥11.1 (±0.5)[a]	77.9	97.0	−52.2	47.4
EVA/K	73 (±5)	≥10.6 (±0.3)[a]	78.3	97.0	−50.6	47.9
EVA/MMT	115 (±12)	8.6 (±0.5)	78.3	97.0	−53.0	47.3
PEAA	40 (±2)	≥7.9 (±0.3)[a]	77.9	97.0	−37.4	32.8
PEAA/K	47 (±2)	6.5 (±0.3)	79.6	98.0	−33.7	32.7
PEAA/MMT	55 (±3)	5.9 (±0.8)	79.3	97.7	−35.6	32.6

Villanueva *et al.* (2009) prepared nanocomposites of various polymers such as polyethylene-grafted-maleic anhydride (PEMA), poly(ethylene-co-acrylic acid) (PEAA), a poly(ethylene-co-

vinyl acetate) (EVA), and an ionomer of poly(ethylene-co-methacrylic acid) containing MMT and kaolinite as the nanofiller. They compared morphology, thermal and mechanical properties of the prepared nanocomposites. It has been reported that MMT platelets had higher aspect ratio, whereas kaolinite nanocomposites resulted in better mechanical properties (Table 2-6). MMT and kaolinite both reduced gas permeability of polymers but the former seemed to be more effective.

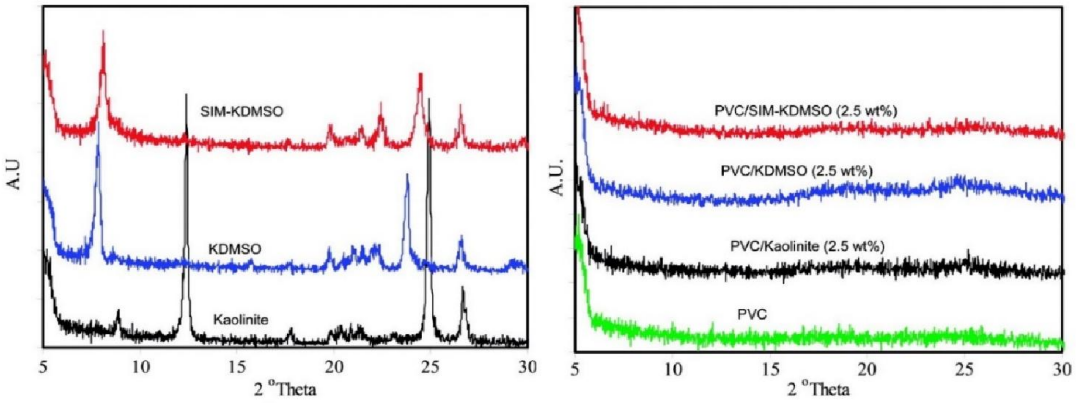

Figure 2-17 XRD patterns of natural and modified kaolinites, PVC and PVC/kaolinite nanocomposites (Turhan et al., 2010).

Turhan *et al.* (2010) prepared a PVC-kaolinite nanocomposite via a solution method; at first the interlamellar spaces were expanded by DMSO and then PVC chains were intercalated into the galleries resulting in a complete exfoliated structure (Figure 2-17).

Sun *et al.* (2010) obtained polyacrylonitrile/kaolinite nanocomposites by *in situ* polymerization of acrylonitrile in the presence of potassium acetate-kaolinite intercalate. Their results showed that kaolinite was well exfoliated and distributed in the form of particles in the range of 1-1000 nm. They found that molecular weight of the polymer was higher in the presence of clay, which was a result of increased interaction between the clay and polymer chains. It was also reported that the nanocomposites had higher thermal stability over the neat polymer.

Zhang *et al.* (2011) prepared kaolin modified polyester fibers with different concentration of the filler. They reported that tensile strength, modulus, and boiling water shrinkage of the kaolin

modified fibers were reduced with the increase of the kaolin content. However, moisture absorption was increased with the increase of the kaolin content They also investigated the non-isothermal crystallization of kaolin modified polyester and observed that the addition of kaolin increased both the melting and crystallization temperature (Zhang *et al*., 2011).

Anjana and George (2012) investigated the effect of nano kaolinite clay on polypropylene/high density polyethylene blends. They claimed to modify kaolinite through ion exchange reactions to make it more compatible with PP/HDPE blend. However, their assumption of replacing the inorganic ions by organic ones is basically wrong, since kaolinite has a very small CEC and technically there is no exchangeable ions in its structure at all. They also reported that addition of kaolinite enhanced the mechanical properties of blends.

George *et al.* (2013) reported that the incorporation of organo-modified kaolin clay (up to 2%) increased tensile strength and tensile modulus of PS/HDPE blends due to improved interfacial adhesion between the particles and the matrix.

2.6 Summary and problem identification

Many studies have been conducted to improve the barrier and mechanical properties of PET through blending with other polymers, coating, and developing multi-layer structures, however, these methods are usually non-economic and give rise to more recycling issues. Dispersing layered materials in a polymeric matrix in order to develop polymer-based nanocomposites has received great attention in recent years. According to the literature it seems that nanocomposites offer improved thermo-mechanical and barrier properties (even with low filler loading) when compared to conventional composite materials. Among the materials with a layered structure which are capable of being dispersed in polymeric matrix, smectite-type clays, such as hectorite, montmorillonite, and synthetic mica are the most investigated. However, no study on the effect of

other clay minerals such as kaolinite and talc on properties of polymers (and specifically PET) has been conducted.

The structure of kaolinite has been extensively studied for years; however, the limitations in dispersion of kaolinite particles, makes this filler less attractive for production of polymer nanocomposites. Only a few studies on intercalation of a variety of small molecules and few polymers such as PEO, PS, and PVC into the lamellar spacing of kaolinite have been reported. They mainly investigated the morphology of resulting composites while the effect of the filler on different properties of polymers has not been considered.

In summary, regarding the economical and environmental effect of polymeric packaging materials, there is a large demand for development of the reduced weight packaging systems. Relatively low barrier and mechanical properties are the main drawbacks of such packaging. Although numerous studies have focused on the barrier and mechanical performance of PET/nanoclay composites, little improvement has been reported. In this work, the influence of kaolin particles, as a nanofiller, on the performance of PET composite films will be investigated.

CHAPTER 3: OBJECTIVES

The main objective of this work is the "development of PET-kaolin nanocomposites with improved mechanical properties (at least 20% improvement) via melt-blending". Although polymeric materials with high mechanical properties are desirable in light weight packaging industry, it is of a great importance not to sacrifice other properties such as optical and barrier properties while improving mechanical properties.

Specific objectives:

- To develop a chemical and/or mechanical treatment method to facilitate the dispersion of kaolin particles during the final mixing process.
- To investigated the effect of chemical and mechanical treatment on morphology and properties of kaolin particles.
- To investigate the effect kaolin clay on the mechanical, barrier, optical and thermal properties of PET nanocomposites.
- To study the effect of secondary processing such as hot-stretching on final properties of PET-kaolin composites.

To meet this objective, two grades of kaolin clay (hydrous and calcined) are used and their level of dispersion is examined. Different chemical and/or mechanical treatments such as KAc, DMSO, and PEO are applied to improve the dispersion of the hydrous kaolin particles in the PET matrix. Subsequently, PET nanocomposite films containing kaolin clay are prepared in a twin screw extruder by cast extrusion technique and the effect of kaolin nanoparticles on the mechanical, barrier, optical and thermal properties of PET nanocomposites is investigated. The calcined kaolin nanoparticles were produced in a stirred media wet grinder prior to mixing with PET. The

application of different types of viscosity modifiers such as *Joncryl* chain extender and phenoxy resin to reduce the effect of degradation on final properties was examined as well. Moreover, the effect of secondary processing (hot stretching) on the properties of composites was studied.

CHAPTER 4: ORGANIZATION OF THE ARTICLES

The following four chapters contain the articles representing the results of this study:

The first article presented in chapter 5 is entitled "*Effect of dry grinding on chemically modified kaolin*". In this work kaolin particles were treated with potassium acetate (KAc) and dimethyl sulfoxide (DMSO) to increase basal spacing of the clay and the effect of dry grinding on the morphology and structure of the treated particles was investigated. The structure and morphological properties of particles are characterized by a combination of XRD, TGA, and FTIR techniques. The variations of particle size and surface characteristics were also investigated. This article has been submitted to *Applied Clay Science*.

The second article presented in chapter 6 is entitled "*Morphology and thermal properties of PET/kaolin nanocomposites*". Kaolin particles are initially treated with potassium acetate. Then, the treated particles are blended with PEO in an internal mixer and in the final step PEO-kaolin masterbatch is diluted with PET in a twin screw extruder. The morphology of the composite is studied by means of XRD, electron microscopy, and rheology. In the second part of this work the effect of kaolin particles on the nonisothermal crystallization of PET is thoroughly investigated.

This article has been submitted to *Polymer Composites*.

The morphology, optical, thermal, barrier and mechanical properties of the products are discussed in details

The third article presented in chapter 7 is entitled "*Preparation of Calcined-Kaolin Nanoparticles via Wet Grinding in Stirred Media Mill and Its Application in the PET Based Nanocomposites*". According to the rheological results of the second article, hydrous kaolin causes remarkable degradation in PET matrix, and hence it is replace with a calcined grade kaolin. Calcined kaolin nano-particles (gUlt) are produced via wet-grinding process in a stirred media mill and are

subsequently mixed with PET in twin and single screw extruders to produce PET-gUlt nanocomposite. The morphology, optical, thermal, barrier and mechanical properties of the products are discussed in details. This article has been submitted to *Polymer International.*

The fourth article presented in chapter 8 is entitled "*PET/Calcined kaolin composites: Effect of uniaxial stretching on the properties*". In this paper the influence of silane coupling agent, chain extension, and post extrusion uniaxial hot-stretching on the final properties of the composites is investigated. Composite films are produced and uniaxially stretched above glass transition temperature under controlled conditions. The morphology of the composites is observed by SEM. Rheological, mechanical and optical properties and oxygen transmission rate (OTR) of the composites before and after stretching are studied. This article has been submitted to *Polymer Engineering & Science.*

CHAPTER 5: ARTICLE 1: EFFECT OF DRY GRINDING ON CHEMICALLY MODIFIED KAOLIN

Khalil Shahverdi-Shahraki[1], Tamal Ghosh[2], Kamal Mahajan[2], Abdellah Ajji[1]*, Pierre J. Carreau[1]

[1] *CREPEC, Department of Chemical Engineering, École Polytechnique de Montréal, Canada*

[2] *PepsiCo Advanced Research - Beverage Packaging, Hawthorne, NY, USA*

Submitted to *Applied Clay Science*.

Abstract

The effect of dry grinding on the morphology and structure of the kaolin particles treated with potassium acetate (KAc) and dimethyl sulfoxide (DMSO) has been investigated. After treatment with KAc, the *d*-spacing of kaolin increased from 0.72 to 1.03, 1.30, and 1.38 nm due to the combined effects of humidity and orientation of KAc molecules**.** The *d*-spacing was increased to 1.13 nm in case of the DMSO treatment. A combination of XRD, TGA, and FT-IR showed that the crystalline structure of kaolin-DMSO and kaolin-KAc were significantly altered by grinding. The intensity of XRD diffraction peaks of ground samples was decreased due to the deterioration of the crystalline structure, and for longer grinding times those peaks almost disappeared. After grinding, the dehydroxylation temperature generally shifted to lower values and a smaller weight loss was observed. The variations of particle size and surface characteristics were also investigated.

Keywords: kaolin, potassium acetate, dimethyl sulfoxide, grinding

5.1 Introduction

Kaolin is a sort of clay primarily composed of kaolinite in association with small quantities of other minerals. It comprises an alumina octahedral sheet and a silica tetrahedral sheet that share a common plane of oxygen atoms [1,2] and a great deal of research has been focused on the methods to make the kaolin into a single layered mineral. However its unique structure creates large superposed dipoles and hydrogen bonds, and subsequently give rise to a large cohesive energy between the layers. As a consequence, only some limited organic molecules, such as alkali salts [3,4] and molecules with strong dipole interactions such as dimethyl sulfoxide [5,6] can intercalate the space between the layers of kaolin. The kaolin-DMSO precursor can be utilized to incorporate other organic molecules or polymers into the kaolin by substitution of the DMSO [7,8].

Intercalation process involves the insertion of organic molecules between the layers of kaolin, which normally increases the interlamellar distance (*d*-spacing). The inserted molecules should be capable of breaking the hydrogen bonds between the layers and of forming new hydrogen bonds with kaolin sheets.

Many researches have been conducted to investigate the effect of grinding on kaolin. It was claimed that milling of kaolin particles was associated with crystal structural deformation (fracturing along the basal planes) remarkable change in the specific surface area [9–11]. It was also reported that grinding, as mechanical treatment, can significantly alter the structure of kaolin and enhance the delamination process of kaolin [12] . Tsunematsu and Tateyama (1999) ground urea-kaolin intercalates in a mechanical mortar and observed that kaolin was easily delaminated. Frost et al. (2001) investigated the effect of grinding on the structure and morphology of kaolin. They found that after grinding, OH groups disappeared and were substituted by water molecules.

In spite of extended studies about kaolin and its intercalated complexes, the effect of mechanical treatment (grinding) on the structure and properties of chemically treated kaolin with KAc and DMSO has not been investigated in detail. This work was undertaken to study the structural and morphological changes that occur due to dry grinding of dimethyl sulfoxide and potassium acetate treated kaolin.

5.2 Experimental Procedure

5.2.1 Materials

A commercial kaolin, a hydrous aluminosilicate, with a density of 2.58 g/cm3 at 25°C was supplied by BASF Corporation. More than ninety percent of particles had a diameter smaller than 2 μm (D_{90}

= 2 μm). Dimethyl sulfoxide (denoted hereafter as DMSO) and potassium acetate (denoted hereafter as KAc) were purchased from Sigma-Aldrich and used as received.

5.2.2 Characterization and Testing

A Philips X'pert diffractometer (CuKα radiation, λ = 1.54056 Å), operating at a voltage of 50 kV and current of 40 mA, was used for wide angle X-ray diffraction (WAXD) measurements. SEM microphotographs of the samples were obtained using a Hitachi S4700 instrument under an acceleration voltage of 2 kV. A thermogravimeter TGA500 TA Instrument was used to study the thermal decomposition. About 10 mg of the samples were heated at 10 °C/min from 30 to 700 °C under nitrogen atmosphere. The infrared spectra in the region 400-4000 cm–1 were obtained using a Spectrum 65 FT-IR Spectrometer (Perkin Elmer) with a resolution of 4 cm^{-1}. Particle size measurements were performed via a Partica LA-950 laser diffraction particle size distribution analyzer (HORIBA Instruments Inc.). The surface area of the samples was measured via an Autosorb-1 surface area analyzer (Quantachrome Instruments) using nitrogen gas as an adsorbate. The samples were outgassed at 150°C for 3 h before the measurements.

5.2.3 Sample Preparation

To obtain the kaolin-DMSO precursor, 70 g kaolin was added to a mixture of 630 mL DMSO and 70 mL distilled water and the suspension was stirred at 70 °C for 96 h. The treated particles were recovered by centrifugation at 5000 rpm for 5 min and dried in a vacuum oven at 70°C for 24 h. The kaolin was also intercalated with KAc via a solution method in which 60 g kaolin was mixed with a KAc solution (50 g KAc dissolved in 120 g water) and stirred at room temperature for 48 h. The particles were dried in a vacuum oven *at 80* °C for 24 h. Kaolin samples were ground using a Shatterbox Laboratory Mill (Model 8510, SPEX SamplePrep, LLC).

5.3 Results and Discussion

5.3.1 X-ray Diffraction

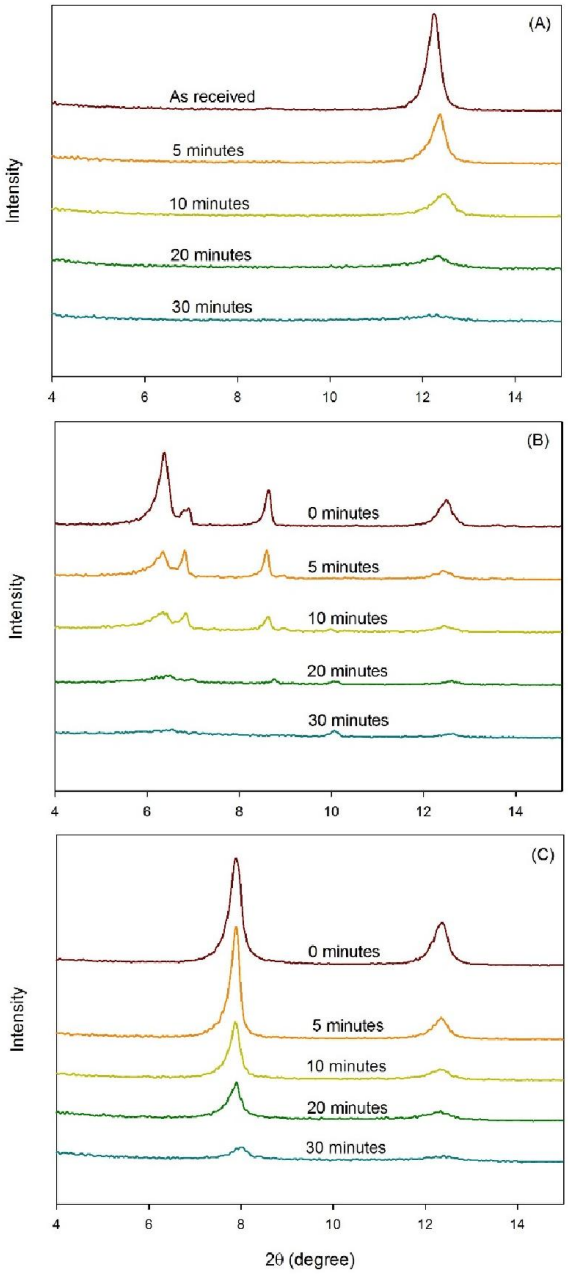

Figure 5-1 XRD patterns of pristine kaolin (A), kaolin KAc (B), and kaolin DMSO (C) as functions of grinding time.

The X-ray diffraction patterns of kaolin samples are presented in Figure 5-1. The characteristic peak of pristine kaolin was at 2θ=12.46° corresponding to *d*-spacing of 0.71 nm. After treatment

with KAc, new peaks appeared at 2θ of 8.56°, 6.79°, and 6.40° corresponding to *d*-spacings of 1.03, 1.30, and 1.38 nm, respectively, while for samples treated with DMSO only one new peak was detected at 2θ of 7.82° (1.13 nm).

Grinding markedly affected the crystalline structure of kaolin regardless of chemical treatments. For samples modified with DMSO or KAc the intensity of the peaks in the XRD patterns decreased with grinding time and after 30 min a broad peak with a very small intensity remained. This phenomenon was assigned to the degradation of the crystalline structure of kaolin. Intense mechanical energy, applied by grinding, lead to the rupture of alumina and silica layers, and therefore, the dimension of particles along the axis perpendicular to the layers becomes smaller.

It is notable that for all the samples, regardless of whether they were modified with DMSO or KAc, the intensity of the characteristic peak at 0.72 nm decreased after grinding but it did not totally disappear. This indicates that, intercalation was not fully achieved and even after chemical treatment, a part of kaolin particles retained their initial structure.

5.3.2 Thermogravimetric Analysis

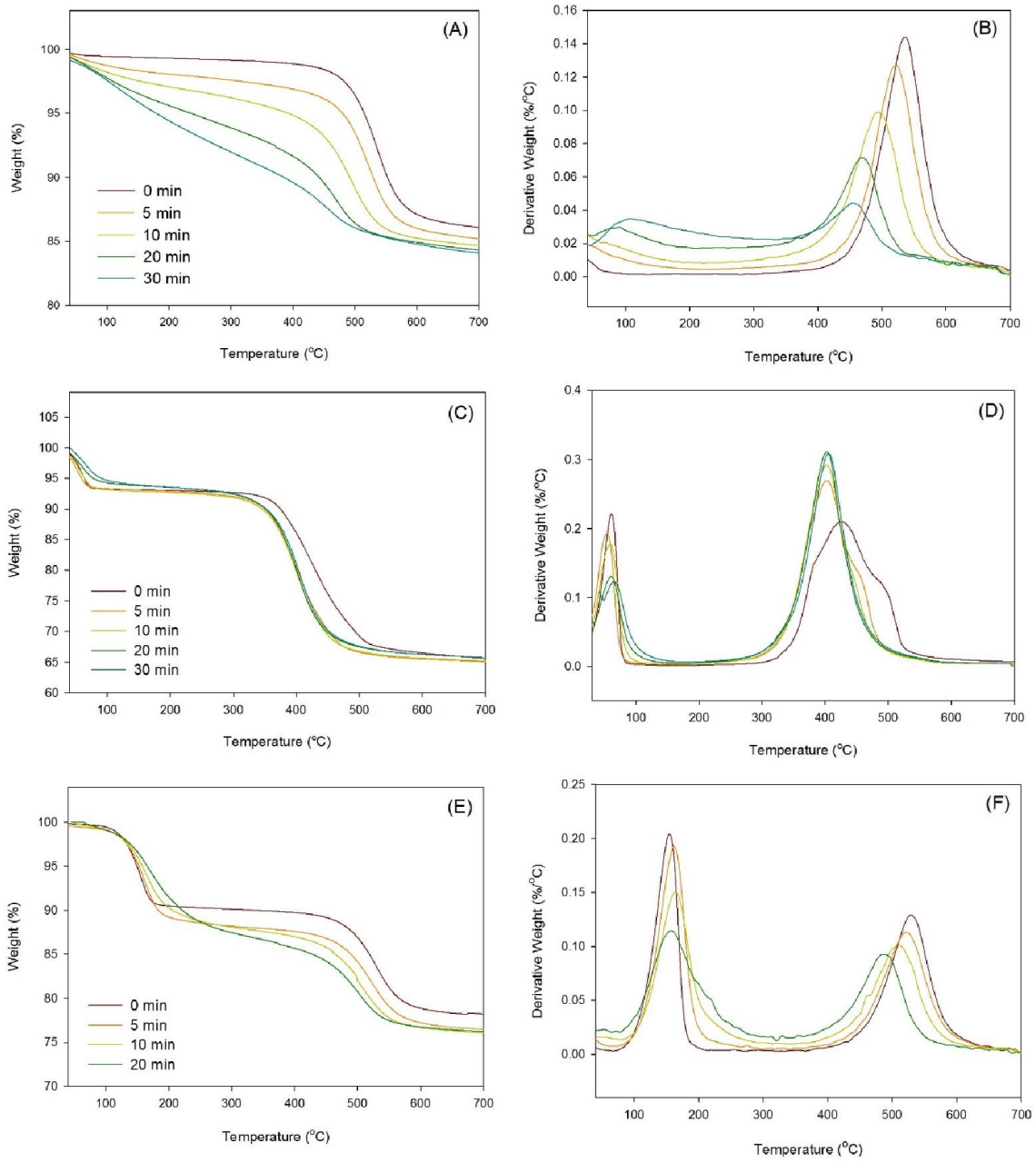

Figure 5-2 TGA thermograms of pristine kaolin (A, B), kaolin KAc (C, D), kaolin DMSO (E, F) as functions of grinding tim.

Figure 5-2 presents thermogravimetry results of kaolin samples ground for different periods of time. The milling process (Figure 5-2B) had two main impacts on the kaolin particles: the first one was the appearance of a new peak around 100°C, associated with the evaporation of water

molecules existing in the structure or adsorbed on the surface, and the second one was the shift of the dehydroxylation temperature to lower values. Not only the position of the dehydroxylation peak changed but its intensity decreased as well. These observations were in agreement with results reported elsewhere [9].

Upon treatment of kaolin particles with KAc, two weight losses were observed in the thermogram (Figure 5-2D). The first one at 60°C was associated with adsorbed water. The second loss was actually composed of three overlapping components at 380, 430, and 495°C: the loss of water in the interlayer of kaolinite (380°C), the removal of surface hydroxyls which are hydrogen-bonded to the intercalating acetate ions (430°C), and the removal of non-reacted hydroxyls (495°C). The liberation of water due to the dehydroxylation was confirmed by analysis of evolved gas at different temperatures [15,16]. Compared to pristine kaolin, the dehydroxylation temperature of KAc-treated samples was shifted from 540°C to lower temperatures. This could be due to the weakened hydrogen bonds after the chemical treatment.

After grinding, the tendency of kaolin-KAc complex to adsorb the moisture subsided. Grinding also reduced the dehydroxylation temperature of kaolin-KAc complex compared to that of the unground sample. By increasing the grinding time, the position of the dehydroxylation peak did not change any more, while its intensity slightly decreased. For the ground samples, the weight loss at 445°C, attributed to the non-reacted hydroxyls, become smaller and eventually disappeared due to the lack of non-reacted hydroxyls in the complex. It suggested that grinding improved the intercalation of KAc into kaolin layers. Once the kaolin particles were intercalated with KAc, grinding had no significant effects on the bonding energy of hydroxyl groups, and therefore, the dehydroxylation temperature did not change. However, the number of OH groups was slightly

reduced due to the partial dehydroxylation (induced by grinding), which resulted in less weight loss.

The TGA diagrams of the kaolin-DMSO intercalate are shown in Figure 5-2E and F. Heating the unground kaolin-DMSO sample caused two intense mass losses around 150°C and 520°C with a weight loss of 10% and 12%, respectively. The first peak was due to the removal and decomposition of DMSO in the interlayer spaces and the second one was attributed to the dehydroxylation of kaolin layers [17,18]. After grinding, the dehydroxylation peak was gradually shifted to lower temperatures. The thermal behavior of ground kaolin-DMSO samples was somehow similar to that of untreated kaolin, except the first loss at 150°C. It suggested that after the removal of DMSO molecules from the interlayer spaces, the thermal behavior of the residuals was basically similar to that of untreated kaolin.

5.3.3 FT-IR analysis

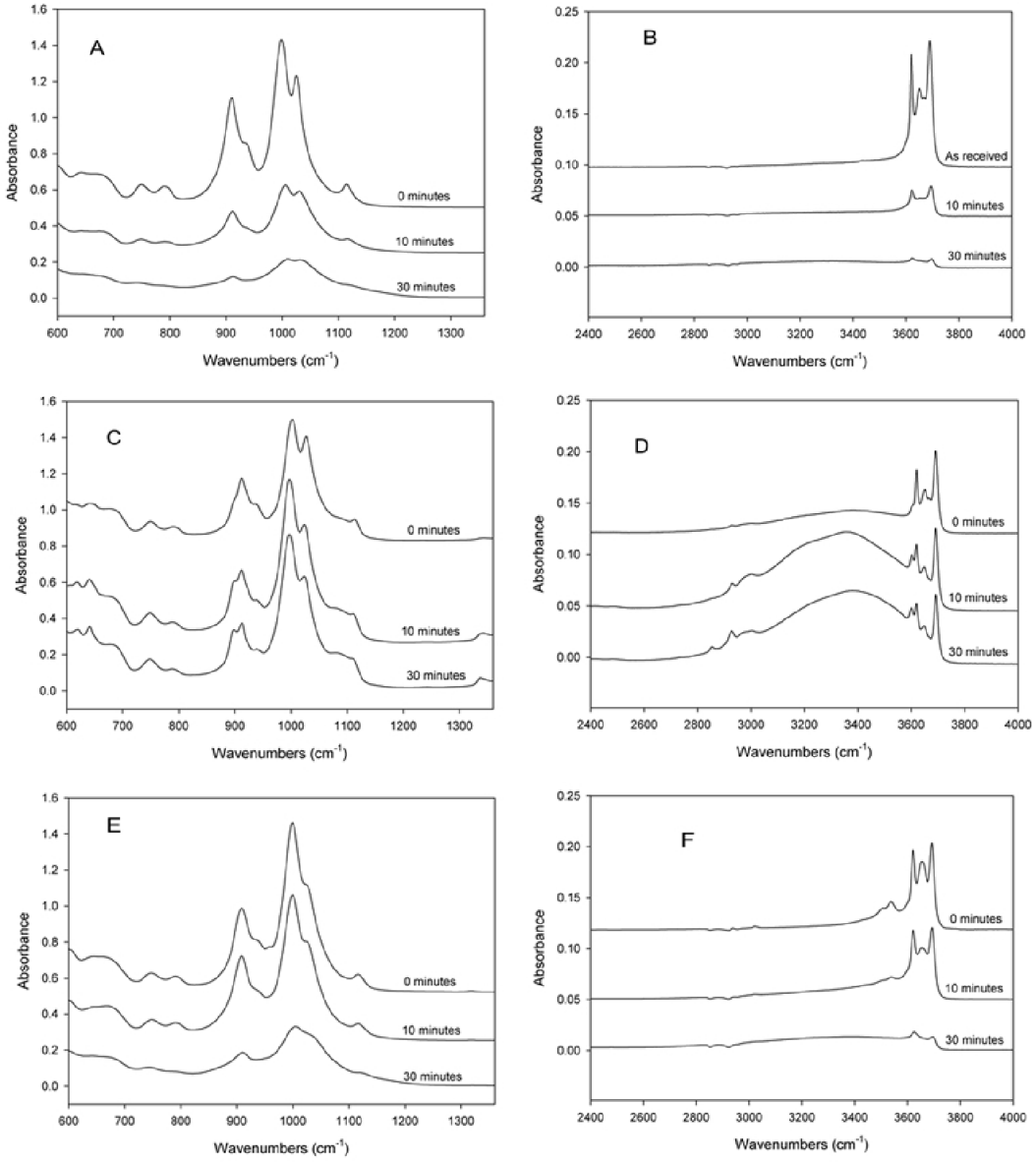

Figure 5-3 FT-IR spectra of the low and high frequency region for the pristine kaolin (A, B), kaolin-KAc (C, D), and kaolin-DMSO (E, F) as functions of grinding time.

Table 5-1 Band component analysis of FT-IR spectra in the high frequency region.

	Grinding time		υ_1	υ_2	υ_3	υ_4	υ_5	υ_6	υ_7
kaolin	0 min	Center (cm^{-1})	-	-	-	3620	3650	3668	3692
		Intensity	-	-	-	0.085	0.067	0.052	0.116
	10 min	Center (cm^{-1})	-	-	-	3622	3653	-	3692
		Intensity	-	-	-	0.020	0.015	-	0.025
	30 min	Center (cm^{-1})	-	-	-	3621	3653	-	3693
		Intensity	-	-	-	0.006	0.004	-	0.006
kaolin-KAc	0 min	Center (cm^{-1})	-	-	3600	3620	3649	3668	3691
		Intensity	-	-	0.010	0.045	0.032	0.023	0.072
	10 min	Center (cm^{-1})	-	-	3600	3620	3650	-	3692
		Intensity	-	-	0.018	0.030	0.017	-	0.061
	30 min	Center (cm^{-1})	-	-	3600	3620	3651	-	3692
		Intensity	-	-	0.018	0.024	0.015	-	0.051
kaolin-DMSO	0 min	Center (cm^{-1})	3505	3544	-	3620	3656	-	3692
		Intensity	0.014	0.019	-	0.052	0.054	-	0.065
	10 min	Center (cm^{-1})	3502	3551	-	3618	3653	-	3690
		Intensity	0.012	0.014	-	0.048	0.037	-	0.054
	30 min	Center (cm^{-1})	3502	3553	-	3617	3653	-	3692
		Intensity	0.005	0.007	-	0.032	0.024	-	0.028

Table 5-2 Band component analysis of FTIR spectra in the low frequency region

	Grinding time		υ_8	υ_9	υ_{10}	υ_{11}	υ_{12}	υ_{13}	υ_{14}	υ_{15}	υ_{16}	υ_{17}
kaolin	0 min	Center (cm^{-1})	751	790	-	913	940	-	998	1027	-	1112
		Intensity	0.042	0.044	-	0.535	0.288	-	0.855	0.635	-	0.110
	10 min	Center (cm^{-1})	752	790	-	912	940	-	998	1028	-	1111
		Intensity	0.016	0.012	-	0.172	0.088	-	0.302	0.274	-	0.075
	30 min	Center (cm^{-1})	751	791	-	912	-	-	1000	1028	-	1112
		Intensity	0.010	0.002	-	0.074	-	-	0.169	0.169	-	0.053
kaolin-KAc	0 min	Center (cm^{-1})	750	790	897	913	941	-	1000	1028	1080	1112
		Intensity	0.047	0.026	0.142	0.269	0.164	-	0.633	0.537	0.123	0.103
	10 min	Center (cm^{-1})	750	790	897	913	941	-	998	1027	1080	1112
		Intensity	0.058	0.019	0.212	0.275	0.181	-	0.868	0.614	0.177	0.129
	30 min	Center (cm^{-1})	750	789	896	913	942	-	998	1026	1079	1111
		Intensity	0.058	0.019	0.203	0.243	0.178	-	0.831	0.589	0.196	0.142
kaolin-DMSO	0 min	Center (cm^{-1})	750	790	-	906	943	962	998	1027	-	1116
		Intensity	0.038	0.030	-	0.412	0.198	0.16	0.864	0.521	-	0.090
	10 min	Center (cm^{-1})	750	791	-	905	942	-	997	1028	-	1116
		Intensity	0.035	0.025	-	0.366	0.176	-	0.658	0.389	-	0.087
	30 min	Center (cm^{-1})	750	790	-	906	943	-	998	1028	-	1116
		Intensity	0.013	0.015	-	0.116	0.080	-	0.243	0.199	-	0.067

Figure 5.3 presents the infrared spectra of the pristine and chemically treated kaolin as functions of grinding time. The results of spectral band deconvolution analysis are presented in Table 5-1 and 5-2. In case of pristine kaolin, the intensity of all hydroxyl stretching bands decreased by grinding and simultaneously a very broad band emerges around 3300 cm^{-1} assigned to water molecules either formed in the interlayer spaces (as confirmed by TGA analysis) or adsorbed on the surface of the particles.

For kaolin-KAc, as shown in Figure 5-3C and D, in addition to the characteristic absorptions bands of kaolin at 3620 (υ_4), 3650 (υ_5), 3668 (υ_6), and 3692 cm^{-1} (υ_7), a new band appeared at 3600 cm^{-1} (υ_3) due to the new hydrogen bonds formed between the inner-surface hydroxyls and the acetate ions [19,20]. The broad band centered at 3350 cm^{-1} was ascribed to the hydroxyl stretching vibrations of water molecules coordinated to either the intercalated KAc molecules or the surface of the particles. After grinding, the increase in the ratio of the intensity of the band at 3600 cm^{-1} (υ_3) to that of 3620 cm^{-1} (υ_4) indicated that the absorbance at 3600 cm^{-1} become more intense with grinding. This confirmed that grinding promoted the intercalation of kaolin particles. Comparing the hydroxyl stretching region of pristine kaolin and kaolin-KAc after grinding, the reduction in the intensity of the bands was more significant in the case of pristine kaolin. This proved that, even after grinding, a large quantity of inner and inner-surface hydroxyls existed in the structure of kaolin-KAc whereas the pristine kaolin was almost dehydroxylated. The inner-surface hydroxyls engendered two different bands in the hydroxyl deformation region, one at 897 cm^{-1} (υ_{10}) assigned to the OH groups hydrogen bonded to the adsorbed water or acetate ions, and another band at 941 cm^{-1} (υ_{12}) attributed to the OH groups hydrogen bonded to basal oxygen atoms of the adjacent silica layer. The intensity of peak at 897 cm^{-1} increased with grinding time as a result of promoted hydrogen bonds between inner-surface hydroxyls and water molecules. However, the band at

941 cm^{-1} lost its intensity due to the lack of hydrogen bonding to the adjacent layer. Furthermore, the sharp band at 913 cm^{-1} (υ_{11}), attributed to the deformation of the inner hydroxyls, did not undergo remarkable changes because inner hydroxyls were somehow shielded with the alumina layer preventing them from interacting with water molecules or acetate ions.

The infrared patterns for the kaolin-DMSO are presented in Figure 5-3E and F. The two new bands observed at 3544 (υ_2) and 3505 cm^{-1} (υ_1) in the hydroxyl stretching region of kaolin-DMSO (Figure 5-3F) were attributed to the inner hydroxyls forming hydrogen bonding with the sulphonyl oxygens of DMSO. In the low frequency region (Figure 5-3E), the interaction of DMSO molecules with silicate layer affected the Si-O vibration modes so that the Si-O stretching band moved from 1112 cm^{-1} (υ_{17}) to 1116 cm^{-1} and the intensity of in-plane vibration band of Si-O-Si at 1027 cm^{-1} (υ_{15}) significantly decreased.

The infrared spectrum of kaolin-DMSO after grinding was almost similar to that of pristine kaolin. A drastic reduction in the intensity of all absorption bands and the appearance of a broad band around 3300 cm^{-1}, which confirmed the existence of water molecule in the structure or on the surface of the particles, were readily observable. The severe reduction in the absorbance peaks at 3553 (υ_2) and 3502 cm^{-1} (υ_1), corresponding to the interaction of DMSO with kaolin, suggested that the majority of DMSO molecules were expelled from the structure due to the grinding process.

Particle Size and Surface Area Characteristics

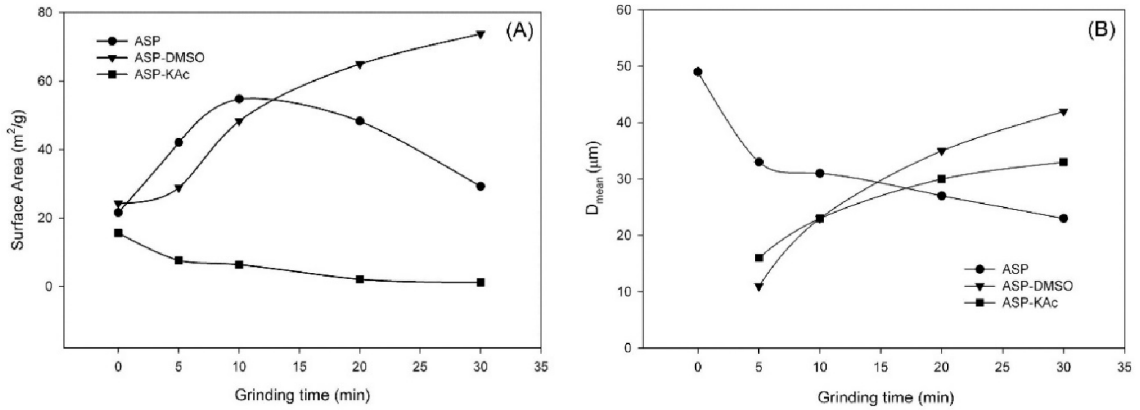

Figure 5-4 BET specific surface area (A) and Mean particle diameter (B) of pristine kaolin, kaolin-KAc, and kaolin-DMSO as functions of grinding time.

Graphs of specific surface area and mean particle size of kaolin samples as a function of grinding time is shown in Figure 5-4. Grinding had a significant effect on the specific surface area of the pristine and chemically treated kaolin, as measured by BET. In the early minutes of grinding, the surface area of pristine clay increased due to the reduced particle size and increased porosity; however, it started to decrease after 10 min. For the as-received kaolin, the mean particle size decreased with grinding time; however, the rate of decrease was higher in the early stages of grinding. This is better illustrated by Figure 5-4B, which reports the diameter of the particles as a function of time. Therefore, in the beginning, the effect of particle size was predominant but after 10 min, the porosity was governing. This led to lower values of the surface area. For both kaolin-DMSO and kaolin-KAc, due to the re-agglomeration of the particles, the mean particle size increased with grinding time (Figure 5-4B). During the grinding process, the surface area of kaolin-DMSO was enhanced (Figure 5-4A), however, for kaolin-KAc the curve shows a downward trend with time after reaching a maximum. The kaolin particles modified by the hygroscopic potassium acetate tend to absorb a large quantity of moisture. This phenomenon might affect the porosity of the particles, which explains the decrease of the surface area.

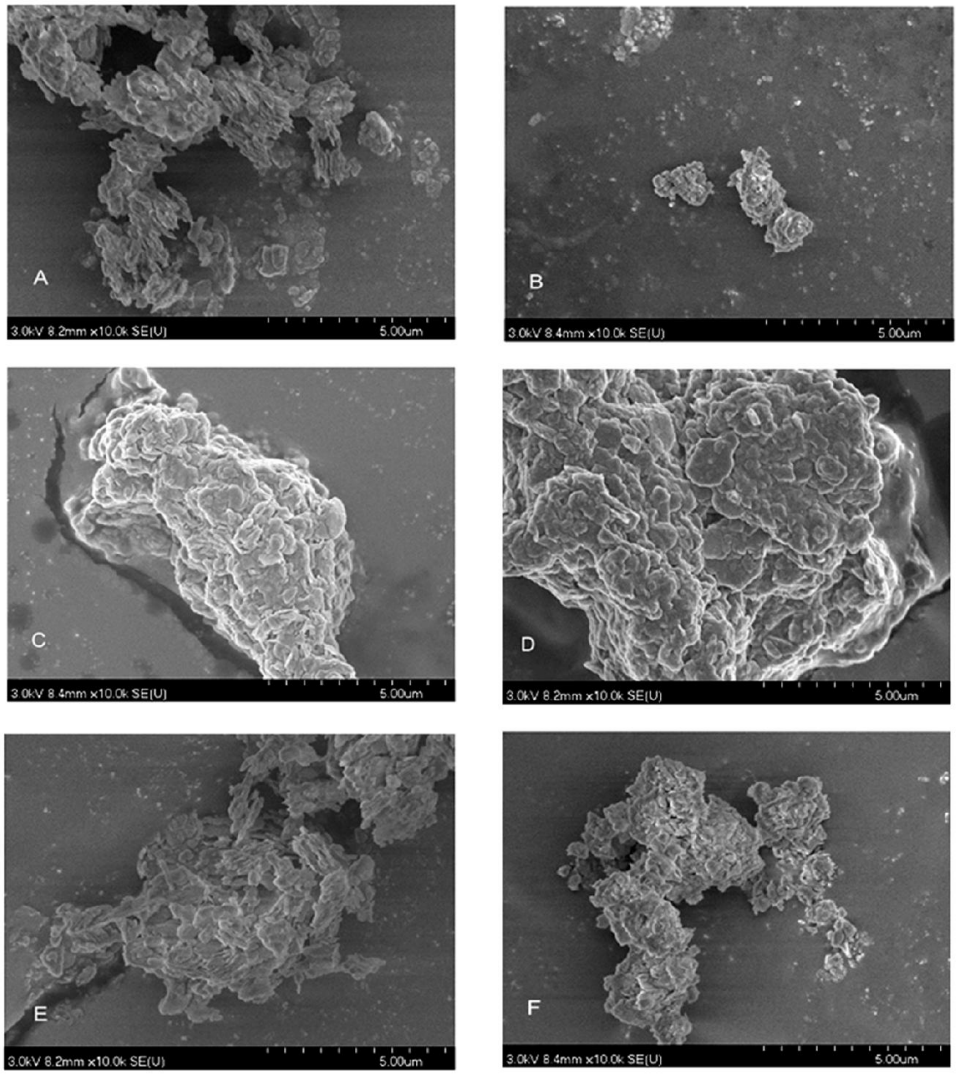

Figure 5-5 SEM micrographs of kaolin (A), kaolin ground for 30 min (B), kaolin KAc (C), kaolin KAc ground for 30 min (D), kaolin DMSO (E), kaolin DMSO ground for 30 min (F).

The variation of particle size with grinding, as obtained using the particle size analyzer, was confirmed by scanning electron microscopy (SEM) and the micrographs are displayed in Figure 5-5. After grinding, the stacks or flakes of pristine kaolin are broken to smaller particles. In cases of kaolin-DMSO and kaolin-KAc the increase of particles size after grinding is clearly shown. The porous texture of pristine kaolin and kaolin-DMSO, compared to that of KAc-treated sample, was readily observed in these images as well.

5.4 Conclusion

Kaolin was intercalated with potassium acetate and dimethyl sulfoxide. The result obtained in this study showed that the grinding process changed the crystalline structure of kaolin and strongly affected the size of the particles. Due to the conversion of hydroxyl groups to water, the weight loss caused by water evaporation during TGA experiments increased with grinding time, while the weight loss associated with the dehydroxylation decreased. It was also noted that dehydroxylation temperature was shifted to lower values after grinding. The data suggested that only the inner-surface hydroxyls are able to interact with the intercalating molecules and the inner-hydroxyls did not undergo significant changes. The grinding process increased the particle size of the kaolin-KAc and kaolin-DMSO samples; however, it decreased that of pristine kaolin. The results finally indicate that the alteration of kaolin structure could fully occur in a relatively short time (30 min), whereas previous works reported a much longer time (many hours) to observe some significant effects.

5.5 Acknowledgements

The authors would like to thank PepsiCo for support of this work.

5.6 References

[1] Huertas FJ, Fiore S, Huertas F, Linares J. Experimental study of the hydrothermal formation of kaolinite. Chem Geol 1999;156:171–90.

[2] Miranda-Trevino JC, Coles CA. Kaolinite properties, structure and influence of metal retention on pH. Appl Clay Sci 2003;23:133–9.

[3] Frost RL, Kristof J, Horvath E, Kloprogge JT. Modification of Kaolinite Surfaces through Intercalation with Potassium Acetate, II. J Colloid Interface Sci 1999;214:109–17.

[4] Frost RL, Kristof J, Mako E, Kloprogge JT. Modification of the Hydroxyl Surface in Potassium-Acetate-Intercalated Kaolinite between 25 and 300° C. Langmuir 2000;16:7421–8.

[5] Vempati RK, Mollah MYA, Reddy GR, Cocke DL, Lauer H V. Intercalation of kaolinite under hydrothermal conditions. J Mater Sci 1996;31:1255–9.

[6] Martens WN, Frost RL, Kristof J, Horvath E, Martens Ray L.; Kristof, Janos; Horvath, Erzsebet WN. F. Modification of Kaolinite Surfaces through Intercalation with Deuterated Dimethylsulfoxide. J Phys Chem B 2002;106:4162–71.

[7] Letaief S, Detellier C. Nanohybrid materials from the intercalation of imidazolium ionic liquids in kaolinite. J Mater Chem 2007;17:1476–84.

[8] Letaief S, Detellier C. Reactivity of kaolinite in ionic liquids: preparation and characterization of a 1-ethyl pyridinium chloride–kaolinite intercalate. J Mater Chem 2005;15.

[9] Sánchez-Soto PJ, del Carmen Jiménez de Haro M, Pérez-Maqueda LA, Varona I, Pérez-Rodríguez JL. Effects of Dry Grinding on the Structural Changes of Kaolinite Powders. J Am Ceram Soc 2000;83:1649–57.

[10] Frost RL, Horváth E, Makó É, Kristóf J. Modification of low- and high-defect kaolinite surfaces: implications for kaolinite mineral processing. J Colloid Interface Sci 2004;270:337–46.

[11] Suraj G, Iyer CSP, Rugmini S, Lalithambika M. The effect of micronization on kaolinites and their sorption behaviour. Appl Clay Sci 1997;12:111–30.

[12] Frost RL, Makó É, Kristóf J, Horváth E, Kloprogge JT. Modification of Kaolinite Surfaces by Mechanochemical Treatment. Langmuir 2001;17:4731–8.

[13] Tsunematsu K, Tateyama H. Delamination of Urea-Kaolinite Complex by Using Intercalation Procedures. J Am Ceram Soc 1999;82:1589–91.

[14] Frost RL, Mako E, Kristof J, Horváth E, Kloprogge JT. Mechanochemical treatment of kaolinite. J Colloid Interface Sci 2001;239:458–66.

[15] Gabor M, Toth M, Kristof J, Komaromi-Hiller G. Thermal behavior and decomposition of intercalated kaolinite. Clays Clay Miner 1995;43:223–8.

[16] Kristóf J, Frost RL, Horváth E, Kocsis L, Inczédy J. Thermoanalytical Investigations on Intercalated Kaolinites. J Therm Anal Calorim 1998;53:467–75.

[17] Letaief S, Detellier C. Application of thermal analysis for the characterisation of intercalated and grafted organo-kaolinite nanohybrid materials. J Therm Anal Calorim 2011;104:831–9.

[18] Franco F, Ruiz Cruz M. Thermal behaviour of dickite-dimethylsulfoxide intercalation complex. J Therm Anal Calorim 2003;73:151–65.

[19] Kohn SC, Brooker RA, Frost DJ, Slesinger AE, Wood BJ. Ordering of hydroxyl defects in hydrous wadsleyite (β-Mg2SiO4). Am Mineral 2002;87:293–301.

[20] Ruan HD, Frost RL, Kloprogge JT, Duong L. Infrared spectroscopy of goethite dehydroxylation. II. Effect of aluminium substitution on the behaviour of hydroxyl units. Spectrochim Acta Part A Mol Biomol Spectrosc 2002;58:479–91.

CHAPTER 6: ARTICLE 2: MORPHOLOGY AND THERMAL PROPERTIES OF POLY(ETHYLENE TEREPHTHALATE)-MODIFIED KAOLIN NANOCOMPOSITES

Khalil Shahverdi-Shahraki[1], Tamal Ghosh[2], Kamal Mahajan[2], Abdellah Ajji[1]*, Pierre J. Carreau[1]

[1] *CREPEC, Department of Chemical Engineering, École Polytechnique de Montréal, Canada*

[2] *PepsiCo Advanced Research - Beverage Packaging, Hawthorne, NY, USA*

Parts of this work have been presented at the 29th *International Conference of The Polymer Processing Society* (July 2013)

Submitted to *Polymer Composites.*

Abstract

Kaolin particles were dispersed in a PET matrix using a displacement procedure in which kaolin was initially treated with potassium acetate and, subsequently, melt-blended with PEO and PET. The disappearance of characteristic peaks in XRD patterns of chemically treated particles revealed that the crystalline form and layered structure of kaolin particles were mainly destroyed. Electron microscopy techniques (SEM, TEM) showed that the thickness of dispersed particles were generally in the range of 10-100 nm. It was also observed that the dispersion level of the chemically treated kaolin was much better than that of "as received" kaolin particles. Rheological studies showed the formation of a network-like structure in samples containing the chemically treated kaolin as a result of improved dispersion of particles. It was also observed that both the kaolin particles and modifiers could accelerate the degradation process and lower the molecular weight of the PET. The introduction of kaolin particles remarkably shifted the crystallization and melting temperatures of PET to lower temperatures. It was observed that the incorporation of a chain extender significantly restricted the crystallization process. The Avrami-Jeziorny analysis confirmed the alteration of the crystalline structure of the filled polymer. Based on TGA thermograms the decomposition temperature of PET-kaolin composites was slightly lower than that of the neat PET.

Keywords: PET, Kaolin, Nanocomposite, Morphology, Crystallinity.

6.1 Introduction

Nanocomposites are a new class of engineering materials, which have found many applications in various industrial fields such as automotive, construction, and packaging due to their excellent properties, low cost and weight. Based on the fact that polymeric materials suffer from lack of thermal stability and low modulus in comparison with other engineering materials such as metals,

different type of fillers have been incorporated to polymer matrices to overcome these shortcomings. The size of these traditional fillers are usually in the range of micrometers [1]. With the development of nanoparticles, many researchers have considered using them as nanofillers to reinforce polymer composites. Nanoparticles can provide a large contact area between different phases in the composite, which may result in a significant reinforcement effect on polymers [2–10].

Kaolin is a layered aluminosilicate in which each layer in the structure comprises two sublayers: an alumina octahedral sheet and a silica tetrahedral sheet that share a common plane of oxygen atoms. Regarding the asymmetric structure of kaolin layers, which creates large superposed dipoles, and hydrogen bonds between oxygen atoms on one side of each layer and hydroxyl groups on the other side of adjacent layers, there will be a large cohesive energy between the layers [11]. As a consequence of this cohesive energy, only some limited organic molecules, such as potassium acetate and dimethyl sulfoxide can intercalate the space between the layers of kaolin [12–20]. Kaolin is extensively used for many industrial applications such as paper, ceramics, paint, rubber, and plastics industries.

Recently a few investigations on the incorporation of organic modified kaolin in polymers have been reported [21–25]. Komori *et al.* [26,27] intercalated poly(vinyl pyrrolidone) into kaolin interlayer spaces at room temperature via a solution method. Liu and coworkers [28] reported the intercalation of poly(styrene/maleic anhydride) into kaolin via *in situ* polymerization using kaolin-DMSO (dimethyl sulfoxide) as a starting material. They achieved a complete exfoliated structure when the kaolin content was in the range of 1-10 wt%. Turhan *et al.* [29] prepared a PVC-kaolin nanocomposite via a solution method; at first the interlamellar spaces were expanded by DMSO and then PVC chains were intercalated into the galleries resulting in a complete exfoliated structure

.Polystyrene was intercalated into kaolin using kaolin-DMSO intermediate [30]. Tunney and coworkers [31] prepared poly(ethylene glycol)/kaolin intercalates using kaolin-dimethyl sulfoxide (kao-DMSO) and reported an expansion in interlayer galleries of kaolin. Itagaki *et al*. [32] prepared kaolin-nylon 6 composites by melt mixing via a twin-screw extruder with an intercalated compound (prepared by the polymerization of 6-aminohexanoic acid (AHA). The results indicated that mechanical properties had been improved.

Numerous studies have focused on the development and on the properties of PET-MMT composites; however, very few reports can be found in the literature about the dispersion of other types of clay mineral in a PET matrix. In this work, the fabrication of PET/kaolin nanocomposite is reported for the first time. The influence of chemical treatment of kaolin particles with KAc and PEO on the morphology and crystallization behavior of PET/kaolin nanocomposites is investigated. The crystallization kinetics was studied in nonisothermal conditions in order to determine the effect of the treated particles on the nucleation and growth of crystals in the crystallization of PET.

6.2 Experimental

6.2.1 Materials

A bottle grade polyethylene terephthalate (PET) resin Laser+® 7000 was supplied by DAK Americas LLC. It had an intrinsic viscosity of 0.84 dL/g, a melting point of 242 °C and 35% crystallinity.

A commercial grade kaolin (denoted hereafter as kao), hydrous aluminosilicate, with a density of 2.58 g/cm^3 at 25°C (particle size: D_{90} = 2 μm) was supplied by BASF Corporation. Poly(ethylene oxide), PEO, with a molecular weight of 100 000 g/mol and potassium acetate (KAc) were

purchased from Sigma-Aldrich and used as received. A 30 wt% masterbatch of PET chain extender (denoted hereafter as ch) supplied by Polyvel Inc. was used to raise the intrinsic viscosity and increase the melt strength of the PET resin during the melt blending. This product has full FDA compliance for food contact applications. It contains Joncryl® ADR 4368-F, which is a styrene-acrylic multifunctional epoxy-based chain extender with a molecular weight (M_w) of 6800 g/mol.

6.2.2 Characterization and Testing

A Philips X'Pert diffractometer (CuK_α radiation, λ=1.54056 A°), operating at a voltage of 50 kV and current of 40 mA, was used for wide angle X-ray diffraction (WAXD) measurements. The scanning rate was 0.02°/s and the 2θ ranged from 2° to 15°. SEM microphotographs of the samples were obtained using a Hitachi S4700 instrument with a cold field emission gun under an acceleration voltage of 2 kV. A JOEL JEM-2100F transmission electron microscopy operating at 200 kV was used to evaluate the tactoid size, presence of agglomerates, and to fully characterize the morphology of the filler. The samples were microtomed into approximately 50-80 nm thick slices using an Ultracut FC microtome (Leica, Germany) with a diamond knife. Rheological measurements were conducted using a parallel plate stress-controlled rheometer (Gemini of Malvern) with a gap size of 1 mm and a plate diameter of 25 mm. Time and frequency sweeps in small-amplitude oscillatory shear were carried out at 270ºC. The rheometer was equipped with a convection oven to control the temperature. In order to prevent the thermal degradation all the measurements were performed under nitrogen atmosphere in the linear viscoelastic regime. Melting and crystallization characteristics of the samples were determined by differential scanning calorimetry (DSC) using a DSCQ1000 TA Instrument under helium atmosphere. A thermogravimeter TGA500 TA Instrument was used to study the thermal properties. About 10 mg of the samples were heated at 10 °C/min from 30 to 700 °C under nitrogen atmosphere.

6.2.3 Sample preparation

A stepwise procedure was followed in order to intercalate the PET resin into the kaolin clay. In the first step kaolin was intercalated by KAc, which is capable of penetrating between the layers and expanding the structure of kaolin. This was the kao-KAc precursor. In the next step this precursor was blended with the PEO and finally intercalation of PET chains proceeded by displacing of KAc and PEO molecules.

The kaolin was intercalated with KAc via a solution method in which 60 g kaolin was mixed with a KAc solution (50 g KAc dissolved in 120 g water) and stirred at room temperature for 48 h. The treated particles were separated from the mixture by centrifugation at 5000 rpm for 5 min and dried in a vacuum oven at 70°C for 24 h.

A PEO-kaolin masterbatch (denoted hereafter as kao-KAc-PEO) was prepared in a Brabender internal mixer. Treated kaolin and PEO were fed into the chamber at a weight ratio of 0.33 and the mixing process was done at 90°C for 10 min with a rotating speed of 100 rpm.

PET granules were ground in liquid nitrogen to obtain a fine powder of PET. The PET powder was manually mixed with a kaolin powder (or ground PEO masterbatch) for a few minutes and then the mixture was melt-blended by extrusion using an 18 mm diameter twin screw extruder (LEISTRITZ Extruder Corp., L/D=40) to obtain a masterbatch containing 20 wt% kaolin particles. The temperature profile was set in the range of 250-275°C and the screw rotating speed was 150 rpm. The masterbatch was eventually diluted with the neat PET to yield the final composites containing 1 wt% filler loadings; the chain extender (1 wt%) was added to the composites at this stage if needed. Since the presence of ppm amounts of moisture in PET during the melt compounding leads to hydrolysis reactions, all the materials were well dried in a vacuum oven at 110°C for 24 h before being processed.

6.3 Results and discussion

6.3.1 X-Ray diffraction results

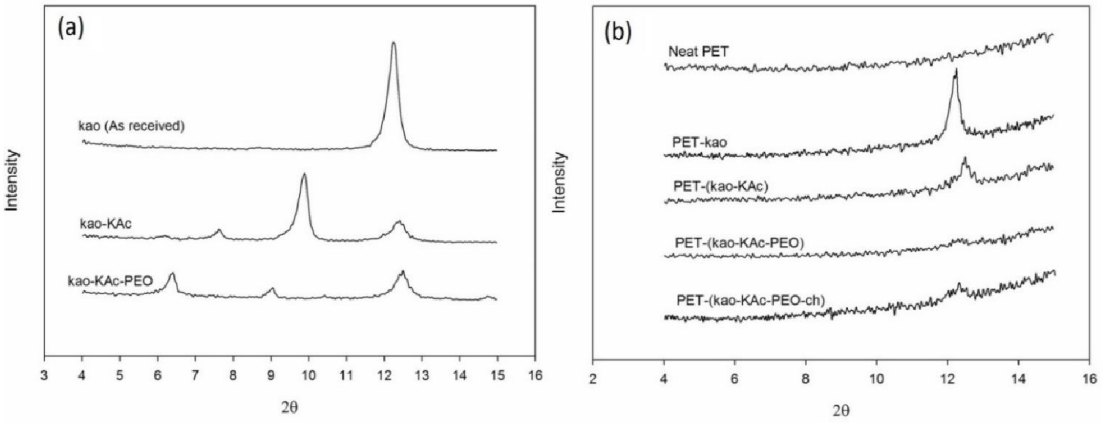

Figure 6-1 XRD patterns: (a) kaolin particles before and after treatment, (b) neat PET and PET/kaolin composites.

It was shown elsewhere that KAc molecules are able to penetrate between the layers of kaolin and increase the basal spacing of layers from 0.72 nm up to 1.4 nm corresponding to 2θ equal to 6.40° in Figure 6-1a that presents the XRD patterns of the pristine kaolin, kao-KAc precursor, and kao-KAc-PEO masterbatch. One can see that by blending the kao-KAc precursor with PEO, PEO molecules intercalate the kaolin galleries as the intensity of the characteristic peak at 0.72 nm (2θ = 12.46°) significantly decreases and also two new peaks appear at 2θ of 9.02° and 6.40°, which correspond to a *d*-spacing of 0.98 and 1.38 nm, respectively. Both PEO and kaolin are known as hydrophilic materials, which possess large quantities of oxygen and hydroxyl groups in their structure. The existence of hydroxyl groups can increase the tendency of PEO chains to interact with kaolin layers during the melt blending. Figure 6-1b presents the XRD patterns of different PET composites. As it is shown, when PET is compounded with the untreated kaolin (as received) there is no change in the XRD pattern and the intense peak at 0.72 nm is clearly observed while for the composite containing KAc-treated kaolin, PET-(kao-KAc), the intensity of this peak is much lower. Eventually when the kao-KAc-PEO masterbatch is diluted with the neat PET the peaks at

0.98 and 1.38 nm disappear and only the characteristic peak of kaolin (0.72 nm) with a very weak intensity can be detected in the pattern. This could be a sign of partial delamination and destruction of crystalline structure of kaolin layers in the PET matrix. Finally, the XRD pattern of PET-(kao-KAc-PEO-ch) is almost the same as PET-(kao-KAc-PEO); thus the addition of chain extender does not seem to have a remarkable effect on morphology of the composite. The chain extender molecules are supposed to react with PET end groups and connect the chains together in order to increase the molecular weight, but they are not likely to have any interactions with kaolin particles. It should be noticed that the existence of the characteristic peak of kaolin (even with very low intensity) in the XRD patterns of all composites reveals that even after chemical treatment and compounding there are still a fraction of particles, which have not undergone any intercalation and retained their initial structure.

6.3.2 SEM and TEM images

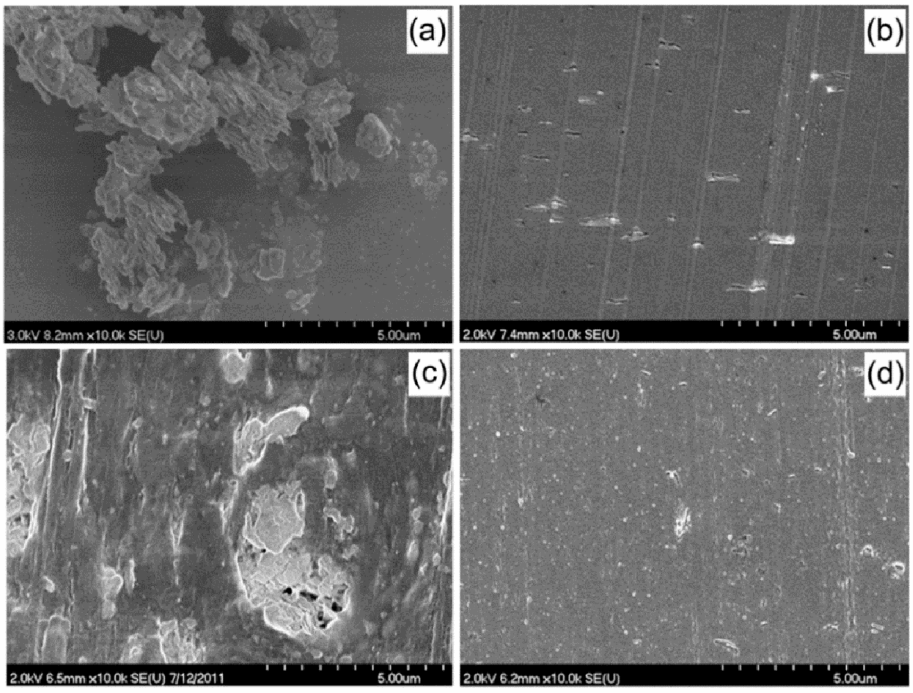

Figure 6-2 SEM images: (a) as received kaolin, (b) PET-kao composite, (c) kao-KAc-PEO masterbatch, (d) PET-(kao-KAc-PEO) nanocomposite.

SEM images of the "as-received" kaolin powder, kao-KAc-PEO masterbatch, PET-kao, and PET-(kao-KAc-PEO) composites are shown in Figure **6-2**. The kaolin particles tend to flocculate and form very big agglomerates, which are 5-20 μm in size. However, when kaolin is mixed with PET, due to de high shear applied during the extrusion the flocculated particles partially break up and form some aggregates in the range of a few microns (Figure 6-2b). As the kao-KAc-PEO masterbatch has a very high filler content (33 wt%) it is no surprise to observe large agglomerates in the SEM image of Figure 6-2c. A comparison between the images of the microtomed PET-Kao and PET-(kao-KAc-PEO) shows that the treatment of kaolin with KAc and blending with PEO can promote the dispersion of particles in the PET matrix; in many parts of the PET-Kao composite image of Figure 6-2b no kaolin particles are found at all while well-dispersed particles are easily observable (white spots) in the micrograph of PET-(kao-KAc-PEO) Figure 6-2d. The morphology of these two composites is totally different: the compound with the untreated kaolin contains a few big agglomerates in different positions of the matrix, whereas numerous fine kaolin particles can be found in the compound with the treated kaolin. This could be explained to the delamination of kaolin particles or breaking-down of the micron-size aggregates under high shear rates, which eventually lead to the dispersion of kaolin particles in the PET matrix.

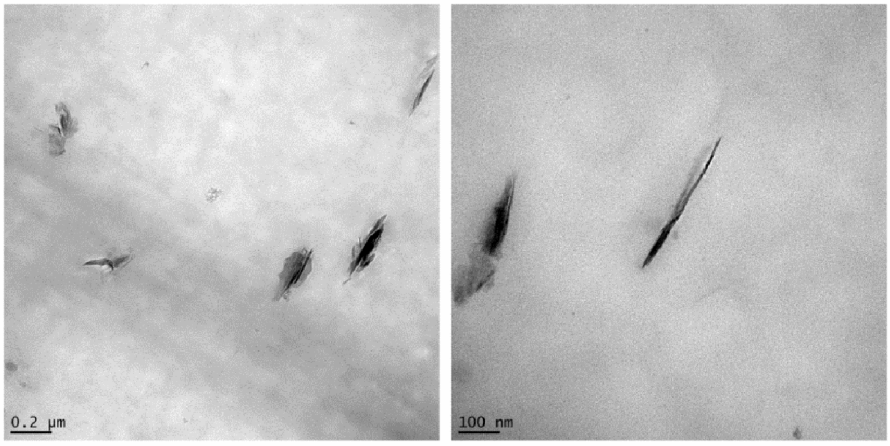

Figure 6-3 TEM images of PET (kao KAc PEO) nanocomposite at different magnifications

Since XRD is not reliable as a stand-alone technique for characterising polymer nanocomposites, TEM images were prepared to support the results of the morphological analysis. TEM images of cross-section of the PET-(kao-KAc-PEO) composite are presented in Figure 6-3. They show that tactoids of several layers of kaolin are distributed in the PET matrix whereas no large-scale aggregates are observed. The length of these tactoids is in the rage of 100-200 nm with an aspect ratio around 10. However, many particles with higher aspect ratio can be found. It should be noted that, due to the specific structure of kaolin it is not categorized as expandable clay minerals such as MMT; therefore the dispersion level of kaolin should not be compared to those of PET-MMT nanocomposites, which are extensively reported in the literature.

6.3.3 Rheological properties

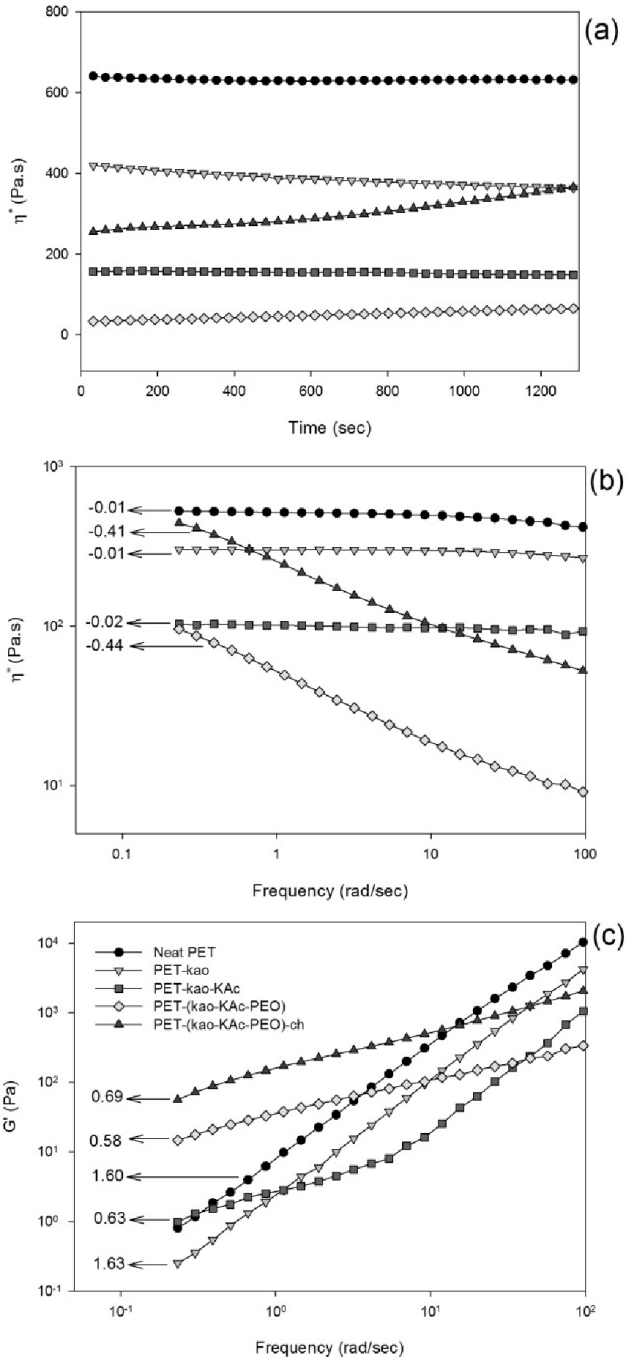

Figure 6-4 Rheological measurements: (a) complex viscosity vs. time, (b) complex viscosity vs. frequency, (c) elastic modulus vs. frequency (Test conditions: temperature = 270 °C, stress amplitude = 15 Pa).

To investigate the effect of chemical treatment and blending, rheological experiments were conducted and the results are presented in Figure 6-4. Figure 6-4a shows the isothermal time sweep

of the melt viscosity for the composites. It is clearly observed that the addition of the kaolin particles to the PET matrix reduces the viscosity with respect to the neat matrix; this effect has been shown elsewhere [33]. The viscosity loss is a result of large decrease in the molecular weight of the resin. There are two possible reasons for this reduction in viscosity: (i) degradation of PET during the melt processing, (ii) apparent slip effect at the walls of the rheometer plates. In order to check if the latter has any influence on the viscosity, two sets of experiments at two different gap heights (1 mm and 2 mm) were performed and result confirmed that there was no slip during the measurements. Hence, the degradation should be the only reason for the severe viscosity reduction. The degradation is induced by the thermal decomposition of the modifiers used to modify the properties of the filler and followed by the hydrolysis of PET. The existence of hydroxyl groups in the structure and on the edges of the kaolin particles has been considered as the main factor that causes the polymer degradation during the processing at high temperature. It seems that the hydroxyl groups in the structure of kaolin act as Brønsted acidic sites and play the most important role in the degradation of the PET chains [34,35]. The effect of the chemical treatment on the shear viscosity of the samples is also displayed in this figure. The viscosity of samples containing the treated fillers is drastically lower than that of the untreated filler. The stability of the samples with time is another point that can be concluded from Figure 6-4a. The complex viscosity of all samples nearly remains constant during the time of experiment (20 min), except the composite containing the chain extender for which the complex viscosity increases significantly during the rheological measurements due the reaction between the chain extender and end groups of the PET molecules [36].

Frequently sweep measurements on the neat PET and PET/kaolin composites were carried out to study the interactions between the polymer matrix and the filler particles. The results presented in

Figure 6-4b & c indicate that the treatment of the kaolin particles with KAc and PEO can improve the dispersion of kaolin particles in the matrix. The strong shear-thinning behavior of the complex viscosity for PET-(kao-KAc-PEO) and PET-(kao-KAc-PEO-ch) observed in Figure 6-4b indicates the formation of a network-like structure due the particle-particle interaction, whereas the other samples exhibit a Newtonian behavior up to frequencies around 100 rad/s. The complex viscosity of PET-(kao-KAc-PEO) nanocomposite at higher frequencies decreases below the value of the PET-kao due to the degradation mechanism described before.The storage (G') modulus of the neat PET and PET/kaolin composites are presented in Figure 6-4c. It is shown than the composite containing treated particles has increased melt elasticity at lower frequencies. Storage modulus is very sensitive towards the morphology of the dispersed phase in the polymer melt. The slope of storage modulus vs. frequency decreases from 1.60 to 0.58 after the introduction of treated kaolin particles indicating that the dependence of G' on ω decreases. The significant change in the slope of G' is typical of a network-like structure of dispersed particles in nanocomposites. The data reveals that the addition of chain extender does not have any influence on the rheological behavior of PET but shifting the curves to higher values. This indicates that the chain extender does not change the morphology of the particles while reacting with PET chains and increasing the viscosity of the matrix.

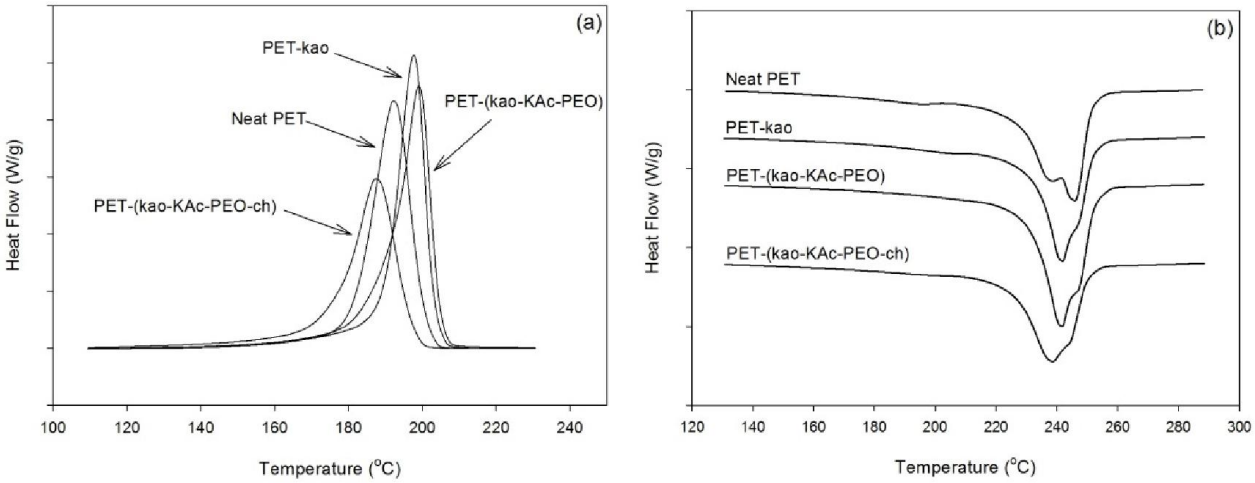

Figure 6-5 Crystallization (a) and melting (b) behavior of different composites at heating/cooling rate of 10 °C/min.

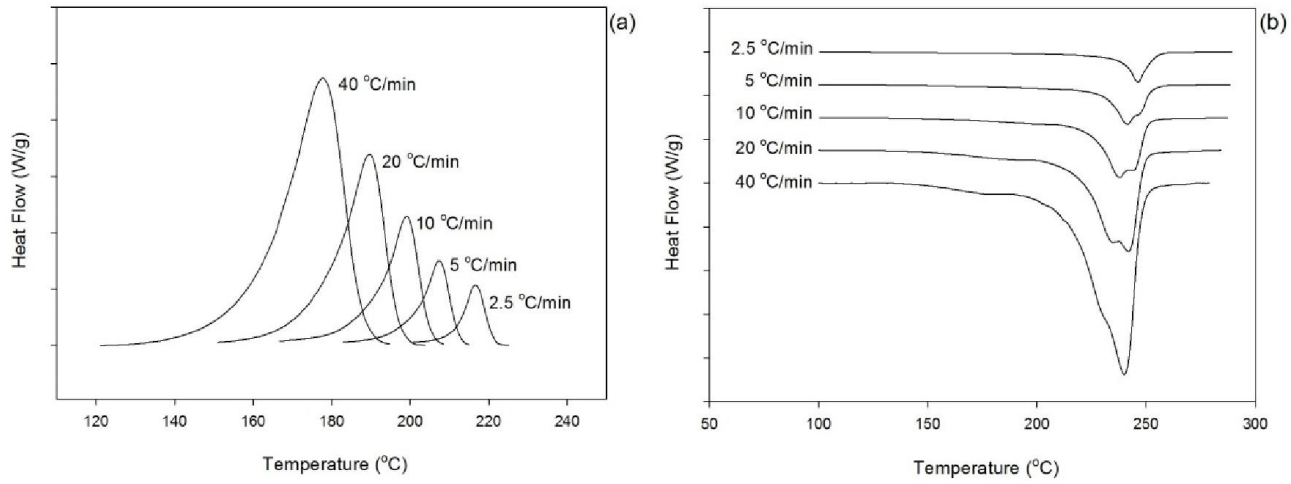

Figure 6-6 Crystallization (a) and melting (b) behavior of PET-(kao-KAc-PEO) at different cooling rates.

6.3.4 Crystallization/Melting (DSC) behavior

The nonisothermal crystallization curves of the neat PET and PET/kaolin composites at heating/cooling rate of 10 °C/min are displayed in Figure 6-5. The onset melting temperature, $T_{m,o}$, the onset crystallization temperature, $T_{c,o}$, the temperature of maximum crystallization rate, $T_{c,max}$, and the degree of crystallinity, X_c, are listed in Table 6-1. X_c was calculated using the following equations:

$$X_c = \frac{\Delta H_m}{\left(1 - W_f - W_p\right) \times \Delta H_0} \qquad \text{(Equation 6-1)}$$

where ΔH_m is the melting enthalpy of sample, ΔH_0 is the melting heat of 100% crystalline PET which is taken 140 J/g according to the literature [37], W_f and W_p denote the filler and PEO weight fractions respectively. It should be noticed that melting of PEO occurs at temperatures (66-75°C) much lower than that of PET (245°C). Therefore PEO is very unlikely to make any contributions in the melting enthalpy of PET.

As shown in Figure 6-5a, for the samples containing kaolin particles the crystallization exotherm becomes narrower and shifts to the higher temperatures. This can be explained by heterogeneous nucleation effects of the kaolin particles in the PET matrix, which accelerates the crystallization process. In fact, the segments of the PET chains can interact with the surface of kaolin particles to develop crystallization nuclei. It was observed that the sample containing chain extender crystallized at temperatures even lower than that of the neat PET. It seems that the chain extender acts as a cross linking bridge between the polymer chains and prevent the rearrangement of PET chains in a crystalline structure.

Table 6-1 Characteristic data for nonisothermal crystallization of PET and PET/kaolin composites.

	φ (°C/min)	$T_{c,o}$ (°C)	$T_{c,max}$ (°C)	$T_{m,o}$ (°C)	X_c (%)
Neat PET	2.5	218.2	206.5	212.3	31.8
	5	206.1	194.8	202.9	30.1
	10	205.5	192.3	193.2	29.6
	20	198.1	182.6	182.6	27.8
	40	190.0	169.1	176.6	24.6
PET-kao	2.5	219.5	210.2	212.1	29.5
	5	214.7	204.5	208.2	29.4
	10	208.3	197.7	200.1	28.1
	20	202.0	188.9	192.9	26.1
	40	193.5	177.4	176.7	25.0
PET-kao-KAc-PEO	2.5	224.4	216.4	215.3	35.7
	5	216.9	207.2	203.8	32.6
	10	208.9	199.0	199.6	29.2
	20	201.8	189.6	190.3	27.1
	40	193.4	177.7	177.8	24.7
PET-kao-KAc-PEO-ch	2.5	221.3	211.7	206.2	30.2
	5	210.8	197.9	193.4	26.9
	10	202.3	187.4	182.0	25.2
	20	192.0	174.0	176.7	22.5
	40	180.5	157.4	163.6	16.8

The total crystallinity of the composite containing untreated kaolin is slightly lower than that of the neat PET, as observed in Table 6-1. This effect was also reported for other type of fillers [38] and could be due to the opposing effects of kaolin particles on crystallization of PET. Although the

filler particles can promote the development of nucleation sites, at the same time, the mobility of PET chains is restricted due to the presence of the particles. Moreover, filler particles can also play the role of physical barriers against the crystal growth and limit the amount of crystals to be formed. However, for PET-kao-KAc-PEO due to the better dispersion of particles, their nucleation effect overcomes the barrier effects at lower cooling rates and crystallinity increases over the neat PET, but at higher cooling rates this is less obvious.

Figure 6-6 displays the crystallization and melting behavior of PET-kao-KAc-PEO nanocomposite at different cooling/heating rates. The crystallization curves become broader and shift to lower temperatures with increasing the cooling rate. At lower cooling rates samples have a longer period of time to form the nuclei; therefore the crystallization occurs at higher temperatures, whereas at higher cooling rates the nucleation takes place at lower temperatures. It has been suggested that at higher cooling rates the motion of PET chains cannot follow the cooling temperature and consequently more supercooling is required to initiate crystallization [39,40].

Figure 6-5b shows a multiple melting behavior for all samples; both neat PET and PET composites display two major melting peaks at two different temperatures. This existence of multiple melting peaks is frequently reported after isothermal crystallization of PET and other semi-crystalline polymers [41]. The first (low temperature) and second (high temperature) melting peaks are attributed to the fusion of secondary and primary crystals respectively [42]. Since the crystals formed by secondary crystallization are smaller than those formed by primary crystallization, they will melt at lower temperatures. The occurrence of multiple melting is more pronounced at higher cooling rates. Considering the fast crystallization rate of PET, at low cooling rates the polymer chains gain enough time for folding and rearrangement, thus crystallization takes place within a narrow temperature region to form relatively stable crystals. It was observed that in case of neat

PET the second peak is predominant for all heating rates; in fact the contribution of the first peak became much smaller at higher heating rates. However, as shown in Figure 6-6b for PET-kao-KAc-PEO at heating rates smaller than 20 °C/min the first peak is dominating but at higher heating rates (>20 °C/min) the second peak shows higher intensities. This behavior could be due to the change in the crystalline structure at higher heating rates. It was shown hereinbefore that Avrami index, *n*, also changed with heating rate which was attributed to the alteration of crystalline structure, a simple comparison between Avrami index values and the heating endotherms reveals that for the samples with a *n* value above 2 the second melting peak is predominant, while *n* value below 2 coincides with dominating of the first peak. Another reason could be the existence of crystallites with different sizes. The variation in the size of crystallites roots in the fact that there are two different populations of nuclei during the crystallization process; the first group which form at the very early times of crystallization and grow up to the final stages of the process (athermal nucleation) and the second population of nuclei that form not at the beginning but throughout the crystallization (thermal nucleation). The former leads to the formation of larger crystallites with thicker lamellas while the latter give rise to premature and small crystalline domains due to the time and space limitations, which restrict the growth of the lamellas.

Considering the importance of crystallization in the processing and final properties of polymers a number of models have been proposed to study their isothermal and nonisothermal crystallization. The Ozawa method [43] and Jeziorny methods [44] are more frequently applied to study the non-isothermal crystallization process. In this work both methods were applied; however, the Ozawa method showed large deviations from experimental data and therefore only the results of the Jeziorny analysis is reported here.

The following equation is used to calculate the relative crystallinity as a function of temperature:

$$X(T) = \frac{\int_{T_{c,o}}^{T} (dH/dT)dT}{\int_{T_{c,o}}^{T_\infty} (dH/dT)dT} \quad \text{(Equation 6-2)}$$

where $T_{c,o}$ and T_∞ denote the onset and end temperatures of crystallization, respectively, and H is the heat flow. This equation can be written as a function of time, $X(t)$, considering the relationship between time and temperature in nonisothermal crystallization:

$$t = \frac{T_{c,o} - T}{\varphi} \quad \text{(Equation 6-3)}$$

where t, T, and φ denote temperature, time, and cooling rate, respectively.

The Avrami equation [37] is widely used to describe the isothermal crystallization of polymers:

$$1 - X(t) = \exp(-Z_t\, t^n) \quad \text{(Equation 6-4)}$$

where $X(t)$ is the relative crystallinity at time t, n is the Avrami index, and Z_t is the kinetic crystallization rate. Jeziorny [44] tried to modify this method for nonisothermal crystallization at constant cooling rate by defining the following parameter:

$$\ln Z_c = \frac{\ln Z(t)}{\varphi} \quad \text{(Equation 6-5)}$$

where φ is the cooling rate, Z_c is the nonisothermal crystallization kinetic rate constant.

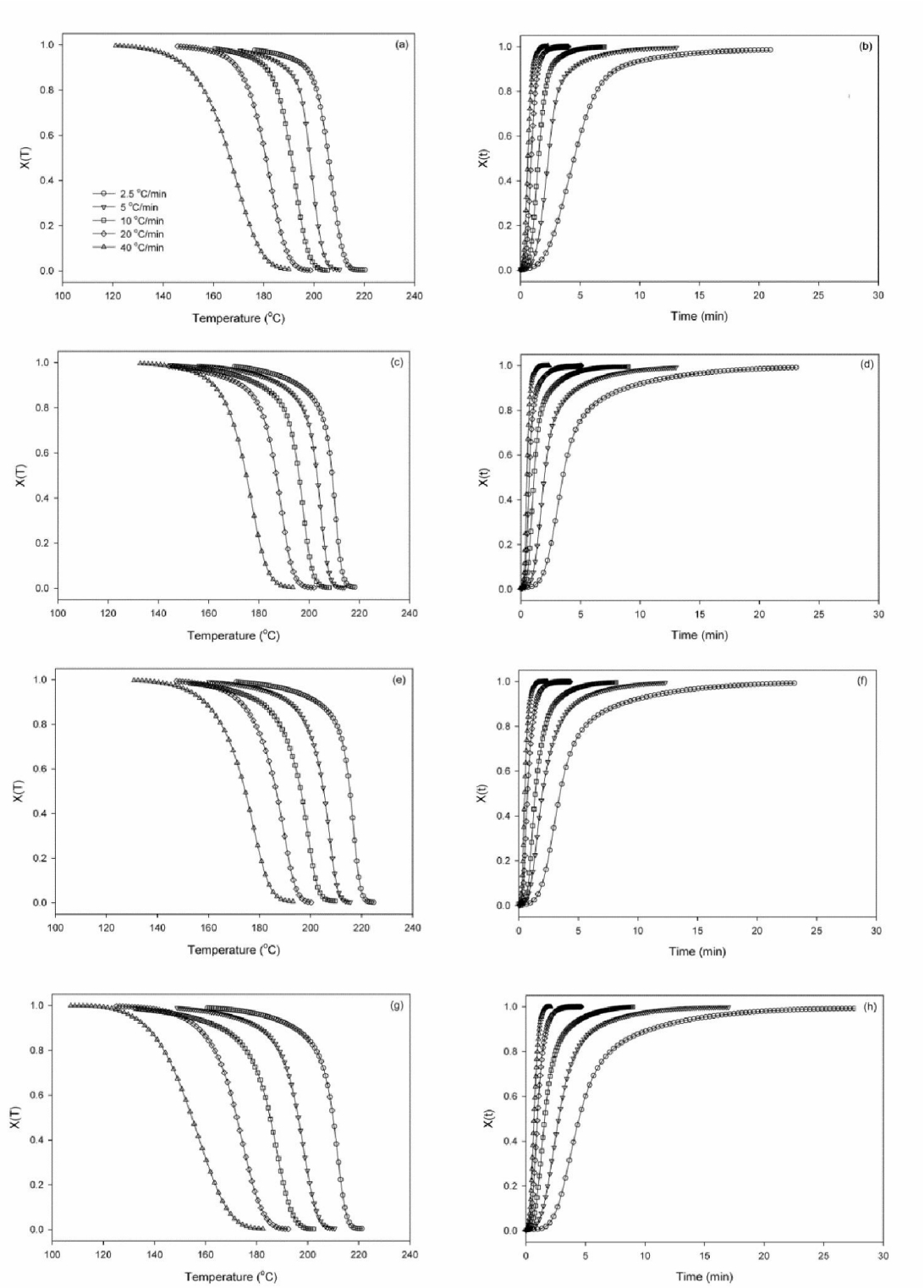

Figure 6-7 Relative crystallinity versus temperature and time at different cooling rates: (a,b) neat PET, (c,d) PET-kao, (e,f) PET-(kao-KAc-PEO), (g,h) PET-(kao-KAc-PEO-ch).

Table 6-2 Result of the Avrami-Jeziorny analysis for nonisothermal crystallization of neat PET and PET composites.

	φ (°C/min)	$T_{c,o}$ (°C)	$T_{c,max}$ (°C)	$t_{1/2}$ (min)	n	$Z_t \times 102$ (min^{-1})	$Z_c \times 10^2$
Neat PET	2.5	218.2	206.5	4.56	2.31	2.08	21.24
	5	206.1	194.8	2.38	2.59	7.33	59.29
	10	205.5	192.3	1.54	2.73	21.38	88.70
	20	198.1	182.6	0.92	2.76	86.04	99.25
	40	190.0	169.1	0.62	2.49	224.5	102.04
PET-kao	2.5	219.5	210.2	3.79	1.87	5.72	31.84
	5	214.7	204.5	2.09	1.89	17.12	70.26
	10	208.3	197.7	1.17	1.89	51.48	93.58
	20	202.0	188.9	0.73	2.26	140.2	101.70
	40	193.5	177.4	0.51	2.86	465.3	103.92
PET-kao-KAc-PEO	2.5	224.4	216.4	3.69	1.84	6.25	32.99
	5	216.9	207.2	2.11	1.73	19.01	71.75
	10	208.9	199.0	1.48	2.00	31.68	89.14
	20	201.8	189.6	0.79	2.10	123.6	101.06
	40	193.4	177.7	0.51	2.39	345.2	103.14
PET-kao-KAc-PEO-ch	2.5	221.3	211.7	4.79	1.94	3.31	25.58
	5	210.8	197.9	2.87	1.98	8.61	61.23
	10	202.3	187.4	1.65	1.87	27.19	87.79
	20	192.0	174.0	0.99	2.35	71.52	98.34
	40	180.5	157.4	0.69	2.57	179.5	101.47

Figure **6-7** shows the plots of relative crystallinity versus temperature and time for different samples.The Avrami equation was directly fitted to the experimental data using Sigmaplot software

and the results are summarized in Table 6-2. One can see that neat PET has a n value larger than 2 regardless of the heating rate. However, for composites n depends on the heating rate; for lower heating rates n is in the range of 1.5 to 2 while it increases to values above 2 for higher heating rates. n values in the range of 2 to 3 imply that the nuclei are growing three-dimensionally, and the shift to values below 2 signifies that the mode of crystallization is probably changed to two-dimensional growth with heterogeneous nucleation. It should be noticed that the Avrami method does not distinguish between the formation of nuclei and their subsequent growth during the crystallization. The nonisothermal crystallization kinetic rate constant increases considerably with the cooling rate; larger values of Z_c imply that the crystallization is faster in the presence of kaolin particles. Compared to the neat PET, the PET-kao composite has a larger Z_c at a given cooling rate. However, in case of PET-kao-KAc-PEO and PET-kao-KAc-PEO-ch the values of Z_c are almost equal to that of the neat PET.

The temperature of maximum crystallization rate, $T_{c,max}$, and crystallization half-time (the time taken for the relative crystallinity of the sample to reach the value of 50%), $t_{1/2}$, are two main parameters that characterize the rate of crystallization. The higher $T_{c,max}$ and smaller $t_{1/2}$ values indicate a higher crystallization rate. As shown, the $t_{1/2}$ values of composites are generally smaller than that of the neat PET; the only exception is PET-kao-KAc-PEO-ch. PET-Kao exhibits the smallest $t_{1/2}$ for all cooling rates. However, when the particles are chemically treated with KAc and PEO, the values of $t_{1/2}$ increase slightly. In spite of the fact that the growth rates are lower at higher temperatures, the high number of nuclei provided by the clay particles generates a large quantity of crystallites that grow concurrently, which compensates the effect of lower growth rates. This indicates that the filler particles act as a heterogeneous nucleation agent and induce the formation of crystals, which subsequently increases the crystallization rate of the sample.

6.3.5 Thermal stability

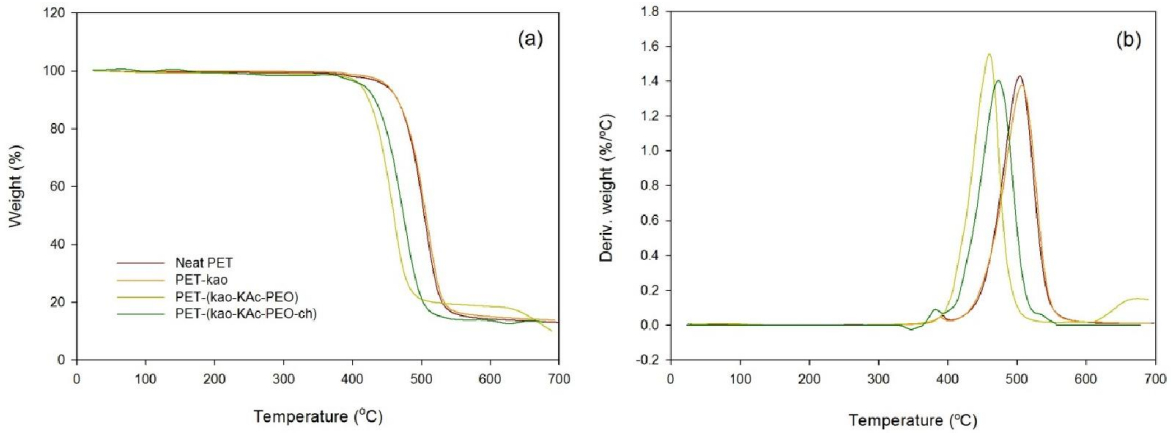

Figure 6-8 Thermal decomposition temperature of neat PET and PET/kaolin composites: (a) weight loss, (b) derivative weight loss.

The TGA thermograms of the neat PET along with those of other composites are presented in Figure 6-8. The onset temperature of degradation (T_{onset}), measured as the temperature required for 5% weight loss, for the neat PET, PET-kao, and PET-(kao-KAc-PEO) are 418, 407, and 397°C, respectively. In spite of the fact that T_{onset} of PET is slightly shifted to lower temperatures as kaolin particles are added to the resin, it seems that the main degrading effect is due to the chemical modifiers and not the kaolin particles. The kaolin particle and chemical modifiers can exert influence not only on the T_{onset}, but also on the temperature at which the maximum mass loss occurs (T_{max}), as shown in Figure 6-8b. The inclusion of the untreated kaolin has a small effect on T_{max} of the composites; however, the TGA data show that for samples treated with KAc and PEO the maximum mass loss occurs at temperatures lower than those of the neat PET. It seems that the decomposition of kao-KAc is the main reason for the shift of T_{max} to lower temperatures. The decomposition of kao-KAc takes place at 455°C and subsequently the decomposition products can give rise to an accelerated degradation of the PET resin. It is also noteworthy that blending with PET seems to improve the thermal stability of PEO, as the T_{max} of PEO is 262 °C while no mass loss is observed for PET-(kao-KAc-PEO) at this temperature.

TGA data shows that the addition of chain extender to the system can slightly improve the thermal stability, as T_{max} is shifted to 473 °C for PET-(kao-KAc-PEO-ch) which is 15 °C higher than maximum decomposition temperature of PET-(kao-KAc-PEO), however, it is still lower than that of the neat PET.

6.4 Conclusion

XRD and TEM indicated that PET/kaolin nanocomposite was achieved via melt blending. It was shown that the treatment of kaolin with KAc and blending with PEO improved its dispersion in a PET matrix. However, a low level of exfoliation was achieved. The size of nanoscale particles ranged from 100 to 200 nm in length and 10-50 nm in thickness in the final nanocomposite. Due to the existence of hydroxyl groups in the structure of kaolin particles, PET undergone a remarkable degradation during the melt mixing step and this effect is more pronounced for chemically treated particles. The kaolin particles, as nucleating agent, affect the crystallization/melting behavior of PET and increase the crystallization rate of the PET. It was also concluded that chemical treatment of particles with KAc and PEO would slightly decrease the thermal stability of nanocomposite.

6.5 Acknowledgments

The authors gratefully acknowledge PepsiCo for support of this work.

6.6 References

[1] Klaus Friedrich, Stoyko Fakirov, Zhong Zhang, Friedrich K, Fakirov S, Zhang Z. Polymer Composites: From Nano- to Macro-Scale. New York: Springer; 2005.

[2] Beake BD, Leggett GJ. Nanoindentation and nanoscratch testing of uniaxially and biaxially drawn poly(ethylene terephthalate) film. Polymer (Guildf) 2002;43:319–27.

[3] Imai Satoshi; Abe, Eiichi; Tateyama, Hiroshi; Abiko, Akimasa; Yamaguchi, Akira; Aoyama, Tomohiro; Taguchi, Hiroaki YN, Imai Y, Nishimura S, Abe E, Tateyama H, Abiko A, et al. High-

modulus poly (ethylene terephthalate)/expandable fluorine mica nanocomposites with a novel reactive compatibilizer. Chem Mater 2002;14:477–9.

[4] S. I, Chang Sung Jong; Joo, Yong Lak; Im, Seungsoon J-HK, Chang J-H, Kim SJ, Joo YL, Im S. Poly (ethylene terephthalate) nanocomposites by in situ interlayer polymerization: the thermo-mechanical properties and morphology of the hybrid fibers. Polymer (Guildf) 2004;45:919–26.

[5] Wu T, Ke Y. The absorption and thermal behaviors of PETâ€“SiO2 nanocomposite films. Polym Degrad Stab 2006;91:2205–12.

[6] Chae DW, Kim BC. Thermal and rheological properties of highly concentrated PET composites with ferrite nanoparticles. Compos Sci Technol 2007;67:1348–52.

[7] Bizarria M, Giraldi ALF de M, de Carvalho CM, Velasco JI, d'Ávila MA, Mei LHI, et al. Morphology and thermomechanical properties of recycled PET-organoclay nanocomposites. J Appl Polym Sci 2007;104:1839–44.

[8] Kim Yun Hyuk; Choi, Soo Myung; Yoon, Kwan Han H-UB, Kim H-U, Bang YH, Choi SM, Yoon KH. Morphology and mechanical properties of PET by incorporation of amine-polyhedral oligomeric silsesquioxane. Compos Sci Technol 2008;68:2739–47.

[9] Choudalakis G, Gotsis AD. Permeability of polymer/clay nanocomposites: A review. Eur Polym J 2009;45:967–84.

[10] Wang Y, Gao J, Ma Y, Agarwal US. Study on mechanical properties, thermal stability and crystallization behavior of PET/MMT nanocomposites. Compos Part B Eng 2006;37:399–407.

[11] Bergaya F, Theng BKG, Lagaly G. Handbook of Clay Science. Elsevier Science; 2011.

[12] Gardolinski Luiz Pereira; de Souza, Gabriel Pinto; Wypych, Fernando JER, Gardolinski JE, Ramos LP, de Souza GP, Wypych F. Intercalation of benzamide into kaolinite. J Colloid Interface Sci 2000;221:284–90.

[13] Frost RL, Kristof J, Paroz GN, Kloprogge JT, Frost J.; Paroz, G. N.; Kloprogge, J. T. RL. K. Intercalation of kaolinite with acetamide. Phys Chem Miner 1999;26:257–63.

[14] Martens WN, Frost RL, Kristof J, Horvath E, Martens Ray L.; Kristof, Janos; Horvath, Erzsebet WN. F. Modification of Kaolinite Surfaces through Intercalation with Deuterated Dimethylsulfoxide. J Phys Chem B 2002;106:4162–71.

[15] Tsunematsu K, Tateyama H. Delamination of Urea-Kaolinite Complex by Using Intercalation Procedures. J Am Ceram Soc 1999;82:1589–91.

[16] Zhang X, Xu Z. The effect of microwave on preparation of kaolinite/dimethylsulfoxide composite during intercalation process. Mater Lett 2007;61:1478–82.

[17] Komori Y, Enoto H, Takenawa R, Hayashi S, Sugahara Y, Kuroda K, et al. Modification of the Interlayer Surface of Kaolinite with Methoxy Groups. Langmuir 2000;16:5506–8.

[18] Murakami J, Itagaki T, Kuroda K. Synthesis of kaolinite-organic nanohybrids with butanediols. Solid State Ionics 2004;172:279–82.

[19] Letaief S, Elbokl TA, Detellier C. Reactivity of ionic liquids with kaolinite: Melt intersalation of ethyl pyridinium chloride in an urea-kaolinite pre-intercalate. J Colloid Interface Sci 2006;302:254–8.

[20] Letaief S, Detellier C. Reactivity of kaolinite in ionic liquids: preparation and characterization of a 1-ethyl pyridinium chloride–kaolinite intercalate. J Mater Chem 2005;15.

[21] Ansari DM, Price GJ. Correlation of mechanical properties of clay filled polyamide mouldings with chromatographically measured surface energies. Polymer (Guildf) 2004;45:3663–70.

[22] Buggy M, Bradley G, Sullivan A. Polymer–filler interactions in kaolin/nylon 6,6 composites containing a silane coupling agent. Compos Part A Appl Sci Manuf 2005;36:437–42.

[23] Liu Q, Zhang Y, Xu H. Properties of vulcanized rubber nanocomposites filled with nanokaolin and precipitated silica. Appl Clay Sci 2008;42:232–7.

[24] Sukumar R, Menon ARR. Organomodified kaolin as a reinforcing filler for natural rubber. J Appl Polym Sci 2008;107:3476–83.

[25] Yahaya LE, Adebowale KO, Menon ARR. Mechanical properties of organomodified kaolin/natural rubber vulcanizates. Appl Clay Sci 2009;46:283–8.

[26] Itagaki T, Komori Y, Sugahara Y, Kuroda K, Itagaki Yoshihiko; Sugahara, Yoshiyuki; Kuroda, Kazuyuki TK. Synthesis of a kaolinite--poly (β-alanine) intercalation compound. J Mater Chem 2001;11:3291–5.

[27] Komori Y, Sugahara Y, Kuroda K. Direct intercalation of poly (vinylpyrrolidone) into kaolinite by a refined guest displacement method. Chem Mater 1998;11:3–6.

[28] Liu X, Zhang H, Yang Z, Ha C, Liu Hongtao; Yang, Zhizhong; Ha, Chengyong XZ. Preparation and characterization of poly (styrene/maleic anhydride)/kaolin nanocomposites. Chinese Sci Bull 2005;50:1320–5.

[29] Turhan Y, DogÌŒan M, Alkan M. Poly(vinyl chloride)/Kaolinite Nanocomposites: Characterization and Thermal and Optical Properties. Ind Eng Chem Res n.d.;49:1503–13.

[30] Elbokl TA, Detellier C. Aluminosilicate nanohybrid materials. Intercalation of polystyrene in kaolinite. J Phys Chem Solids 2006;67:950–5.

[31] Tunney JJ, Detellier C. Aluminosilicate Nanocomposite Materials. Poly(ethylene glycol)-Kaolinite Intercalates. Chem Mater 1996;8:927–35.

[32] Itagaki T, Matsumura A, Kato M, Usuki A, Kuroda K, Itagaki A.; Kato, M.; Usuki, A.; Kuroda, K. T. M. Preparation of kaolinite--nylon6 composites by blending nylon6 and a kaolinite--nylon6 intercalation compound. J Mater Sci Lett 2001;20:1483–4.

[33] Sanchez-Solis A, Garcia-Rejon A, Manero O. Production of nanocomposites of PET-montmorillonite clay by an extrusion process. Macromol Symp 2003;192:281–92.

[34] Xu X, Ding Y, Qian Z, Wang F, Wen B, Zhou H, et al. Degradation of poly(ethylene terephthalate)/clay nanocomposites during melt extrusion: Effect of clay catalysis and chain extension. Polym Degrad Stab 2009;94:113–23.

[35] Qin H, Zhang S, Liu H, Xie S, Yang M, Shen D. Photo-oxidative degradation of polypropylene/montmorillonite nanocomposites. Polymer (Guildf) 2005;46:3149–56.

[36] Ghanbari A, Heuzey MC, Carreau PJ, Ton-That MT. A novel approach to control thermal degradation of PET/organoclay nanocomposites and improve clay exfoliation. Polymer (Guildf) 2013;54:1361–9.

[37] Brandrup J, Immergut EH, Grulke EA, Abe A, Bloch DR. Polymer Handbook (4th Edition) n.d.

[38] Xin F, Li L, Chan SH, Zhao J. Influences of carbon fillers on electrical conductivity and crystallinity of polyethylene terephthalate. J Compos Mater 2012;46:1091–9.

[39] Xu W, Ge M, He P. Nonisothermal crystallization kinetics of polypropylene/montmorillonite nanocomposites. J Polym Sci Part B Polym Phys 2002;40:408–14.

[40] Kim JY, Park HS, Kim SH. Unique nucleation of multi-walled carbon nanotube and poly(ethylene 2,6-naphthalate) nanocomposites during non-isothermal crystallization. Polymer (Guildf) 2006;47:1379–89.

[41] Lee B, Shin TJ, Lee SW, Yoon J, Kim J, Ree M. Secondary Crystallization Behavior of Poly(ethylene isophthalate-co-terephthalate): Time-Resolved Small-Angle X-ray Scattering and Calorimetry Studies. Macromolecules 2004;37:4174–84.

[42] Papageorgiou GZ, Karayannidis GP. Crystallization and melting behaviour of poly(butylene naphthalene-2,6-dicarboxylate). Polymer (Guildf) 2001;42:2637–45.

[43] Ozawa T. Kinetics of non-isothermal crystallization. Polymer (Guildf) 1971;12:150–8.

[44] Jeziorny A. Parameters characterizing the kinetics of the non-isothermal crystallization of poly(ethylene terephthalate) determined by d.s.c. Polymer (Guildf) 1978;19:1142–4.

CHAPTER 7: ARTICLE 3: PREPARATION OF CALCINED-KAOLIN NANOPARTICLES VIA WET GRINDING IN STIRRED MEDIA MILL AND ITS APPLICATION IN THE PET BASED NANOCOMPOSITES

Khalil Shahverdi-Shahraki[1], Tamal Ghosh[2], Kamal Mahajan[2], Abdellah Ajji[1]*, Pierre J. Carreau[1]

[1] *CREPEC, Department of Chemical Engineering, École Polytechnique de Montréal, Canada*

[2] *PepsiCo Advanced Research - Beverage Packaging, Hawthorne, NY, USA*

Submitted to *Polymer International*.

Abstract

The aim of this study was to produce calcined kaolin nano-particles (gUlt) and to investigate their effect on the morphology and properties of poly(ethylene terephthalate) nanocomposites. The calcined kaolin was ground via a wet-grinding process in which the production of nanometer and submicron range particles is possible due to higher energy densities in the grinding chamber. PET-gUlt nanocomposites were prepared via two-step melt extrusion in twin and single screw extruders, respectively. SEM and TEM micrographs along with rheological measurements confirmed the dispersion of nano-size particles in the PET matrix. The final properties of the nanocomposites were measured and compared to those of neat PET so that mechanical and barrier properties of PET were improved after the incorporation of gUlt particles, however, the optical properties deteriorated to some extent. A decrease in viscosity of gUlt-filled PET melts due to the lower molecular weight of nanocomposites was the major drawback, and therefore phenoxy resin additive was used during the melt mixing step in order to compensate this effect. gUlt nanoparticles affected the melting/crystallization behavior of PET to some extent, however, TGA data confirmed that they did not have any impacts on the thermal stability and decomposition temperature of PET.

Keywords: calcined kaolin, PET, nanocomposite, grinding, melt extrusion.

7.1 Introduction

PET is a commodity thermoplastic that has found many applications particularly in packaging industries and fiber production. In order to overcome the shortcomings of PET such as lack of thermal stability and low modulus, hybrid systems were produced by incorporation of an external filler and more specifically nano-size particles. The clay minerals have been extensively used as nanoparticles due to their natural abundance, high aspect ratio, and low cost [1]. Intercalation

and/or exfoliation of smectite clays (montmorillonite) in different polymeric matrices has been widely reported in the literature [2–5]. However, few studies have been conducted regarding the dispersion of non-expanding clay minerals such as kaolin.

Kaolin is a white, soft powder principally composed of the mineral kaolinite with minor amounts of impurities such as quartz and feldspar. Kaolinite ($Al_2O_3.2SiO_2.2H_2O$) is a 1:1 aluminosilicate having an octahedral aluminum hydroxide sheet and a tetrahedral silica sheet in each layer [6]. Kaolin has found a wide range of applications in the ceramic, cosmetic, pulp and paper industries. Calcined-kaolin is a thermally treated grade of kaolin which is produced by firing the powder to a temperature around 650°C to remove the adsorbed and structural water and make the material more hydrophobic. Calcination at higher temperatures results in complete dehydroxylation and eventually at temperatures above 950°C a fully calcined kaolin with an amorphous spinel structure are produced [7].

Our previous studies have demonstrated that hydrous kaolin had a strong degrading effect on PET which was mainly due to the large number of hydroxyl groups on the surface of particles. A calcined grade of kaolin, which is mainly dehydroxylated, seems to be more compatible with PET. However, due to the absence of any reactive functional groups on the surface of calcined kaolin, no chemical modifications can be performed to increase its affinity for polymer matrices. Therefore, the dispersion of particles by grinding prior to melt-mixing with PET may be an appropriate alternative.

Nano particles may be produced either by self-assembly of atoms (chemical synthesis) which is referred to as bottom-up method or by applying mechanical forces to grind larger size particles (top-down method) [8]. Wet-grinding in a stirred media mill was used as a suitable method for the production of nanoparticles from large agglomerates [9,10]. The nano particles produced in the

grinder has the potential to be used as a nano filler in the polymer matrices [11]. It has been reported that operating parameters such as pH, the surfactant concentration, grinding media loading, and media size may have a great influence on the stability and particle size distribution of the final product [9,12–15].

Considering the difficulties in the dispersion of kaolin particles onto another substance, the wet grinding seems to be an effective method for this purpose. In this paper, we report the preparation of calcined-kaolin nanoparticles in a wet grinding process and their incorporation into PET to produce PET/calcined-kaolin nanocomposites. The morphological investigations and the impact of nanoparticles on the final properties of nanocomposites are reported as well.

7.2 Experimental

7.2.1 Materials

The Polyethylene terephthalate (PET) resin used in this study was Laser+® 7000 supplied by DAK Americas LLC. It is a bottle grade PET resin with an intrinsic viscosity of 0.84 dL/g, a melting point of 242 °C and 35% crystallinity. The filler was a calcined grade kaolin, denoted hereafter as CKao, with a specific gravity of 2.63 g/cm^3 supplied by BASF Corporation. Sodium hexametaphosphate (SHMP), purchased from Sigma-Aldrich, was added to the grinding media, to prevent agglomeration in the grinder. Phenoxy resin additive (PKHA), a linear poly hydroxy ether provided by InChem Corporation, was used in this work to modify the molecular weight of PET. Analytical grade sodium hydroxide (NaOH) and nitric acid (HNO_3), purchased from Sigma-Aldrich, were used as pH regulators.

7.2.2 Characterization and Testing

Scanning electron microscope (SEM) microphotographs were obtained using in a Hitachi S4700 instrument with a cold field emission gun under an acceleration voltage of 2 kV. A JOEL JEM-2100F transmission electron microscope (TEM) operating at accelerating voltage of 200 kV was used to observe ultrathin sections of the samples and fully characterize the morphology. The samples were microtomed into approximately 50-80 nm thick slices using an Ultracut FC microtome (Leica, Germany) with a diamond knife.

Wide angle X-ray diffraction (WAXD) measurements were accomplished using a Philips X'Pert diffractometer (CuKα radiation, λ=1.54056 A°), operating at a voltage of 50 kV and current of 40 mA. The scanning rate was 0.02 °/s and the 2θ ranged from 2° to 15°.

Rheological measurements were performed using a parallel plate stress-controlled rheometer (Gemini of Malvern) with a gap size of 1 mm and a plate diameter of 25 mm. Frequency sweeps were carried out in small-amplitude oscillatory mode at 270°C in the frequency range of 0.628-628 rad/s. It was verified that all the measurements were in the linear viscoelastic range. The measurements were performed under nitrogen flow to avoid the thermal degradation and the temperature was controlled by a convection oven installed on the rheometer.

Differential scanning calorimetry (DSC) was done on a DSC Q1000 TA Instrument to study the melting and crystallization characteristics of the samples. The heating/cooling ramps with constant heating rate of 10 °C/min were applied under helium atmosphere in the temperature range of 30-300°C. The thermal decomposition was studied by use of a TGA Q500 TA Instrument thermogravimeter. About 10 mg of the samples were heated at 10 °C/min from 30 to 700°C under a nitrogen atmosphere.

Dynamic mechanical analysis (DMA) was performed by using a DMA 2980 TA Instruments. The measurements were carried out on rectangular molded samples in the bending mode with a constant heating ramp of 5.00°C/min from 30 to 170°C and a frequency of 1 Hz. An *Instron* universal tensile machine (Model 3365) with 500 N load-cell and a strain rate of 25 mm/min was used to measure the mechanical properties of PET nanocomposites at room temperature.

The oxygen transmission rate (OTR) was measured at 23°C under barometric pressure 700 mmHg using an Ox-Tran oxygen permeability MD Module (Model 2/21) from Mocon Incorporation. The permeability coefficients were reported after normalizing by the films thickness (OTR × thickness).

Optical properties were determined according to ASTM D1003 using a LAMBDA 1050 spectrophotometers from PerkinElmer.

Partica LA-950 laser diffraction particle size distribution analyzer (HORIBA Instruments Inc.) was used to obtain the particle size distribution of the particles. The measurements were performed on a diluted aqueous suspension of the particles (sonicated for 20 sec).

7.2.3 Sample preparation

7.2.3.1 Grinding of particles

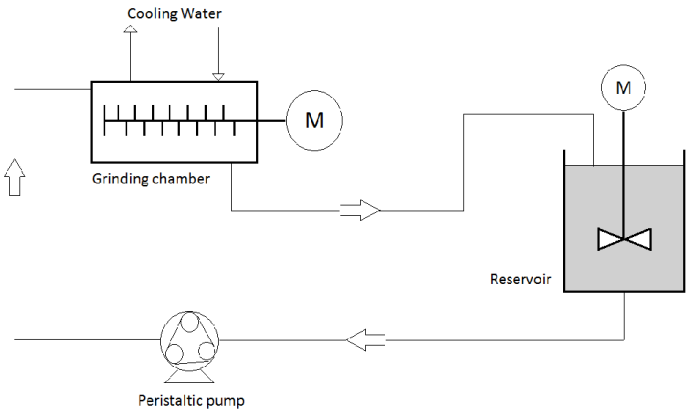

Figure 7-1 Schematic diagram of the grinder setup.

For this work, the grinding of the calcined kaolin particles was carried out in a MINIFER agitator bead mill (NETZSCH, Germany) in circulation mode. A schematic diagram of the grinder setup is given in Figure 7-1. Zirconium oxide beads (NETZSCH, Germany) rage from 0.1 to 0.2 mm in diameter were used as grinding media. The rotation speed of the agitating shaft was set at 2000 rpm. The particles were dispersed in distilled water and 1 wt% SHMP was added to the mixture under vigorous agitation. pH was adjusted in the range of 7-8 by drop wise addition of diluted NaOH and/or HNO_3. The suspension was put in the reservoir to be pumped into the grinding chamber for a given period of time.

7.2.3.2 Preparation of nanocomposites

The nanocomposites were prepared in a two-step process. PET granules were initially ground in liquid nitrogen and then were mixed with ground calcined kaolin (gUlt) in a co-rotating twin-screw extruder (Berstorff ZE25, screw diameter (D) = 25 mm, L/D = 28) in order to obtain a 15 wt% masterbatch. The processing temperature and screw speed were set at 270°C and 150 rpm respectively. In the second step, PET-gUlt masterbatch was diluted with neat PET in a Killion single screw extruder (D = 45 mm) to produce the final nanocomposites with given filler loadings. The temperature profile was set in the range of 250-275 °C and the screw rotating speed was 25 rpm. PKHA (4 wt%) was added to the composites in the second extrusion step. All the materials were well dried in a vacuum oven at 110 °C for 24 h before being processed to eliminate the moisture and avoid degradation reactions in PET during the melt compounding.

7.3 Result and Discussion

7.3.1 Grinding process

The operating conditions of the grinder such as grinding media loading, pH, surfactant concentration, rotation speed, and grinding media size were optimized and kept constant during the experiments. These operating conditions did not have a great effect on the final product except for the dispersant aid and the pH adjustment. Nanoparticles have a high tendency to aggregate in the grinding chamber, where the particles collide to each other and aggregation is very likely. Therefore addition of grinding aid (surfactant) to the media seems to be inevitable. SHMP can affect the grinding process by acting as a dispersant which can hold the particle apart by electrostatic or steric repulsion. The grinding aid also makes it possible to increase the particle loading in wet grinder by reducing the viscosity of the suspension.

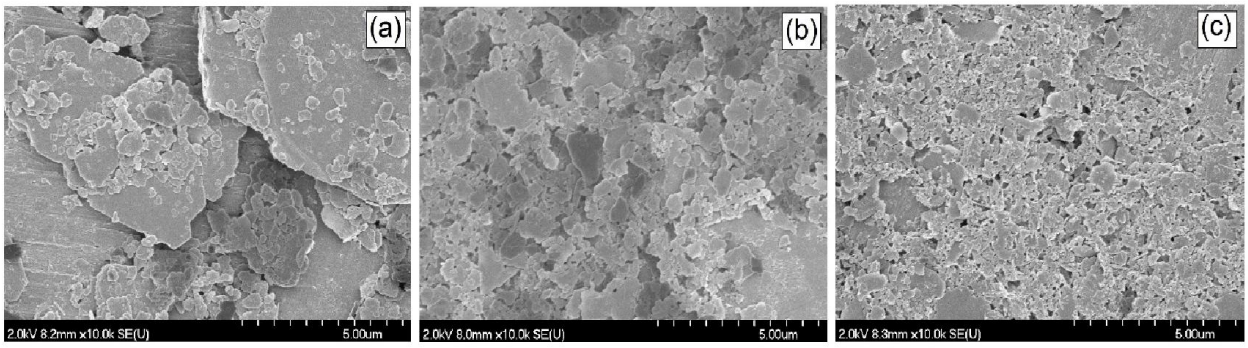

Figure 7-2 SEM micrographs of calcined-kaolin ground for different periods of time: (a) 0 min, (b) 60 min, and (c) 180 min.

Figure 7-2 shows SEM images of calcined kaolin ground for different periods of time. For asreceived material, there are a number of fine particles alongside some large flat crystal planes. In fact a mixture of primary particles and large agglomerates with sizes ranging from hundred nanometers to 20 μm are seen in the image. After 60 min, large particles are disappeared and smaller particles (<1 μm) can be observed. The grinding process causes the breakage of large platelet and formation of some finer particles, although some larger platelets remain. After 180 min

of grinding the alteration of structure of particles is clearly observed, the large plates does not exist anymore and many nanoparticles with sizes around 250 nm are appeared instead.

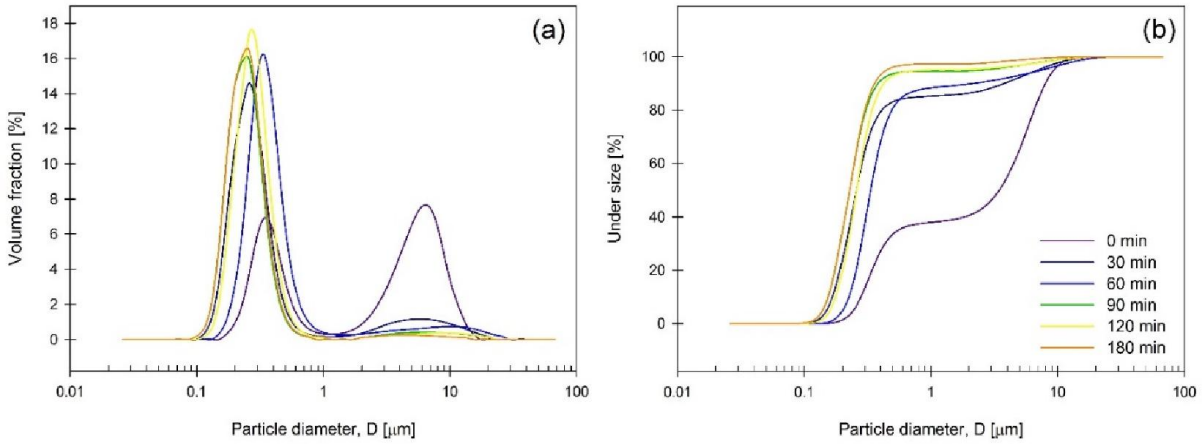

Figure 7-3 Particle size distribution (PSD) as a function of grinding time.

Figure 7-3 illustrates the particle size distribution (PSD) of samples as a function of grinding time (up to 180 min) measured with a laser particle size analyzer. Particle size measurements were performed on the feed and product material and then the mean particle size was calculated. After 60 min of grinding, 90% or more of the products were 1 μm or less, and after 120 min, a small fraction of the particles (< 4%) were bigger than 1 μm. Although the mean particle size decreased with time, it was noted that after 120 min it approached a constant value about 240 – 260 nm and remained almost unchanged thereafter. It seems that there is a limitation for the smallest size we can achieve and excessive grinding does not decrease the particle size anymore.

7.3.2 Morphology of nanocomposites

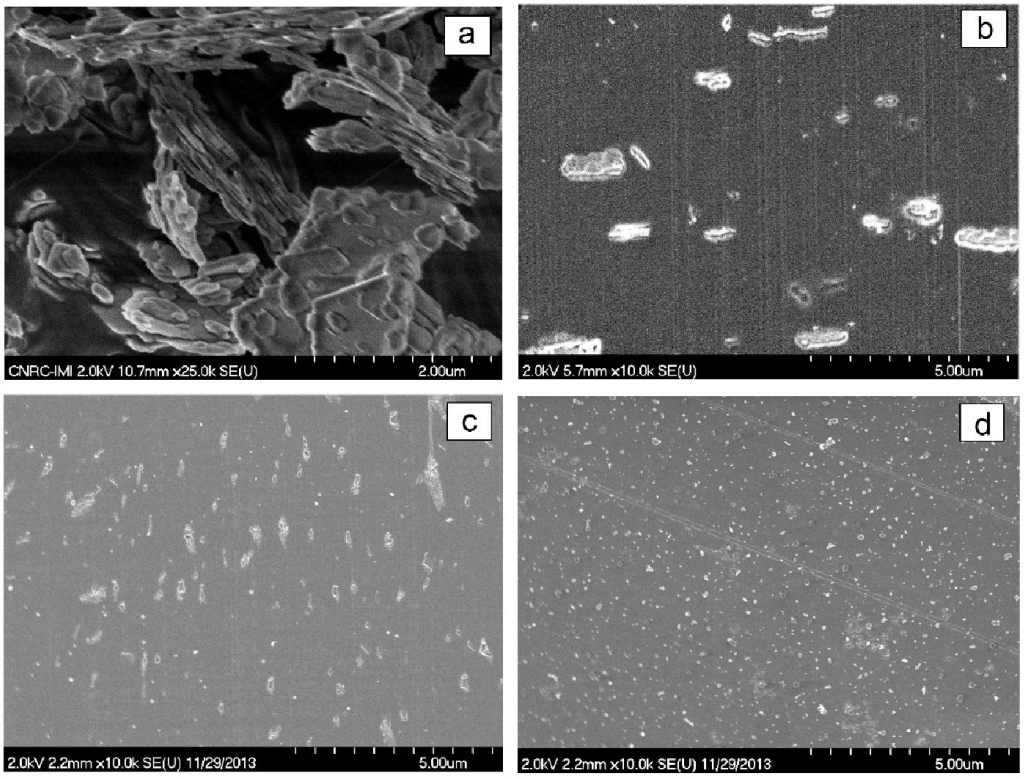

Figure 7-4 SEM micrographs: (a) asreceived CKao, (b) PET-CKao 2%, (c) PET-gUlt 2%, and (d) PET-gUlt 2%-PKHA

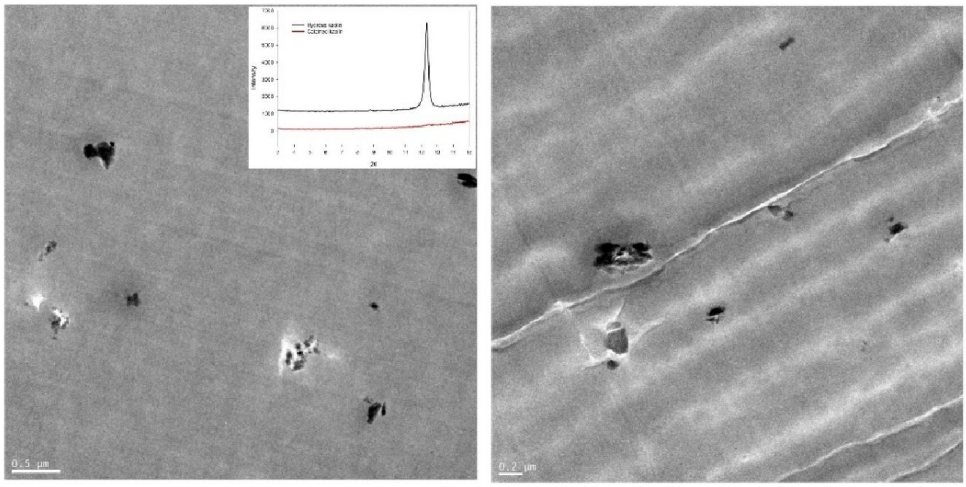

Figure 7-5 TEM micrographs of the PET-gUlt 2%-PKHA nanocomposite.

The SEM images in Figure 7-4 show the morphology of asreceived calcined kaolin and PET-gUlt nanocomposites. One can see that large agglomerates of calcined kaolin particles are dispersed and submicron particles, observed as white spots, are distributed within the PET matrix.

The transmission electron micrograph (TEM) of the PET-gUlt 2%-PKHA nanocomposite is shown in Figure **7-5**. The nanocomposite seems to have a particulate nanostructured morphology. It is obvious that the morphology of calcined kaolin particles is different from what observed for other layered-structure nanocomposites so that the irregularly shaped particles, sized in the range from 50 to 200 nm, are observed rather than individual layers. It should be noticed that layers of calcined kaolin were not observed even at very high magnifications. Since the calcination process is associated with the collapse of the interlayer spaces and a disappearance of the basal distances, calcined kaolin may not be considered as a layered structure [16]. A simple comparison between the XRD patterns of calcined and hydrous kaolin (shown in Figure **7-5**) confirms the structural alternation of particles as a result of calcination. It is shown that the characteristic peak of hydrous kaolin at 2θ=12.4°, indicating the d-spacing of 0.72 nm between the layers, is not observe for calcined kaolin.

7.3.3 Rheology

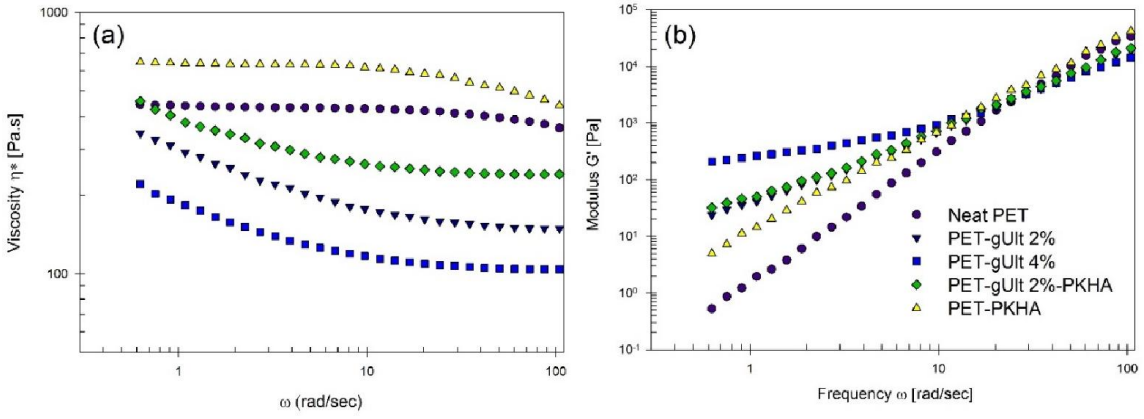

Figure 7-6 (a) Complex viscosity and (b) elastic modulus of neat PET and the PET nanocomposites measured at 270°C as a function of frequency.

Figure 7-6a shows the complex viscosity (η^*) of neat PET and PET nanocomposites measured at 270°C as a function of frequency. The neat PET and PET-PKHA exhibited a Newtonian behaviour at low frequencies with a shear thinning exponent, *n,* of −0.02. For PET-PKHA the Newtonian plateau was shorter due to the effect of phenoxy resin. The PET-gUlt nanocomposite with 2 wt% filler content showed shear thinning behavior with an exponent *n* equal to -0.30. As the loading increased, the complex viscosity curve shifted to lower values, however, the shear thinning trend remained the same. The viscosity loss is due to the degradation of PET during the melt processing which consequently decreases the molecular weight of the polymer. The addition of PKHA could compensate this loss to some extent, as shown in Figure **7-6**a.

Storage modulus (G') of neat PET and PET-gUlt composites measured as a function of frequency and the results are presented in Figure **7-6**b. The rheological behavior of the nanocomposites was totally different from that of neat polymer. The typical power law rule, $G' \sim \omega^2$, was valid for unfilled polymer (PET and PET-PKHA) at low frequencies. The rheological behavior in the terminal zone was however altered after the introduction of gUlt particles to the system so that G' increased dramatically and the dependence of G' on ω became smaller at low frequency. This behaviour was also observed for other polymer nanocomposites such as poly(propylene) [17], polystyrene [18] and polyamide-12 [19], and poly(lactic acid) [20] and was attributed to a pseudo-solid-like structure or a network of nanoparticles in the material which restrains the long-range motion of polymer chains. By increasing the filler loading from 2 to 4 wt%, storage modulus increased at low frequencies and the terminal slope of the G' declined from 1.04 to 0.42. The addition of PKHA slightly affected the G' and reduced the terminal slope to 0.90 which highlights the important role of matrix viscosity on the dispersion of particles.

At high frequencies, the effect of gUlt particles on the rheology is not considerable and the behavior of melt will be dominated by the PET matrix. The nanoparticles may restrain the large-scale relaxations of polymer chains in a nanocomposites, however, they do not have a remarkable impact on the short-range dynamics of the chains in length scales comparable to the entanglement length [21]. At high frequencies, the difference between the G' of neat and filled PET was much smaller and G' decreased with particle loading due to possible degradation of the PET matrix.

7.3.4 Tensile properties

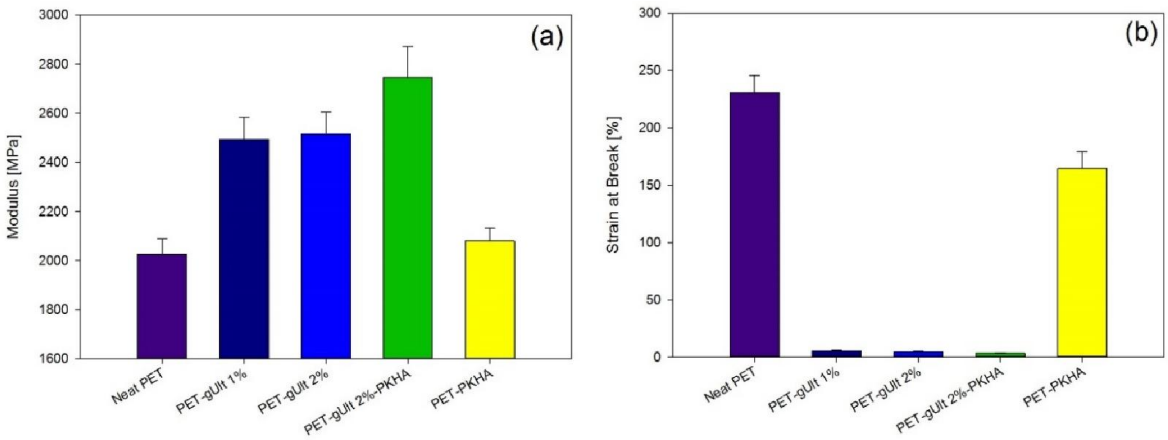

Figure 7-7 (a) Tensile modulus and (b) elongation at break of neat PET and PET-gUlt nanocomposites.

Generally speaking, the addition of nanoparticles into polymer matrices is expected to improve the final properties. The tensile modulus and the elongation at break of neat PET and PET-gUlt nanocomposites were determined by tensile machine and are shown in Figure **7-7**. It was observed that the elastic modulus increased upon the addition of 1 wt% gUlt particles. However, with increasing the filler content to 2 wt% further improvement was not observed. Since the enhancement of composites is directly depends on the interactions between the filler and the matrix in the interface, the dispersion level and surface area of the particles might be a critical parameter affecting the final properties. It seems that increasing the filler loading leads to the partial aggregation of particles which subsequently decreases the surface area.

With the addition of PKHA the improvement was higher and 35.6% improvement was observed in elastic modulus. This could be assigned to the increased molecular weight of PET matrix in presence of phenoxy resin, as shown by rheological measurements.

Transition from ductile to brittle behavior in the stress-strain response is one the characteristics of polymer nanocomposite. As shown in Figure **7-7**b, the improvement in modulus of PET nanocomposites was associated with a drastic reduction in elongation at break. The same effect has been reported for other nanocomposite and some reasons such as restricted mobility of the polymer chains due to the interaction with nanoparticles, stress concentration around the particles, and failure of filler aggregates have been mentioned to explain this brittle behavior [22–24].

7.3.5 Thermo-mechanical properties

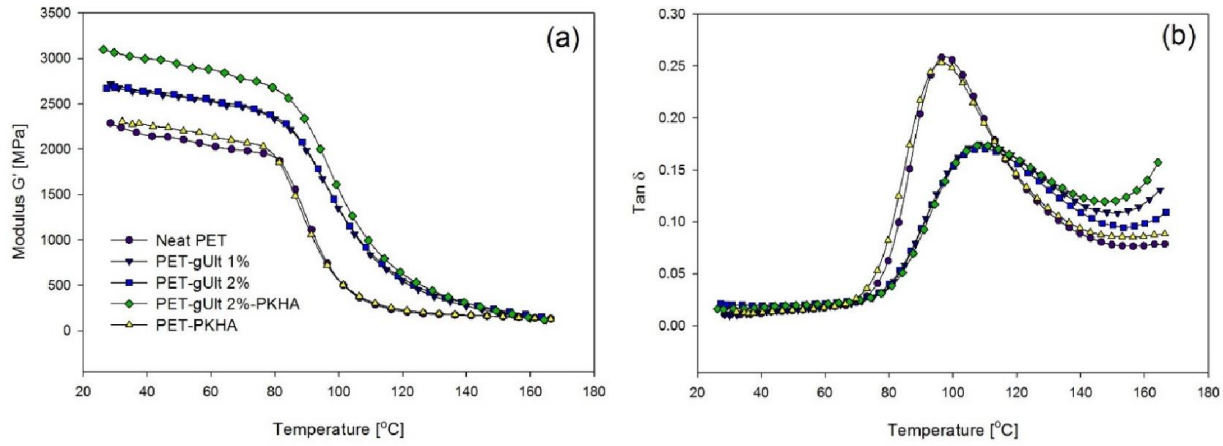

Figure 7-8 Temperature dependence of (a) storage modulus and (b) tan δ measured by DMA at 1 Hz.

The storage modulus and tan δ temperature dependencies for neat PET and the PET-gUlt nanocomposites are shown in Figure 7-8. The nanocomposites exhibited higher storage modulus over the entire temperature range (25-170°C) compared to neat PET. Table 7-1 presents the ratio of the storage modulus of the composite (G'_{com}) to that of neat PET (G'_{PET}) at 40°C. With the addition of 2 wt% gUlt, the modulus was improved by 21% and the improvement was more pronounced in case of samples containing both gUlt and PKHA (40%). This may be ascribed to

the higher molecular weight of PET-gUlt-PKHA compared to that of PET-gUlt. As shown by rheological measurements, PKHA can lessen the degradation of PET during the extrusion process which results in a higher molecular weight of the PET matrix.

As displayed in Figure 7-8b, the tan δ that corresponds to the dissipation of the energy showed a peak at about 97 and 110 °C for the neat PET and the nanocomposites, respectively. This peak is attributed to the glass transition temperature. After incorporation of gUlt nanoparticles, the tan δ peak shifted to higher temperatures by approximately 11-13 °C, furthermore the area under the tan δ peak decreased. The shift of the tan δ peak to a higher temperature may be assigned to restricting effect of particles on cooperative motion of PET chains. This effect was reported for other composite systems such as polyimide-clay nanocomposites [22] and PVDF-clay nanocomposites [25].

The decrease in the height of tan δ peak could be attributed to the confinement of polymer chains by nanoparticles. The magnitude of tan peak is directly proportional to the free motion of polymer chains within the amorphous phase, therefore the neat PET with higher amorphous fraction exhibits higher tan δ peak. The crystallinity and particle–polymer interactions may constrain the PET chains and hinder their free motion. By incorporation of gUlt particles, the crystallinity of the samples did not change (Table 7-1), however, the volume fraction of polymer constricted by particles would increase which resulted in a lower magnitude of tan δ peak [26].

Table 7-1 Crystallinity of samples and the ratio of the storage modulus of the composite (G'_{com}) to that of neat PET (G'_{PET}).

	Relative crystallinity X_c [%]	**G'_{com}/ G'_{PET}**
Neat PET	28.8	1
PET-gUlt 1%	29.8	1.22
PET-gUlt 2%	29.7	1.23
PET-gUlt 2%-PKHA	29.3	1.40
PET-PKHA	26.8	1.05

7.3.6 Barrier properties

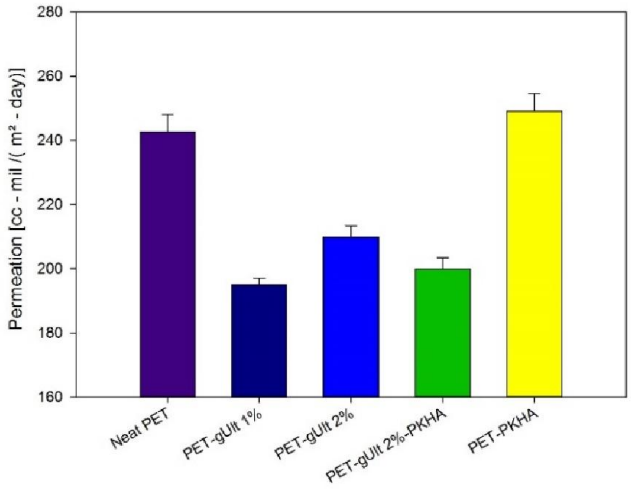

Figure 7-9 Oxygen permeability of neat PET and its nanocomposites.

Figure 7-9 shows the measured oxygen permeability of neat PET and its nanocomposites. For all the filled samples, the permeability was lower than that of neat PET due to both the presence of gUlt particles and a higher crystallinity. By incorporation of gUlt nanoparticles to PET, about 20% reduction in oxygen permeability was observed. However, increasing the filler loading from 1 to 2 wt% slightly deteriorated the barrier properties which could be due to the agglomeration of particles by increasing the filler content. The improvement in barrier properties of polymer nanocomposites was reported elsewhere [5,27,28] and was attributed to the decrease of solubility (due to the reduced polymer matrix volume) and more tortuous path for penetrant molecules. The silicate particles distributed in the polymer matrix are assumed to be impermeable barriers which induce a longer diffusion pathway for diffusing molecules.

7.3.7 Optical properties

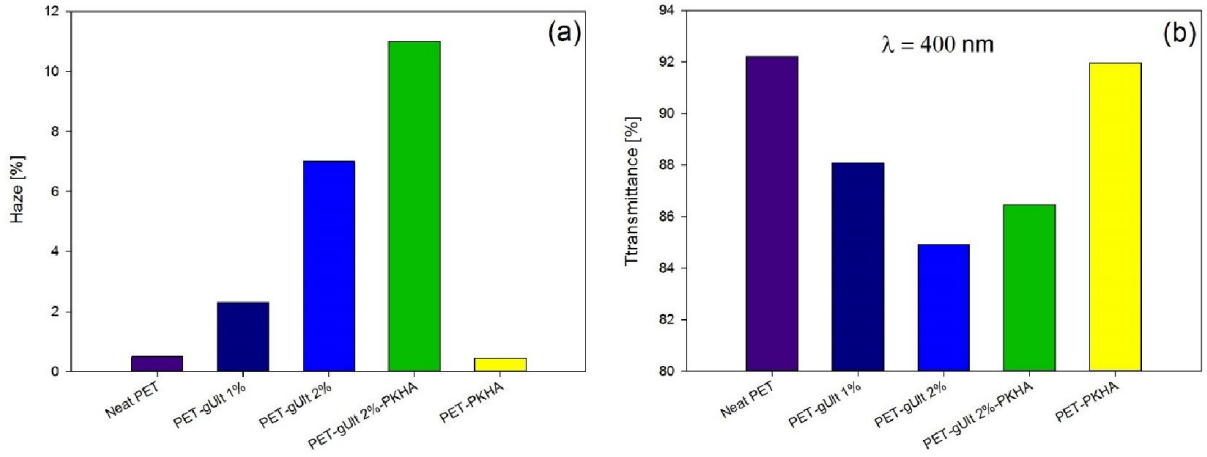

Figure 7-10 Optical properties of PET and its nanocomposites (a) Haze and (b) Light transmittance.

Haze percentage and light transmittance of neat PET and its nanocomposites are shown in Figure 7-10. Due to scattering and absorption of light, all the nanocomposites had higher haze and lower transmittance with respect to neat PET. As shown in Figure 7-10a, the haze jumped from 0.5% to 2.5 and 7% after incorporation of 1 and 2 wt% of particles, respectively and this increase in haze percentage was associated with a loss in transmittance. The addition of phenoxy resin did not have a big effect on optical properties of PET, however, a synergistic effect was observed in presence of gUlt particles. A material is considered to be transparent as long as the haze is lower than 30% [29], therefore one can say that all the PET nanocomposites prepared were optically transparent.

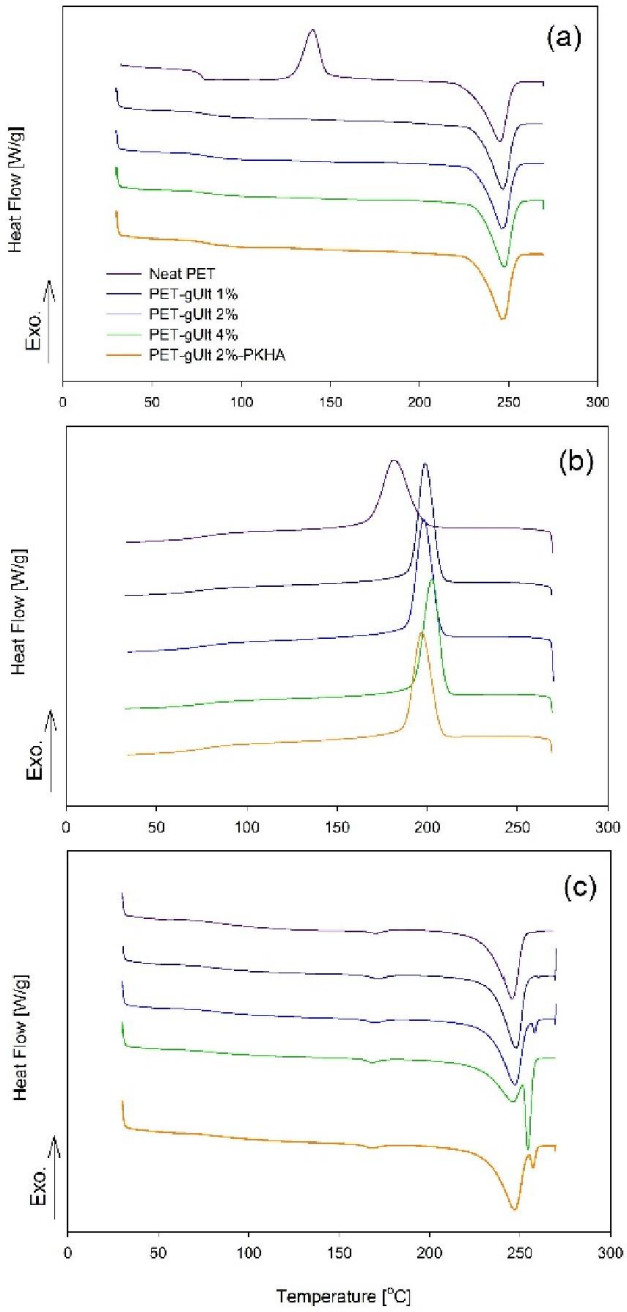

Figure 7-11 DSC thermograms PET and its composites: (a) heating, (b) cooling, and (c) heating after annealing at 200°C.

7.3.8 Thermal properties

7.3.8.1 DSC

Figure 7-11a and b show the heating (melting) and cooling (crystallization) cycles for neat PET and its nanocomposites, respectively. The incorporation of gUlt did not have any effects on the

melting behavior of PET and the melting peaks were observed around 246°C in all cases, as shown in Figure 7-1a. However, the relative crystallinity (X_c) of the nanocomposites was significantly higher than that of the neat PET, as observed in Table 7-2. The cold crystallization peak, observed for neat PET at 140°C, did not exist for nanocomposites. This indicates that recrystallization is hindered due to the incorporation of gUlt particles.

Table 7-2 DSC data of PET and its nanocomposites.

	T_m (°C)	$T_{c,m}$ (°C)	X_c [%]
Neat PET	245.3	181.3	9.2
PET-gUlt 1%	246.8	198.8	28.2
PET-gUlt 2%	246.8	198.0	28.7
PET-gUlt 4%	246.5	202.1	29.2
PET-gUlt 2%-PKHA	246.9	188.2	27.6

The crystallization temperature ($T_{c,m}$) of nanocomposites was higher than that of the neat PET (Figure 7-11b). The higher $T_{c,m}$ observed for the nanocomposites was reported elsewhere [30,31] and was related to the heterogeneous nucleation effect of the gUlt particles which could provide higher number of nuclei in the PET matrix. In presence of gUlt the segments of the PET chains may interact with the particles to form the crystallization nuclei.

Figure 7-11c shows the heating cycle of samples annealed for 1 h at 200°C. The melting of annealed PET nanocomposites was reflected by a double-melting behavior, so that a new sharp peak appeared at about 257°C and its magnitude gradually increases with increasing filler content. This behavior could be assigned to the melting/recrystallization of primary crystals during the heating process which results in the formation of two crystalline phases with different sizes, thickness and ordering. The melting of crystals restrained by the filler particles could be another reason [32,33].

7.4 Conclusion

Ground calcined-kaolin nanoparticles (gUlt) were prepared by use of stirred media wet-grinder and then were dispersed in a PET matrix via melt extrusion technique to form PET-gUlt nanocomposite. SEM and TEM micrographs revealed that the ground particles are uniformly dispersed in the matrix. It was also shown that the addition of viscosity modifier (PKHA) can significantly improve the dispersion of particles. Rheological frequency measurements confirmed the formation of a network-like structure in the samples due to the particle-particle or particle-polymer interactions. It was also noticed that the incorporation of particles resulted in a viscosity loss. However the addition of a phenoxy resin modifier (PKHA) could compensate this viscosity loss to some extent.

DMA and tensile tests showed that the modulus of all nanocomposites were enhanced. The highest improvement (about 40%) was observed for the composite containing 2 wt% of gUlt and phenoxy resin (PKHA), however, the elongation at break was remarkably reduced due to brittleness induced by the presence of nanoparticles. The incorporation of gUlt particles improved the barrier properties of PET as well. The particles caused more haziness in the films, however, the nanocomposites were still transparent. Due to the degrading effect of gUlt particles on PET chains, the nanocomposites exhibited smaller viscosity compared to that of neat PET. The thermal properties such as crystallinity and crystallization temperature of PET were considerably altered as a result of nucleating role of particles.

7.5 Acknowledgment

The authors gratefully acknowledge PepsiCo for support of this work.

7.6 References

[1] Oya A, Kurokawa Y, Yasuda H. Factors controlling mechanical properties of clay mineral/polypropylene nanocomposites. J Mater Sci 2000;35:1045–50.

[2] Vaia RA, Ishii H, Giannelis EP. Synthesis and properties of two-dimensional nanostructures by direct intercalation of polymer melts in layered silicates. Chem Mater 1993;5:1694–6.

[3] P. D, Alexandre M, Dubois P. Polymer-layered silicate nanocomposites: preparation, properties and uses of a new class of materials. Mater Sci Eng R 2000;28:1–63.

[4] Fischer H. Polymer nanocomposites: from fundamental research to specific applications. Mater Sci Eng C 2003;23:763–72.

[5] Ghanbari A, Heuzey M-C, Carreau PJ, Ton-That M-T. Morphology and properties of polymer/organoclay nanocomposites based on poly(ethylene terephthalate) and sulfopolyester blends. Polym Int 2013;62:439–48.

[6] Bergaya F, Theng BKG, Lagaly G. Handbook of Clay Science. Elsevier Science; 2011.

[7] Kakali G, Perraki T, Tsivilis S, Badogiannis E. Thermal treatment of kaolin: the effect of mineralogy on the pozzolanic activity. Appl Clay Sci 2001;20:73–80.

[8] Alexe M, Harnagea C, Visinoiu A, Pignolet A, Hesse D, Gösele U. Patterning and switching of nano-size ferroelectric memory cells. Scr Mater 2001;44:1175–9.

[9] Mende S, Stenger F, Peukert W, Schwedes J. Mechanical production and stabilization of submicron particles in stirred media mills. Powder Technol 2003;132:64–73.

[10] Stenger F, Götzinger M, Jakob P, Peukert W. Mechano-Chemical Changes of Nano Sized α-Al2O3 During Wet Dispersion in Stirred Ball Mills. Part Part Syst Charact 2004;21:31–8.

[11] Sakthivel S, Pitchumani B. Production of Nano Talc Material and Its Applicability as Filler in Polymeric Nanocomposites. Part Sci Technol 2011;29:441–9.

[12] Weit H, Schwedes J. Scale-up of power consumption in agitated ball mills. Chem Eng Technol 1987;10:398–404.

[13] Joost B, Schwedes J. Comminution of white fused alumina and wear of grinding beads in stirred media mills. PT. 1. The effect of the grinding chamber geometry and the hardness of the grinding beads on the grinding result. Ceram. Forum Int., vol. 73, 1996, p. 365–71.

[14] Bilgili E, Hamey R, Scarlett B. Production of pigment nanoparticles using a wet stirred mill with polymeric media. China Particuology 2004;2:93–100.

[15] Stenger F, Mende S, Schwedes J, Peukert W. Nanomilling in stirred media mills. Chem Eng Sci 2005;60:4557–65.

[16] Sperinck S, Raiteri P, Marks N, Wright K. Dehydroxylation of kaolinite to metakaolin-a molecular dynamics study. J Mater Chem 2011;21:2118–25.

[17] Solomon MJ, Almusallam AS, Seefeldt KF, Somwangthanaroj A, Varadan P. Rheology of Polypropylene/Clay Hybrid Materials. Macromolecules 2001;34:1864–72.

[18] Zhao J, Morgan AB, Harris JD. Rheological characterization of polystyrene–clay nanocomposites to compare the degree of exfoliation and dispersion. Polymer (Guildf) 2005;46:8641–60.

[19] Hoffmann B, Kressler J, Stöppelmann G, Friedrich C, Kim G-M. Rheology of nanocomposites based on layered silicates and polyamide-12. Colloid Polym Sci 2000;278:629–36.

[20] Wu D, Wu L, Wu L, Zhang M. Rheology and thermal stability of polylactide/clay nanocomposites. Polym Degrad Stab 2006;91:3149–55.

[21] Du F, Scogna RC, Zhou W, Brand S, Fischer JE, Winey KI. Nanotube Networks in Polymer Nanocomposites: Rheology and Electrical Conductivity. Macromolecules 2004;37:9048–55.

[22] Agag T, Koga T, Takeichi T. Studies on thermal and mechanical properties of polyimide–clay nanocomposites. Polymer (Guildf) 2001;42:3399–408.

[23] Cho JW, Paul DR. Nylon 6 nanocomposites by melt compounding. Polymer (Guildf) 2001;42:1083–94.

[24] Fischer B, Ziadeh M, Pfaff A, Breu J, Altstädt V. Impact of large aspect ratio, shear-stiff, mica-like clay on mechanical behaviour of PMMA/clay nanocomposites. Polymer (Guildf) 2012;53:3230–7.

[25] Priya L, Jog JP. Poly(vinylidene fluoride)/clay nanocomposites prepared by melt intercalation: Crystallization and dynamic mechanical behavior studies. J Polym Sci Part B Polym Phys 2002;40:1682–9.

[26] Shelley JS, Mather PT, DeVries KL. Reinforcement and environmental degradation of nylon-6/clay nanocomposites. Polymer (Guildf) 2001;42:5849–58.

[27] Gain O, Espuche E, Pollet E, Alexandre M, Dubois P. Gas barrier properties of poly(ε-caprolactone)/clay nanocomposites: Influence of the morphology and polymer/clay interactions. J Polym Sci Part B Polym Phys 2005;43:205–14.

[28] Russo GM, Simon GP, Incarnato L. Correlation between Rheological, Mechanical, and Barrier Properties in New Copolyamide-Based Nanocomposite Films. Macromolecules 2006;39:3855–64.

[29] Ram A. Fundamentals of Polymer Engineering. Springer; 1997.

[30] Wang Y, Gao J, Ma Y, Agarwal US. Study on mechanical properties, thermal stability and crystallization behavior of PET/MMT nanocomposites. Compos Part B Eng 2006;37:399–407.

[31] Ghasemi H, Carreau PJ, Kamal MR. Isothermal and non-isothermal crystallization behavior of PET nanocomposites. Polym Eng Sci 2012;52:372–84.

[32] Phang IY, Pramoda KP, Liu T, He C. Crystallization and melting behavior of polyester/clay nanocomposites. Polym Int 2004;53:1282–9.

[33] Carli LN, Crespo JS, Mauler RS. {PHBV} nanocomposites based on organomodified montmorillonite and halloysite: The effect of clay type on the morphology and thermal and mechanical properties. Compos Part A Appl Sci Manuf 2011;42:1601–8.

CHAPTER 8: ARTICLE 4: POLYETHYLENE TEREPHTHALATE/CALCINED KAOLIN COMPOSITES: EFFECT OF UNIAXIAL STRETCHING ON THE PROPERTIES

Khalil Shahverdi-Shahraki[1], Tamal Ghosh[2], Kamal Mahajan[2], Abdellah Ajji[1]*, Pierre J. Carreau[1]

[1] *CREPEC, Department of Chemical Engineering, École Polytechnique de Montréal, Canada*

[2] *PepsiCo Advanced Research - Beverage Packaging, Hawthorne, NY, USA*

Submitted to *Polymer Engineering & Science.*

Abstract

This paper aimed at investigating the effect of calcined kaolin filler (CKao) on polyethylene terephthalate (PET). The influence of silane coupling agent, chain extension, and post extrusion uniaxial hot-stretching on the final properties of the produced composites were studied as well. PET-CKao films were prepared via melt blending in a twins screw extruder followed by stretching above glass transition temperature at controlled conditions. The morphology of the composites before and after stretching was observed by SEM. Rheological measurements were also performed to characterize the polymer melts. Mechanical and optical properties as well as oxygen transmission rate (OTR) of the composites were also investigated. The results showed that addition of calcined kaolin particles, even at low filler content, had a great reinforcing effect on mechanical and barrier properties of PET matrix. This effect was more pronounced in case of hot-stretched samples. The main drawback observed with this calcined kaolin particles was an increased haze in the final composites. Processing parameters including stretching temperature and stretching ratio were found to have a significant effect on final properties, however the influence of stretching rate was negligible.

Keywords: PET composite, Calcined kaolin, Stretching, Properties

8.1 Introduction

PET is a commodity grade polyester which has found many applications such as textile fibers and food packaging materials due to its good chemical resistance, thermal stability, and mechanical properties. However, to minimize the economic and environmental impacts of PET (as raw or waste material), it is always preferable to improve its various physical properties through mixing with fillers, particularly if they are less costly.

Polymer/layered silicate nanocomposites, as a new class of composite materials, have received an extensive attentions in the last 20 years [1–5]. Generally speaking, layered silicates incorporate improved mechanical performance, thermal stability, and barrier properties to polymer materials, at relatively low filler contents compared to that of conventional composites [6–10]. However, the majority of research on polymer nanocomposites has been conducted on a limited number of fillers including montmorillonite clay, silica, and calcium carbonate.

Kaolin is a type of clay primarily composed of the mineral kaolinite with minor amounts of impurities such as quartz, feldspar and other clay minerals. Kaolinite ($Al_2O_3.2SiO_2.2H_2O$) is a hydrated aluminosilicate with 1:1 layer structure consisting of an octahedral aluminum hydroxide sheet and a tetrahedral silica sheet [11]. Kaolin is relatively low-cost and readily available worldwide. It has a wide range of application in the ceramic, cosmetic and pulp and paper industries. Pristine kaolin is calcined by firing the powder to a temperature around 650°C to lose both surface-adsorbed and chemically bonded water (lattice water). Calcination at higher temperatures leads to the complete dehydroxylation and formation of partially crystalline metakaolin. Fully calcined products are produced above 950°C which has an amorphous spinel structure [12].

Since the surface of mineral fillers is generally hydrophilic, they are incompatible with the polymer matrix. It has been known for many years that chemical treatment of a filler surface can promote the compatibility and dispersion of the particles into a polymer matrix. Treatment of particles with silane coupling agent has been extensively applied to different types of fillers such as TiO_2 [13] and clay minerals [14–16]. In this research, an epoxy functional silane was used to examine the effect of silane treatment of calcined kaolin on the properties of PET composites.

Polymer science and technology involves in general two steps: i) the synthesis and production of raw materials and ii) the processing of the previous materials for the fabrication of end-use plastic products. Many industrial polymer forming processes such as blow molding or thermoforming involve secondary processing including uniaxial and biaxial stretching. Therefore, having a good knowledge of how this type of deformation can influence the polymer-clay composites is of great importance. It has been demonstrated that biaxial stretching of PET-silica can significantly affects the filler dispersion [17]. Litchfield and Baird studied uniaxial stretching of spun fibers above their glass transition temperature (T_g) and concluded that secondary processing can enhance the mechanical properties [18].

It has been previously shown that chemically modified kaolin can be dispersed in a PET matrix, however, the existence of hydroxyl groups in the structure resulted in degradation and molecular weight loss which spoils the final properties of the composite. In this paper, the effect of calcined kaolin particles on morphological, mechanical, optical, and gas-barrier properties of PET resin was investigated. Secondary processing, such as hot-stretching, effect on the properties of PET-CKao composites are also investigated.

8.2 Experimental

8.2.1 Materials

A commercial grade PET resin (Laser+® 7000) with an intrinsic viscosity of 0.84 dL/g provided by DAK Americas LLC was used as polymer matrix. A commercial calcined grade kaolin (Ultrex® 96), denoted hereafter as CKao, from BASF Corporation was used in this study. It is a dehydroxylated aluminosilicate with a density of 2.63 g/cm3 (at 25°C) and an average particle size of 1.2 μm. In order to raise the melt viscosity and molecular weight of the PET resin, an FDA-

approved masterbatch of PET with a chain extender (denoted hereafter as ch), from Polyvel Inc., was added during the melt mixing. A silane coupling agent, 3-(Glycidoxy-propyl) trimethoxysilane (denoted hereafter as SiE), supplied by Gelest was used for silanization of the surface of particles.

8.2.2 Characterization and Testing

A Hitachi S4700 SEM instrument with a cold field emission gun under an acceleration voltage of 2 kV was used to examine the morphological characteristics of the composites. The samples were microtomed using an Ultracut FC microtome (Leica, Germany) with a diamond knife and gold coating was subsequently applied to make them conductive.

The structure and crystal size of the composites were investigated by wide angle X-Ray diffraction (WAXD). The WXRD patterns were recorded over scattering angles, 2θ, range from 10 to 40° on a Philips X'pert diffractometer (CuKα radiation, λ=1.54056 A°) operating at a voltage of 50 kV and current of 40 mA.

Rheological measurements were carried out under nitrogen atmosphere on a stress-controlled rheometer (Bohlin Gemini HR nano, Malvern) with a parallel plate geometry using 25 mm diameter plates and 1 mm gap size. The rheometer was equipped with a convection oven to control the temperature at 270°C for all the samples.

Melting and crystallization characteristics of the samples were determined by differential scanning calorimetry (DSC) using a DSCQ1000 TA Instrument at a heating/cooling rate of 10 ºC/min under helium atmosphere. Thermal gravimetric analysis (TGA) was carried out on a TGA500 TA Instrument. About 10 mg of the samples were heated at 10°C/min from 30 to 700°C under nitrogen atmosphere.

The mechanical properties were measured in tensile mode at room temperature using an Instron universal testing machine (Model 3365) with 500 N load-cell at a strain rate of 25 mm/min.

In order to determine barrier properties of the composites, oxygen transmission rates (OTRs) were measured at 23°C under a barometric pressure 700 mmHg using an Ox-Tran oxygen permeability MD Module (Model 2/21) from Mocon. The permeability coefficients were calculated by normalizing (multiplying) measured OTR values by the films thickness.

Haze values were determined according to ASTM D1003 using a LAMBDA 1050 spectrophotometers from PerkinElmer.

8.2.3 Sample preparation

8.2.3.1 Applying silane coupling agent

Modification of CKao particles was accomplished via aqueous alcohol solutions method. An ethanol-deionized water (90/10 wt%) solution was adjusted to pH 4.5-5.5 with acetic acid. The required amount of silane coupling agent was added drop wise to yield a 4% final concentration and the mixture was stirred for 10 min for hydrolysis and silanol formation. Then, the temperature was increased to at 80°C, CKao particles were added into the solution and the grafting reaction was completed under stirring for 2 hr. The product was filtered and extensively washed with ethanol in order to remove the excess silane and finally dried at 50 °C in a vacuum oven.

8.2.3.2 Preparation of the PET-CKao composites

The PET powder (PET granules were ground in liquid nitrogen to obtain a fine powder of PET) was manually mixed with CKao for a few minutes and then the mixture was melt-blended via a twin screw extruder (LEISTRITZ Extruder Corp., L/D=40) to obtain a 20 wt% masterbatch. The

temperature profile was set in the range of 250-275°C and the screw rotating speed was 150 rpm. The masterbatch was eventually diluted with neat PET and the final films with 2-8 wt% filler content were prepared via cast film extrusion process. Unless otherwise indicated, for all the composites, the filler loading was 2 wt% and PET-CKao-ch composite contains 0.5 wt% chain extender. Prior to processing, all the materials were dried in a vacuum oven at 110°C for 24 h to eliminate the moisture and prevent hydrolysis reactions during the melt compounding.

8.2.3.3 Uniaxial Stretching of composites

Rectangular PET sheets having 10 cm wide, 40 mm long and 100 μm thick, cut from the extruded films, were uniaxially stretched in an Instron mechanical testing machine (ElectroPuls™ E3000) equipped with an environmental chamber. The stretching temperature was set in the range of 90 to 120ºC and specimens were strained up to draw ratios of 2 to 4 and rapidly cooled down to room temperature with air flow.

8.3 Results and discussion

8.3.1 Effect of Silane coupling agent and chain extender

8.3.1.1 Morphology

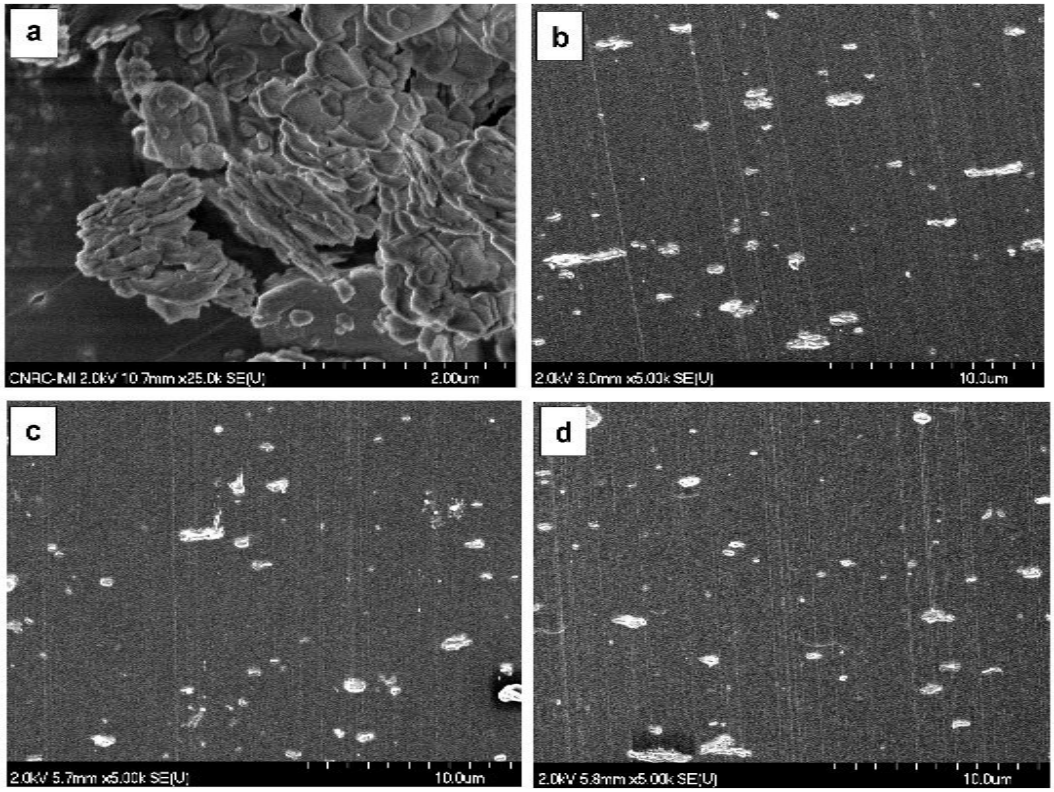

Figure 8-1 SEM micrographs of (a) Neat PET, (b) PET-CKao, (c) PET-CKao-SiE, and (d) PET-CKao-ch

SEM images of as-received calcined kaolin, PET-CKao, PET-CKao-SiE, and PET-CKao-ch composites are shown in Figure 8-1. As-received kaolin has a layered structure (Figure 8-1a). During the calcination process at high temperatures, dehydroxylation occurs, the layers collapse and a tightly-stacked structure is formed. However, this process does not change the layered structure of the material. After blending with PET, large CKao aggregates break up to form smaller particles (<1 μm) uniformly dispersed in the matrix (Figure 8-1b). However, very few particles in the range of 2-3 μm could be still observed in the image. It seems that the silane treatment and

addition of chain extender has a small effect on the morphology of composites as well. The size of dispersed particles is slightly smaller in the case of samples treated with silane coupling agent (Figure 8-1c) or those containing a small amount of chain extender (Figure 8-1d). The chain extender can react with the end groups of PET chains and provide a chemical link between them, so increases molecular weight and subsequently the viscosity of PET during the melt process. Due to increased viscosity, the particles in the extruder will undergo a higher shear field which promotes the breaking of particles and results in a smaller particle size.

8.3.1.2 Rheology

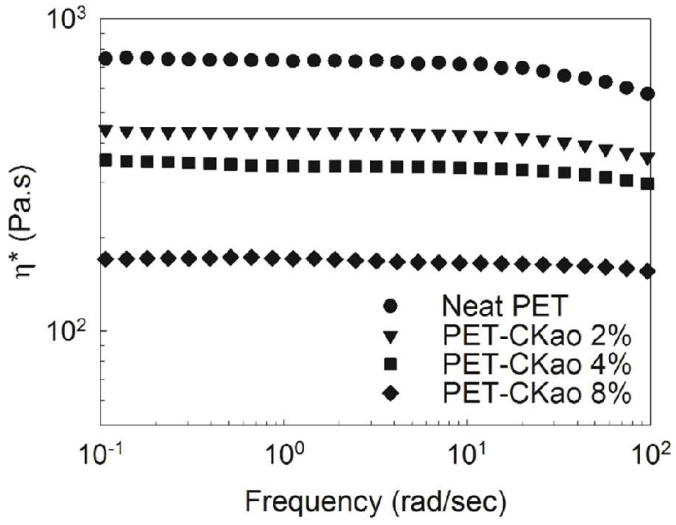

Figure 8-2 Complex viscosity of Neat PET and PET-CKao composites

The rheological properties of neat PET and PET-CKao with different filler loadings are presented in Figure 8-2. From frequency sweep measurements, one can clearly see that PET and its composites show a Newtonian behavior in most of the frequency range examined. At high frequencies, the viscosity becomes slightly shear thinning. The constant melt viscosity at low frequencies is known as the zero shear viscosity and is proportional to molecular weight of a polymer to the power 3.4 [19]. Filled PET generally shows a complex viscosity lower than that of neat PET and increasing the filler loading results in even lower viscosities. This effect suggests

that the presence of calcined kaolin particles intensify the degradation of PET chains, which lowers the molecular weight and the melt viscosity of samples.

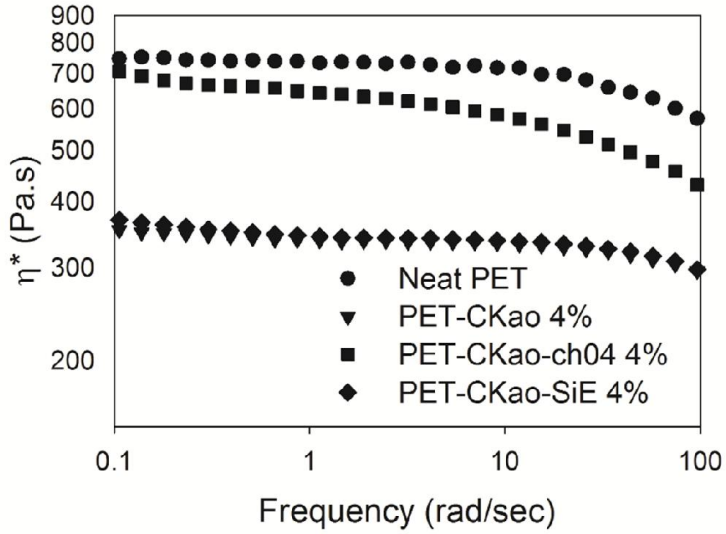

Figure 8-3 Effect of chain extender and silane coupling agent on the melt viscosity of PET-CKao composites.

Furthermore, to find the effect of chain extender and silane coupling agent on the viscosity of the samples, the frequency (ω) dependence of the complex viscosity (η*) for PET-CKao, PET-CKao-ch, and PET-CKao-SiE composites with 4 wt% of filler are presented in Figure 8-3. Modification of CKao with silane coupling agent does not seem to have a significant effect on the rheological properties of PET. However, the composite containing the chain extender displays higher viscosity and a pronounced shear thinning behavior. The chain extender acts as a bridge connecting the polymer chains and increases the molecular weight of PET. Thus, the shear thinning behavior could be due to the formation of long chain branches and broadening of the molecular weight distribution of PET because of the possible reactions with the chain extender. Long chain branching develops an entanglement network that confine the mobility of the polymer chains and consequently affect the rheological behavior of PET [20,21].

8.3.1.3 Thermal properties

8.3.1.3.1 DSC

Table 8-1 DSC Data of neat PET and PET-CKao composites (second heating).

Samples	T_g (°C)	Cold crystallization		Melting		T_c (°C)	x_c (%)
		T_{cc} (°C)	ΔH_{cc} (J/g)	T_m (°C)	ΔH_m (J/g)		
Neat PET	78.9	134.8	22.5	245.3	32.6	180.7	7.2
PET-CKao (2 wt%)	78.4	132.0	3.8	247.0	36.4	201.5	23.5
PET-CKao-ch (2 wt%)	76.1	135.9	19.8	243.6	30.1	187.2	7.4
PET-CKao-SiE (2 wt%)	75.8	134.2	19.8	245.2	34.2	190.7	10.4

Table 8-1 exhibit non-isothermal DSC Data of neat PET and PET-CKao composites. Melting temperature (T_m) and glass-transition temperature (T_g) of the composites remains approximately the same regardless of CKao incorporation. However, crystallization temperature (T_c) shifted to higher temperatures, which is attributed to the nucleating effect of CKao particles [21]. Furthermore, this effect results in higher crystallinity (X_c) in the composites. It is also shown that addition of a chain extender has a hindering effect on the crystallization of PET matrix, as is revealed by the decrease in the crystallization temperature. Apparently, chain extender molecules can act as branching point and cause difficulty for chains mobility and their rearrangement in the crystalline structure. The Data presented in Table 8-1 also shows that silane modification has a similar effect on the crystallization behavior of PET. It seems that the silane coupling agent molecules cover the particles, obstructing the migration and diffusion of PET chains to the surface of the CKao (as nucleus).

8.3.1.3.2 TGA

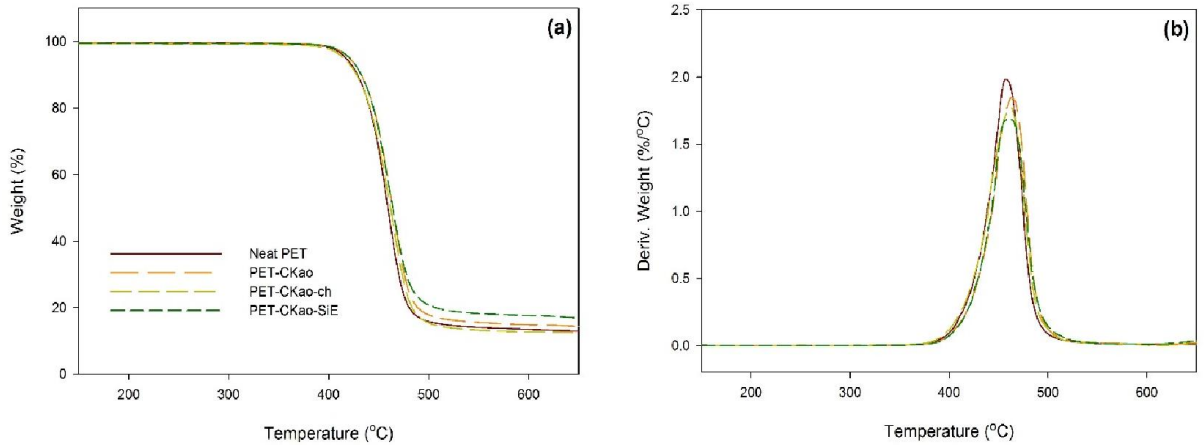

Figure 8-4 TGA Data PET and PET-CKao composites with 2 wt% filler content under Nitrogen atmosphere at heating rate 10°C/min: (a) weight loss, (b) derivative weight loss.

Thermal stability of neat PET and the composites under inert atmosphere (nitrogen) was investigated by TGA and the results are presented in Figure 8-4. A single decomposition step was observed for all samples. The decomposition of neat PET started around 390°C and an identical temperature was observed for all the composites. However, for the composites the temperature of maximum decomposition rate ($T_{d,max}$) is slightly increased (by 4-7°C) compared to that of neat polymer. These results suggest that the incorporation of CKao can slightly enhance the thermal stability of PET.

8.3.1.4 Mechanical properties

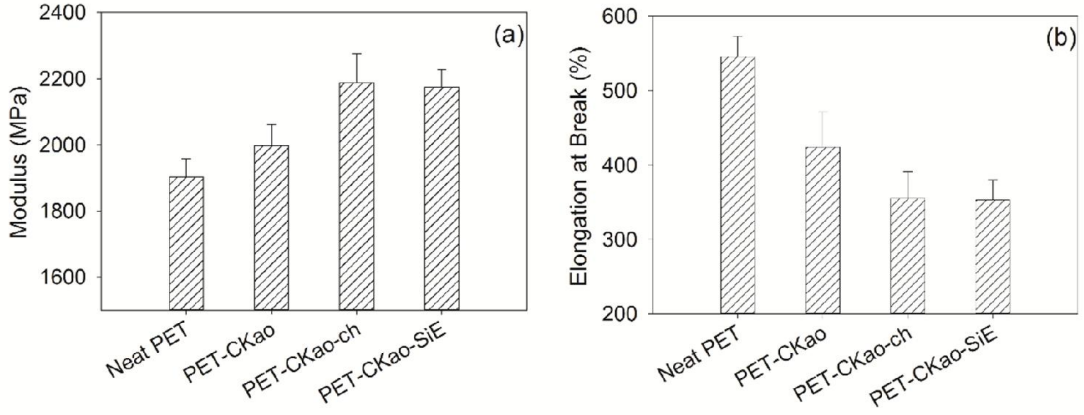

Figure 8-5 Effect of silane coupling agent and chain extender on (a) modulus and (b) elongation at break of PET-CKao composites with 2 wt% filler content

Figure 8-5 exhibits tensile properties of neat PET and PET-CKao composites. For neat PET, the tensile modulus was 1930 MPa and with the addition of 2 wt% CKao, the modulus raised to 2050 MPa. It is well known that filler particles can diminish polymer chain mobility, resulting in less flexibility and higher modulus [22]. The improvement of modulus is more pronounced for PET-CKao-SiE composite. Silane treatment provides a stronger interaction (chemical bonds) between PET molecules and filler particles, and thus results in better stress transfer and more enhancement of modulus. It is also shown that addition of a chain extender has a reinforcing effect on the tensile properties of the composite, probably due to the increased molecular weight and formation of a long chain branching structure [23]. On the other hand, the incorporation of CKao particles had an adverse influence on ductility of samples, thus the increment in modulus was accompanied with 130% and 200% decrease in the elongation at break of PET-CKao and PET-CKao-SiE, respectively, compared to that of neat PET (Figure 8-5b). Similar observation have been previously reported for other polymer/clay composites such as epoxy/organoclay, PLA/MMT, and PET/MMT [24–26].

8.3.2 Effect of Stretching on PET-CKao composites

8.3.2.1 Mechanical properties

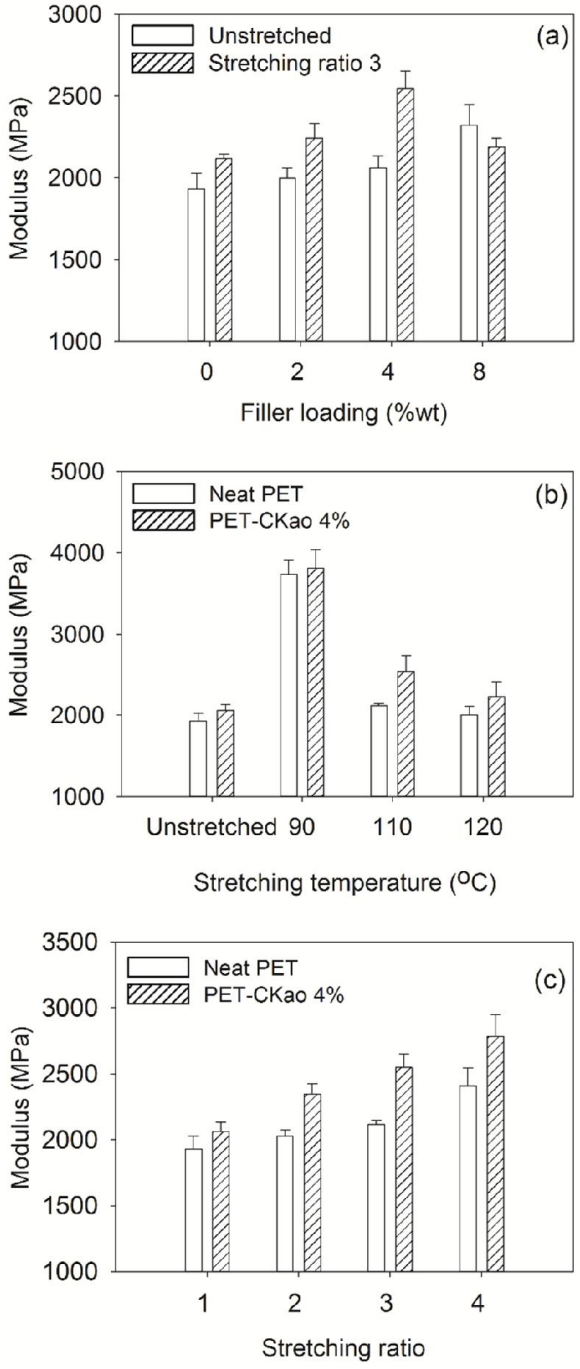

Figure 8-6 Tensile modulus of neat PET and PET-CKao composites: (a) effect of filler loading, (b) effect of stretching temperature, and (c) effect of stretching ratio.

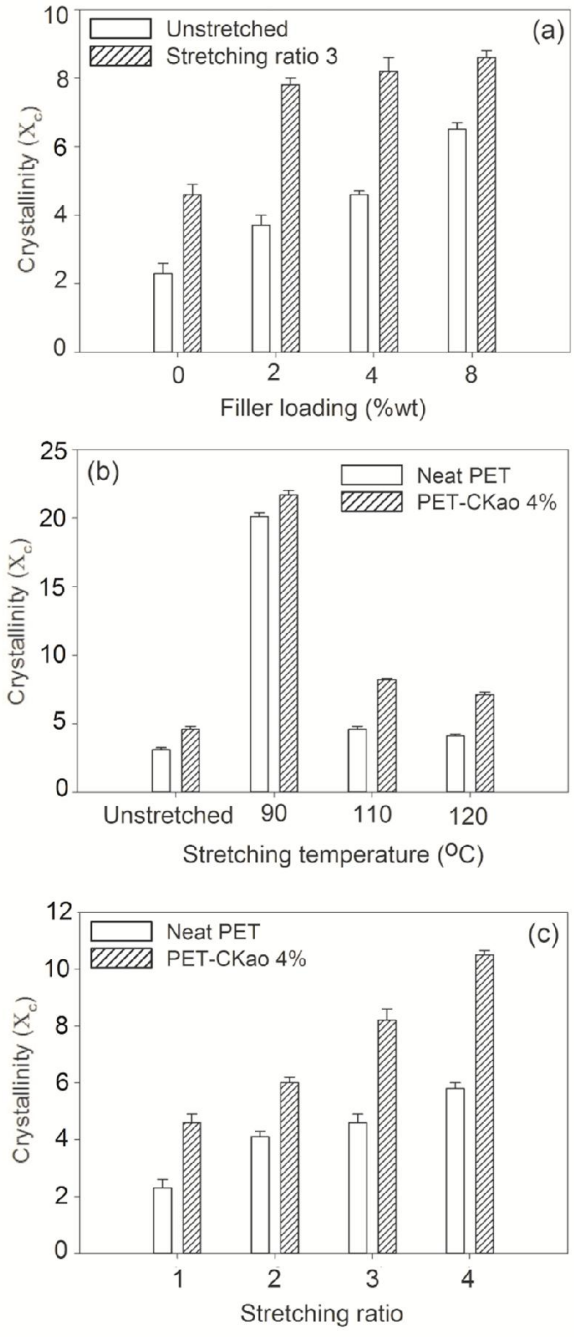

Figure 8-7 Relative crystallinity of neat PET and PET-CKao composites: (a) effect of filler loading, (b) effect of stretching temperature, and (c) effect of stretching ratio.

Figure **8-6**a displays the modulus of stretched and unstretched neat PET and PET-CKao composites with different filler content. The results show that, in case of unstretched samples, modulus increases gradually as filler loading increases from 0 to 8 wt%. However, this effect was more remarkable at higher filler contents. This improvement in Young's modulus can be attributed to the reinforcing effect of CKao particles dispersed in the PET matrix.

Two main parameters are considered to have the greatest influence on the mechanical properties of composite materials; the incorporation of particles which have relatively higher elastic modulus compared to polymer matrix and the relative crystallinity of the samples, since the crystalline domains act as high stiffness domains. The crystallinity of neat PET and PET-CKao composites was determined by DSC and are displayed in

Figure **8-7**. It is shown that the crystallinity of unstretched PET-CKao composites increases with filler content, however, it does not change after being stretched (

Figure **8-7**a).

For composites with the same filler content, hot-stretched ones have significantly higher tensile modulus. This is attributed to the increased molecular orientation and strain-induced crystallization of the PET chains during the stretching process. The only exception to this is the composite with 8 wt% of CKao. One should note that, during the melt mixing of samples with higher filler contents, formation of aggregates occurs which can significantly decrease the specific surface area of the filler and deteriorate filler-matrix adhesion. Moreover, this can negatively affect the wetting of filler by polymer matrix which subsequently gives rise to development of voids and micro-cracks

in the composite [27]. The vicinity of these voids and flaws are considered as stress concentration points that impair the effective load transfer through the interface between the matrix and the filler. In contrast to stretched samples, this phenomenon is not significant in the case of unstretched films, because the stretched samples have already undergone a debonding between the phases during the hot-stretching step.

Figure **8-6**b shows the effect of stretching temperature on tensile modulus of neat PET and PET composites. It can be clearly observed that, for both neat and filled PET, samples stretched at lower temperatures have significantly higher modulus which could be assigned to the effect of crystals formed during the stretching and higher orientation developed at lower stretching temperatures. As presented in

Figure **8-7**b, the relative crystallinity of composite stretched at 90 °C is much higher than unstretched ones or those stretched at 110 °C.

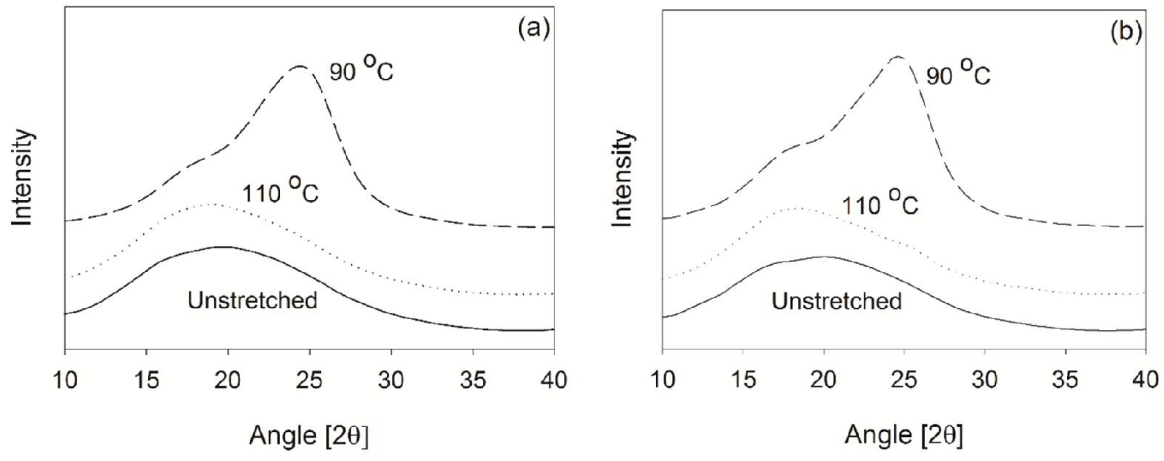

Figure 8-8 XRD patterns of (a) Neat PET and (b) PET-CKao4%. Stretching ratio was 4 for both samples.

The wide-angle X-ray diffraction patterns for the neat PET and the 4wt% calcined kaolin filled composites are displayed in Figure 8-8a and b, respectively. A characteristic diffraction pattern of PET is generally broad and composed of the amorphous phase and reflections of the crystalline phase. The diffractogram of samples stretched at 90℃ shows a diffraction pattern with a new single peak centered on 2θ=25° indicating the formation of the crystalline phase in the samples due to molecular orientation and crystallization during the stretching process. The molecular orientation gives rise to a narrow distribution of both the amorphous and the crystalline phase [28]. In case of unstretched samples and those stretched at high temperatures (110°C) the diffractogram displays a very broad peak centered around 2θ=20°. This is characteristic of glassy PET and is attributed to the amorphous phase. It is also noticeable that the crystalline phase is formed for all samples stretched at 90 °C regardless of the addition of CKao.

The effect of stretching ratio on tensile modulus is displayed in

Figure **8-6**c. One can see that for both neat PET and PET-CKao modulus is increased by stretching ratio. This is assigned to the increased orientation of PET chains and strain-induced crystallization at higher stretching ratios. In all cases, stretched PET-CKao films have higher modulus compared to stretched neat PET. More improvement in the modulus of PET–CKao, compared to neat PET, is likely to be a result of combined effect of incorporation of CKao particles and enhanced crystallinity (due to the particles, as shown in

Figure **8-7**). It has also been reported that this could be due to the better alignment of filler particles and the reduced agglomeration after stretching [29,30].

8.3.2.2 Barrier properties

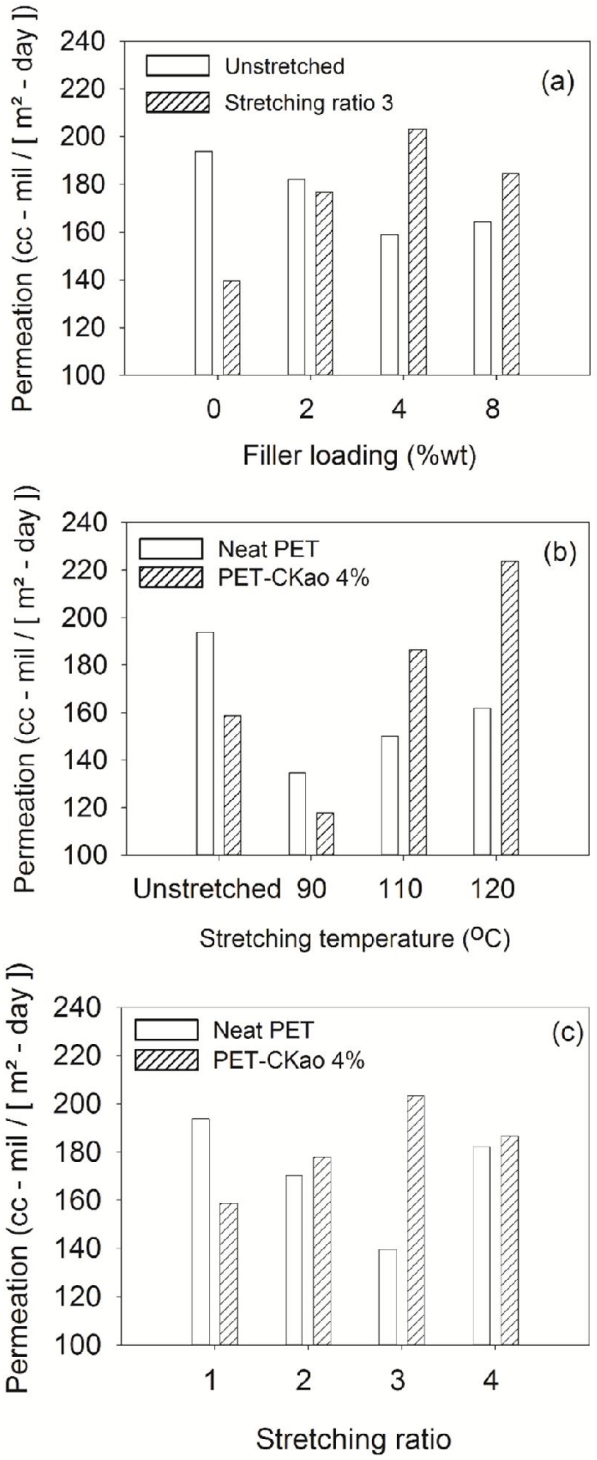

Figure 8-9 Oxygen permeability of neat PET and PET-CKao composites: (a) effect of filler loading, (b) effect of stretching temperature, and (c) effect of stretching ratio.

Figure 8-9 displays oxygen permeability of neat PET and PET-CKao composites as a function of filler loading, temperature, and stretching ratio respectively. As shown in Figure 8-9a, the PET-CKao composites have better barrier properties (lower OTR) than neat PET. The main reasons for this barrier improvement are: (i) decrease of the solubility of oxygen due to the reduced volume fraction of PET in composites (PET volume fraction < 1) compared to neat PET samples (PET volume fraction = 1) and (ii) increase in the tortuosity of the gas diffusion path by CKao particles [9]. There was an 18% reduction in OTR coefficient at 4 wt% CKao loading. However for filler loadings higher than 4 wt%, due to the agglomeration of particles, the filler content does not significantly influence the permeability. As can be observed, permeability of 8 wt% composite is only slightly higher than that of 4 wt% composite.

After stretching, an opposite trend is observed in the barrier properties. For stretched samples the permeability increases with the filler content. Three different parameters can affect the permeability of composites: the barrier effect of particles as impermeable obstacles, the amount of crystalline domains in the sample, and the agglomeration of particles. Increasing the CKao content enhances the relative crystallinity of PET (

Figure **8-7**) and, at the same time, facilitates the formation of agglomerates in the composite. For stretched samples with filler content up to 4 wt%, the effect of crystallinity is dominant. However, at higher filler loadings, agglomeration of particles, debonding at the interface, and formation of voids compensate for crystallinity effect and augment OTR values.

Figure 8-9b displays the oxygen permeability of samples stretched at different temperatures. The lowest oxygen permeation was observed for samples stretched at 90°C and it was increased at higher stretching temperatures because the orientation and crystallinity of the samples stretched at

90°C are much higher than that of the others. PET-CKao composites stretched at temperatures higher than 90°C show higher permeation compared to neat PET which again can be assigned to the effect of crystallinity and formation of micro-voids as discussed in previous section.

The effect of the stretching ratio on the permeability of PET composites has been studied as well, and the results are shown Figure 8-9c. The permeation of neat PET decreases by applying higher stretching ratio up to 3, after which it shows an increase. However exactly the opposite trend was observed in case of filled PET.

8.3.2.3 Optical properties

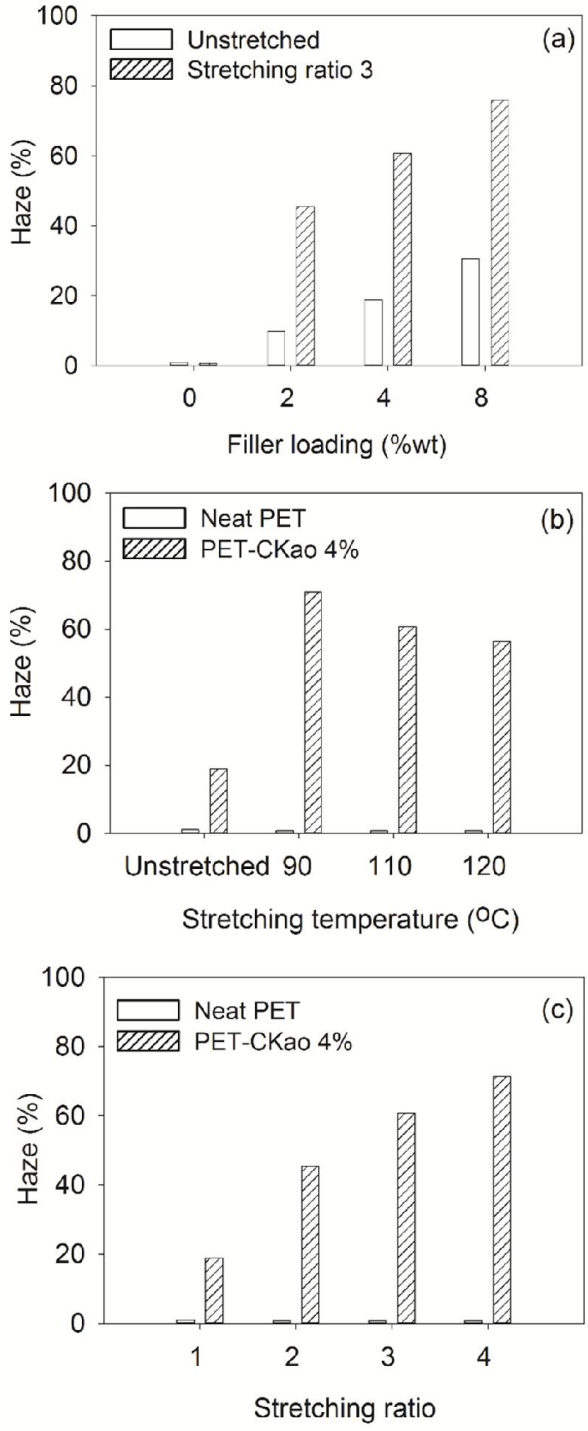

Figure 8-10 Haze of neat PET and PET-CKao composites: (a) effect of filler loading, (b) effect of stretching temperature, and (c) effect of stretching ratio.

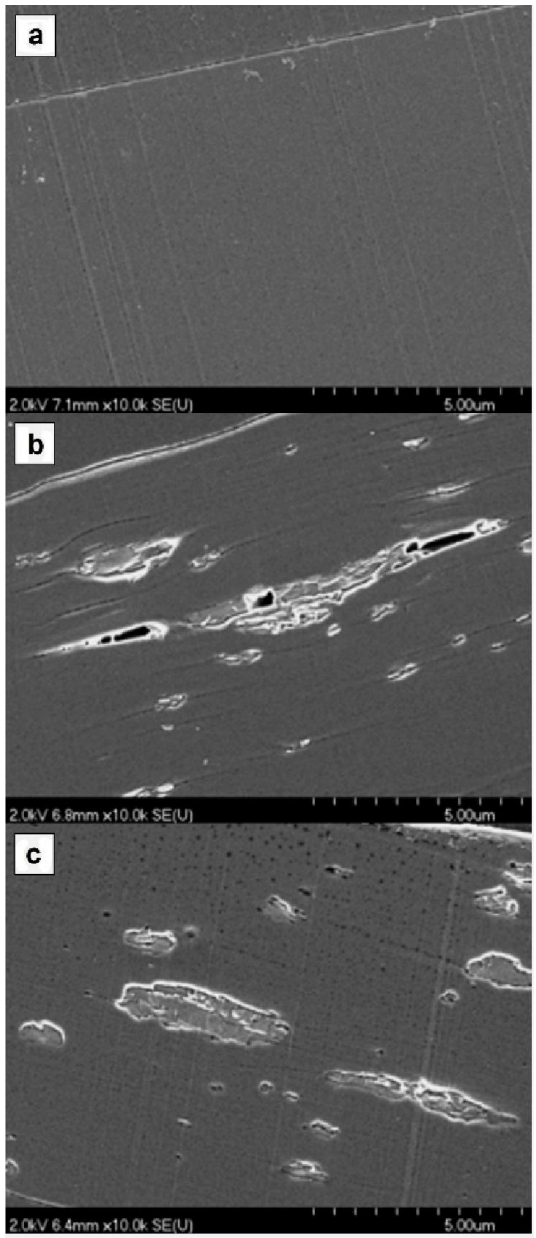

Figure 8-11 SEM micrographs of (a) neat PET stretched at 90℃, (b) PET-CKao (4 wt%) stretched at 90℃, and (c) PET-CKao (4 wt%) stretched at 120℃. Stretching ratio was 3 for all samples.

Figure 8-10 depicts the haze values of neat PET and PET-CKao films as a function of filler loading, temperature, and stretching ratio respectively. Haze describes the ability to divert light in a material (lower is the haze, more transparent is the material) and is defined as the percentage of light that is deflected more than 2.5° from the incident light direction [31]. The haze is remarkably affected by the presence of the filler and increases with the CKao content. The higher the concentration of filler and larger are the aggregates, the more haziness in the film would be observed. As shown in Figure 8-10a, the haze jumped from 0.8 % for neat PET to 30 % for PET-CKao 8%. This can be explained by the dispersion level and size of the CKao particles inside the PET matrix. Figure 8-11 displays SEM micrographs of the cross section of stretched neat PET and PET-CKao composites. It is evident from the images that the size of the dispersed particles is of the order of magnitude of the wavelength of visible light which can cause light diffraction and make the samples hazier [32].

Figure 8-10a shows also that hot stretching has a significant influence on the haziness of PET-CKao films. After being stretched, the haze jumped from 10% to 45%, from 19% to 60%, and from 30% to 75% for PET-CKao composites containing 2 wt%, 4 wt%, and 8 wt% CKao, respectively. One should note that the haze can be affected by many factors other than particle dispersion. The formation of voids and micro-cracks in the sample seems to be one of the main reasons. As discussed above, during the stretching process, debonding between filler particles and the PET matrix takes place and some voids and cracks are formed around the particles. These voids, that are elongated in the stretching direction (Figure 8-11b), can cause additional scatter of light. The size of the voids in the film increases as a result of stretching and cause more haziness in the films.

Figure 8-10b shows the effect of stretching temperature on the haze. In the case of neat PET, the haze value remains less than 1 % regardless of stretching temperature. By contrast, the haze of filled samples depends on the stretching temperature. As the stretching temperature increases, haze

value decreases. According to the DMA results (not shown in this paper) glass transition temperature (T_g) of PET falls between 85°C and 90°C, therefore the modulus of PET would be remarkably decreased (more than 80%) when temperature is changed from 90°C to 120°C. Therefore, due to low modulus at higher temperatures debonding is less likely to occur in the interface. Stretching ratio is another parameter that can affect the haze of composites. As shown in Figure 8-10c, the higher stretching ratio results in higher haze in the samples. But again for neat PET the haze value is not changed by stretching ratio.

8.4 Conclusion

PET and calcined kaolin were melt mixed in a twin screw extruder to produce PET-CKao composites. SEM images revealed that the final average size of dispersed particles was sub-micron. Rheological study exhibited that degradation of PET occurs during the melt mixing with CKao and leads to lower melt viscosity and a loss in the molecular weight. Nevertheless, modulus enhancement was still observed despite the reduction in the molecular weight. It was demonstrated that the incorporation of calcined kaolin has a positive effect on the thermo-mechanical and barrier properties of PET, however the presence of CKao impair the optical properties of PET and lead to more haziness. DSC results showed that crystallization temperature of PET-CKao was shifted to higher values, compared to neat PET, due to the nucleation effect of filler particles and TGA analysis indicated a slight improvement of thermal stability of PET after the introduction of CKao particles. A silane treatment of particles and addition of chain extender were shown to promote the final properties of composites as well.

The composites with different amount of filler were subjected to uniaxial stretching under various processing conditions. It was concluded that stretching of samples above Tg had a great effect on

neat PET and PET-CKao composites, however this effect was more pronounced in case of filled samples. Furthermore, this improvement was attributed to a stress induced crystalline structure and orientation of PET chains. Decreasing stretch temperature significantly improved mechanical and barrier properties of the samples while stretch ratio had a smaller effect. SEM images showed that debonding between the filler and PET matrix was the main reason for increased haziness in samples after stretching.

8.5 Acknowledgment

The authors gratefully acknowledge PepsiCo for the support of this work.

8.6 References

[1] Yano K, Usuki A, Okada A, Kurauchi T, Kamigaito O. Synthesis and properties of polyimide–clay hybrid. J Polym Sci Part A Polym Chem 1993;31:2493–8.

[2] Ma J, Qi Z, Hu Y. Synthesis and characterization of polypropylene/clay nanocomposites. J Appl Polym Sci 2001;82:3611–7.

[3] Tsai T-Y, Li C-H, Chang C-H, Cheng W-H, Hwang C-L, Wu R-J, et al. Preparation of Exfoliated Polyester/Clay Nanocomposites. Adv Mater 2005;17:1769–73.

[4] Costache MC, Heidecker MJ, Manias E, Wilkie CA. Preparation and characterization of poly(ethylene terephthalate)/clay nanocomposites by melt blending using thermally stable surfactants. Polym Adv Technol 2006;17:764–71.

[5] Ghasemi H, Carreau PJ, Kamal MR, Uribe-Calderon J. Preparation and Characterization of PET/Clay Nanocomposites by Melt Compounding. Polym Eng Sci 2011;51:1178–87.

[6] Yangchuan K, Chenfen L, Zongneng Q, Z.N. Q, Ke Y, Long C, et al. Crystallization, properties, and crystal and nanoscale morphology of PET-clay nanocomposites. J Appl Polym Sci 1999;71:1139–46.

[7] Pegoretti A, Kolarik J, Peroni C, Migliaresi C. Recycled poly(ethylene terephthalate)/layered silicate nanocomposites: morphology and tensile mechanical properties. Polymer (Guildf) 2004;45:2751–9.

[8] Wang Y, Gao J, Ma Y, Agarwal US. Study on mechanical properties, thermal stability and crystallization behavior of PET/MMT nanocomposites. Compos Part B Eng 2006;37:399–407.

[9] Ghasemi H, Carreau PJ, Kamal MR, Tabatabaei SH. Properties of PET/clay nanocomposite films. Polym Eng Sci 2012;52:420–30.

[10] Ghanbari A, Heuzey M-C, Carreau PJ, Ton-That M-T. Morphology and properties of polymer/organoclay nanocomposites based on poly(ethylene terephthalate) and sulfopolyester blends. Polym Int 2013;62:439–48.

[11] Bergaya F, Theng BKG, Lagaly G. Handbook of Clay Science. Elsevier Science; 2011.

[12] Kakali G, Perraki T, Tsivilis S, Badogiannis E. Thermal treatment of kaolin: the effect of mineralogy on the pozzolanic activity. Appl Clay Sci 2001;20:73–80.

[13] Zhao J, Milanova M, Warmoeskerken MMCG, Dutschk V. Surface modification of TiO2 nanoparticles with silane coupling agents. Colloids Surfaces A Physicochem Eng Asp 2012;413:273–9.

[14] Wen B, Xu X, Gao X, Ding Y, Wang F, Zhang S, et al. Highly Exfoliated Poly(Ethylene Terephthalate)/Clay Nanocomposites via Melt Compounding: Effects of Silane Grafting. Polym Plast Technol Eng 2011;50:362–71.

[15] Spencer MW, Hunter DL, Knesek BW, Paul DR. Morphology and properties of polypropylene nanocomposites based on a silanized organoclay. Polymer (Guildf) 2011;52:5369–77.

[16] Kim ES, Shim JH, Woo JY, Yoo KS, Yoon JS. Effect of the silane modification of clay on the tensile properties of nylon 6/clay nanocomposites. J Appl Polym Sci 2010;117:809–16.

[17] Jéol S, Fenouillot F, Rousseau A, Masenelli-Varlot K, Gauthier C, Briois J-F. Drastic Modification of the Dispersion State of Submicron Silica during Biaxial Deformation of Poly(ethylene terephthalate). Macromolecules 2007;40:3229–37.

[18] Litchfield DW, Baird DG. The role of nanoclay in the generation of poly(ethylene terephthalate) fibers with improved modulus and tenacity. Polymer (Guildf) 2008;49:5027–36.

[19] Fetters LJ, Lohse DJ, Richter D, Witten TA, Zirkel A. Connection between Polymer Molecular Weight, Density, Chain Dimensions, and Melt Viscoelastic Properties. Macromolecules 1994;27:4639–47.

[20] Dealy JM, Wissbrun KF. Melt Rheology and Its Role in Plastics Processing: Theory and Applications. Springer; 1999.

[21] Macosko CW. Rheology: Principles, Measurements, and Applications. Wiley; 1994.

[22] Gu A, Kuo S-W, Chang F-C. Syntheses and properties of PI/clay hybrids. J Appl Polym Sci 2001;79:1902–10.

[23] Najafi N, Heuzey MC, Carreau PJ, Wood-Adams PM. Control of thermal degradation of polylactide (PLA)-clay nanocomposites using chain extenders. Polym Degrad Stab 2012;97:554–65.

[24] Lai M, Kim J-K. Effects of epoxy treatment of organoclay on structure, thermo-mechanical and transport properties of poly(ethylene terephthalate-co-ethylene naphthalate)/organoclay nanocomposites. Polymer (Guildf) 2005;46:4722–34.

[25] Najafi N, Heuzey MC, Carreau PJ. Polylactide (PLA)-clay nanocomposites prepared by melt compounding in the presence of a chain extender. Compos Sci Technol 2012;72:608–15.

[26] Ghanbari A, Heuzey MC, Carreau PJ, Ton-That MT. A novel approach to control thermal degradation of PET/organoclay nanocomposites and improve clay exfoliation. Polymer (Guildf) 2013;54:1361–9.

[27] Premalal HGB, Ismail H, Baharin A. Comparison of the mechanical properties of rice husk powder filled polypropylene composites with talc filled polypropylene composites. Polym Test 2002;21:833–9.

[28] Nunes RAX, Costa VC, Calado VM de A, Branco JRT. Wear, friction, and microhardness of a thermal sprayed PET: poly (ethylene terephthalate) coating. Mater Res 2009;12:121–5.

[29] Shen Y, Harkin-Jones E, Hornsby P, McNally T, Abu-Zurayk R. The effect of temperature and strain rate on the deformation behaviour, structure development and properties of biaxially stretched PET–clay nanocomposites. Compos Sci Technol 2011;71:758–64.

[30] Soon K, Harkin-Jones E, Rajeev RS, Menary G, Martin PJ, Armstrong CG. Morphology, barrier, and mechanical properties of biaxially deformed poly(ethylene terephthalate)-mica nanocomposites. Polym Eng Sci 2012;52:532–48.

[31] Meeten GH. Optical properties of polymers. Elsevier Applied Science Publishers; 1986.

[32] Hyun K, Chong W, Koo M, Chung IJ. Physical properties of polyethylene/silicate nanocomposite blown films. J Appl Polym Sci 2003;89:2131–6.

CHAPTER 9: GENERAL DISCUSSION

The incorporation of smectite type layered silicates in PET resins in order to develop a nanocomposite with improved final properties has been extensively studied. The dispersion of silicate particles, compatibility between PET and modified clay, thermal stability of the modifier and PET itself at elevated processing temperatures are the main challenges in this area. In this study, rather than just focusing on smectite type clay (montmorillonite), the dispersion of another class of silicate material (kaolin) in PET matrix was examined. Our findings showed that despite the high bonding energy and adherence between the layers of kaolin, the delamination of particles in PET was possible using an indirect procedure (displacement method).

To overcome the strong bonding forces between the layers and facilitate the dispersion of kaolin layers, the particles were initially modified through a chemical and mechanical treatment. For the chemical part, the particles were treated with potassium acetate (KAc) and/or dimethyl sulfoxide (DMSO). Upon pre-intercalation with KAc and DMSO, new diffraction peaks in the XRD patterns at 2θ lower than that of pristine kaolin appeared. This is interpreted as the opening of kaolin structure and represents larger *d*-spacing values between the layers. The mechanical treatment (dry grinding) decreases the intensity of the peaks and after 30 min, just a broad peak with a very small intensity remains. This phenomenon is ascribed to the degradation of the crystalline structure of kaolinite due to rupture of the alumina and silica layers. Although grinding can reduce the particle size by applying mechanical energy, it is associated with chemical phenomena, which can alter the molecular structure of kaolin. FTIR and TGA results revealed that for longer grinding times the hydroxyl groups in the structure of kaolin are converted to water (dehydroxylation).

In the second step, the pre-intercalated kaolin particles were blended with polyethylene oxide (PEO) and PET, respectively. High molecular weight and long chains of PET may provide more

shear forces for the melt mixing process in the extruder. However, these chains cannot penetrate easily into the gallery spaces of kaolin. Therefore, PEO, as a hydrophilic polymer with relatively low molecular weight, was initially blended with the particles in order to facilitate their dispersion. When KAc-treated kaolin was blended with PET, the intensity of the characteristic diffraction peak of hydrous kaolin ($2\theta=12.46°$ corresponding to a *d*-spacing of 0.72 nm) was considerably reduced. This implied that kao-KAc was more delaminated in the PET matrix. Eventually, for the PET-(kao-KAc-PEO) nanocomposite, due to the partial delamination and destruction of the crystalline structure of kaolin layers in the PET matrix, no peaks was detected in the diffraction pattern. The SEM and TEM micrographs showed nano-size tactoids, comprising a few layers of kaolin within the PET matrix, while no large-scale aggregates were observed. This indicated that the quality of the distributive mixing and the dispersion of the particles was good: however, a complete exfoliation was not achieved. On the average, the size of nanoscale particles ranged from 100 to 200 nm in length and 10-50 nm in thickness in the PET/kaolin nanocomposite.

DSC results revealed the heterogeneous nucleation effects of the kaolin particles on the crystallization of PET, which lowered the crystallization temperature and increased the crystallization rate. However, the total crystallinity of PET did not undergo a considerable change because the particles may act as physical barriers against the crystal growth compensating their nucleating effect. Nonisothermal crystallization kinetic of PET/kaolin nanocomposites was carried out based on the Avrami equation. The kinetic parameters of crystallization (n and Z_c) were a function of cooling rate. For nanocomposites, n was in the range of 1.5 to 2 while it increased to values above 2 for higher heating rates indicating the three-dimensional growth of crystals. Furthermore the incorporation of kaolin particles led to a larger Z_c at a given cooling rate indicating that crystallization was faster in the presence of particles; however, the addition of chain extender

eliminated this effect and retained Z_c of composites almost equal to that of neat PET.

TGA data showed that chemical treatment of particles with KAc and PEO influenced the thermal stability of PET and shifted the decomposition temperature to slightly lower values. Our studies revealed that hydrous kaolin caused considerable degradation during melt processing and reduced the molecular weight of PET. This effect was more pronounced in the case of chemically treated particles and might be caused by different mechanisms such as mechanical, thermal and chemical (hydrolysis) degradation. The existence of hydroxyl groups on the surface of kaolin layers might be one of the main reasons, which could catalyze the degradation reactions during the melt mixing of PET (Ghanbari *et al*., 2013). Dehydroxylation of kaolin to remove the hydroxyls might be a solution for this problem.

Calcined kaolin, which is practically dehydroxylated, was substituted to the hydrous grade to be compounded with PET. From a morphological point of view, it was observed that sub-micron calcined kaolin particles were dispersed in the PET matrix; however, an exfoliated structure was not achieved. Rheological studies revealed that even by using calcined kaolin, the degradation of PET occurred during the melt mixing; the degradation was not as severe as in the case of hydrous kaolin, but compatibility between the kaolin particles and PET still remained a critical issue. The incorporation of CKao improved the modulus and this effect was more notable at higher filler contents. CKao had also a great effect on the crystallinity of PET. In presence of 2 wt% of CKao, the crystallinity was increased by 18% over that of neat PET. According to the TGA data, the incorporation of calcined kaolin could slightly enhance the thermal stability of PET.

In view of our finding about the effect of kaolin particles on the end-use properties of PET composites, effect of secondary processes such as hot-stretching on the morphology, mechanical, optical, and gas-barrier properties was also studied. After hot-stretching, due to the increased

molecular orientation and strain-induced crystallization of the PET chains, the tensile modulus increased significantly. However, the presence of the particles had a deteriorating effect on the optical properties of PET and increased haze, as expected for the case of incomplete exfoliation and debonding at the interface.

Substitution of hydrous kaolin with calcined grade lowered the degradation to some extent; however, the dispersion of particles was very poor. Calcined kaolin is produced at very high temperatures and therefore all the functional groups are technically removed from the structure during this thermal treatment. This limited the application of chemical treatments and required the application of mechanical treatment (grinding) in order to improve the dispersion of particles. In order to increase the efficiency of the wet grinder, adjustment of process conditions such as pH and surfactant concentration were crucial.

Electron microscopy images showed that the ground calcined kaolin particles sized around 200 nm were dispersed in the PET matrix. The good dispersion of particles was also confirmed by rheological measurements where the formation of a network-like structure in the composites, due to polymer-particle or particle-particle interactions, was detected by rheometry at low frequencies. DMA and tensile measurements showed that in the presence of ground calcined kaolin, the elongation at break were much smaller, whereas the Young modulus and oxygen barrier properties were improved. The improvement in modulus was smaller than our expectation, which may be attributed to the degradation and molecular weight loss during melt processing. Although calcined kaolin caused less degradation compared to hydrous kaolin, it could not completely hinder the viscosity loss. The addition of chain extenders such as *Joncryl* during the extrusion could be a simple solution for this problem; however, based on our experiments, *Joncryl* was proved to have a destructive effect on optical properties. Recently, some phenoxy-based additives have been

produced, which can react with PET end groups and increase its molecular weight. Our experiments showed that the addition of a phenoxy resin during melt mixing could considerably compensate the molecular weight reduction of PET and resulted in higher modulus and barrier properties of the nanocomposites. In comparison with as received calcined kaolin, the ground particles had a much smaller impact on the optical properties of the composites due to the improved dispersion and smaller particle size. Our DSC results showed that the crystallization/melting behavior of PET in presence of calcined kaolin is more or less the same as with hydrous kaolin.

CHAPTER 10: CONCLUSIONS AND RECOMMENDATIONS

10.1 Conclusion

In this dissertation, PET/kaolin nanocomposites were prepared via melt-compounding in twin and single screw extruders and the final properties of the nanocomposites such as morphological, rheological, thermal, optical, mechanical and barrier properties were characterized by different techniques.

Different chemical and/or mechanical treatments were applied in order to improve the dispersion of particles in the polymer matrix. Potassium acetate (KAc) and dimethyl sulfoxide (DMSO) were eventually chosen for chemical treatment because of higher thermal stability and their capability for intercalation of kaolin particles. The impact of chemical treatment and grinding on the structure and properties of particles were extensively studied. The results showed that grinding would alter the particles size of kaolin and change its crystalline structure at the same time. FT-IR and TGA results revealed that, regardless of the chemical treatment, dehydroxylation of kaolin particles occurred during the grinding process, which was assigned to the conversion of structural hydroxyl groups to water molecules.

The precursor, prepared in the first step, was blended with neat PET to obtain the final nanocomposites. PET nanocomposite films containing hydrous kaolin were produced by cast extrusion. State of dispersion and morphology of nanocomposites were studied by electron microscopy and WAXD techniques. The composites depicted dispersed tactoids and stacked platelets; however, a totally exfoliated structure was not achieved. According to XRD patterns, the intensity of the characteristic peak of kaolin was significantly reduced after blending with PET, which indicates that the particles are dispersed and less ordered. Rheological measurements showed that neat PET followed a Newtonian behavior while a shear-thinning behavior was

observed for the nanocomposites, which was attributed to the formation of a network-like structure of kaolin particles. The melt viscosity of the nanocomposites at high frequencies was much lower than that of the neat PET. This was assigned to severe degradation of PET chains in the presence of the kaolin particles. In spite of the dispersion of particles, no significant improvement was observed in the mechanical properties of the nanocomposites. This was related to the induced degradation during the melt processing, which would result in a considerable reduction in the molecular weight of PET. DSC results showed that the kaolin particles had an effect on the crystallization/melting behavior of PET, so that the crystallization rate of PET was increased in the presence of kaolin particles. TGA thermograms revealed that chemical treatment of particles with KAc and PEO would slightly decrease the thermal stability of the nanocomposites.

We extended our studies using a calcined grade kaolin as a filler, which seems to be more compatible with PET due to the absence of hydroxyl groups in its structure. Because of the lack of functional groups on the surface of calcined kaolin no chemical treatment was applicable. Therefore, the particles were ground in a wet-grinder. Particle size analysis and SEM images showed that this technique could reduce the particle size to few hundred nanometers. When melt-mixed with ground calcined kaolin, PET chains underwent a degradation and molecular weight loss. The addition of phenoxy-based additives could lessen the degradation effect and improved the final properties of the nanocomposite. With 2 wt% of particle loading about 40% and 20% improvement was observed in elastic modulus and barrier properties, respectively. On the other hand, the elongation at break was markedly decreased.

Finally, in the last part of this thesis the effect of secondary processes (hot-stretching) on the final properties of composites was studied. Stretching above T_g had a great effect on both neat PET and PET-CKao composites. Stretched films generally exhibited improved properties and this

was more pronounced in the case of the composites. XRD and DSC results confirmed that the improvement was due to the crystalline structure and orientation of PET chains. The stretching temperature had the greatest effect on the properties, so that lower stretching temperatures let to higher mechanical and barrier properties. Increasing the stretching ratio slightly improved the final properties as well, however, it was not as effective as stretching temperature. An increased haze value in the final films was the major disadvantage of calcined particles.

10.2 Original contributions

Most of the relevant studies focused on preparation of PET nanocomposite with an expandable organoclay (montmorillonite). To best of our knowledge, very few studies have been conducted on the preparation and properties of kaolin nanoparticles as a potential nanofiller for a polymer matrix. In this work, we proposed to prepare PET/kaolin nanocomposite films via melt-mixing in an extrusion process. The microstructure, thermal, mechanical and barrier properties of the obtained nanocomposites were also deeply studied.

Considering the unique structure of kaolin, chemical and mechanical treatment of particles was inevitable in order to disperse them in PET matrix. Effect of chemical treatment and grinding (mechanical treatment) on hydrous kaolin were separately addressed in the literature; however, their simultaneous effect was thoroughly studied in this dissertation.

In spite of the high cohesive energies between the layers of hydrous kaolin, particles were dispersed in the PET matrix via a displacement technique. The calcined kaolin nanoparticles were produced via wet grinding in a stirred-media mill and subsequently blended with PET. To the best of our knowledge, the preparation and properties of PET/calcined kaolin nanocomposites are reported for the first time.

We showed that higher level of dispersion might be achieved for hydrous kaolin; however, extensive degradation during the melt-compounding spoiled the reinforcing impact of particles. On the other hand, the incorporation of calcined kaolin resulted in lower dispersion; however, it was more compatible with PET matrix and caused less thermal degradation.

In the last part of this dissertation, the effect of secondary process (hot-stretching) on the PET/Calcined kaolin composites was investigated. It was exhibited that stretching above T_g had a significant effect on the properties of both neat PET and PET-CKao composites, however this effect was more pronounced in the case of filled samples.

10.3 Recommendations

1. In PET production plants, SSP is applied for the fabricating high molecular weight PET resin. The effect of SSP on the PET/kaolin nanocomposites could be studied to see if SSP can compensate the molecular weight loss caused by melt processing.
2. Melt-mixing conditions and more specifically screw size and configuration (e.g. width of kneading elements, staggering angle…) may have a great effect on the dispersion state of particles within a polymer matrix. Optimization of these parameters for production of PET/kaolin nanocomposites should be taken into consideration.
3. Since kaolin particles cause a considerable degradation in PET, which may spoil the effect of particles, it is strongly recommended to blend kaolin with polymers less sensitive to degradation (e.g. PE, PP) to have a better idea about the reinforcing effect of particles.
4. As pointed out earlier in this study, PET nanocomposites were prepared by melt-compounding technique. Other techniques such as in-situ polymerization could also be applied to produce PET/kaolin nanocomposites in order to avoid degradation during the melt processing step.

5. The effect of uniaxial stretching on the nanocomposites was studied in this thesis. However, the effects of biaxial stretching, as a primary process in blow molding should be studied as well.

6. Recently the intercalation of kaolinite by ionic liquids has been reported. The thermal stability and capability of these materials for treatment of kaolin particles should be investigated.

REFERENCES

Agag, T., Koga, T., & Takeichi, T. (2001). Studies on thermal and mechanical properties of polyimide–clay nanocomposites. *Polymer*, *42*(8), 3399–3408.

Alexe, M., Harnagea, C., Visinoiu, A., Pignolet, A., Hesse, D., & Gösele, U. (2001). Patterning and switching of nano-size ferroelectric memory cells. *Scripta Materialia*, *44*(8–9), 1175–1179.

Anjana, R., & George, K. E. (2012). Reinforcing effect of nano kaolin clay on PP/HDPE blends. *International Journal of Engineering Research and Applications*, *2*(4), 868 – 872.

Ansari, D. M., & Price, G. J. (2004). Correlation of mechanical properties of clay filled polyamide mouldings with chromatographically measured surface energies. *Polymer*, *45*(11), 3663–3670.

Barber, G. D., Calhoun, B. H., Moore, R. B., & R.B., M. (2005). Poly(ethylene terephthalate) ionomer based clay nanocomposites produced via melt extrusion. *Polymer*, *46*(17), 6706.

Beake, B. D., & Leggett, G. J. (2002). Nanoindentation and nanoscratch testing of uniaxially and biaxially drawn poly(ethylene terephthalate) film. *Polymer*, *43*(2), 319–327.

Bear, F. E. (1955). *Chemistry of the Soil*. Reinhold Publishing Corporation.

Bégin-Colin, S., Girot, T., Caër, G. Le, & Mocellin, A. (2000). Kinetics and Mechanisms of Phase Transformations Induced by Ball-Milling in Anatase TiO2. *Journal of Solid State Chemistry*, *149*(1), 41–48.

Bergaya, F., Theng, B. K. G., & Lagaly, G. (2011). *Handbook of Clay Science*. Elsevier Science.

Bilgili, E., Hamey, R., & Scarlett, B. (2004). Production of pigment nanoparticles using a wet stirred mill with polymeric media. *China Particuology*, *2*(3), 93–100. doi:http://dx.doi.org/10.1016/S1672-2515(07)60032-3

Bizarria, M., Giraldi, A. L. F. de M., de Carvalho, C. M., Velasco, J. I., d'Ávila, M. A., Mei, L. H. I., & Maria L. F. de M. Giraldi; Cesar, M. de Carvalho; Jose, I. Velasco; Marcos, A. d'Ávila; Lucia, H. I. Mei, T. M. B. A. (2007). Morphology and thermomechanical properties of recycled PET-organoclay nanocomposites. *Journal of Applied Polymer Science*, *104*(3), 1839–1844.

Black, P. M. (2009). *Geologic Inventory of North Island Aggregate Resources: Influences on Engineering Materials Properties*.

Boldyrev, V. V, Pavlov, S. V, & Goldberg, E. L. (1996). Interrelation between fine grinding and mechanical activation. *International Journal of Mineral Processing*, *44–45*(0), 181–185.

Bounekhel, M., & McNeill, I. C. (1995). Thermal degradation studies of terephthalate polyesters: 2. Poly (ether-esters). *Polymer Degradation and Stability*, *49*(3), 347–352.

Brady, P. V, Cygan, R. T., & Nagy, K. L. (1996). Molecular Controls on Kaolinite Surface Charge. *Journal of Colloid and Interface Science*, *183*(2), 356–364.

Braggs, B., Fornasiero, D., Ralston, J., Smart, R. S., & others. (1994). The effect of surface modification by an organosilane on the electrochemical properties of kaolinite. *Clays and Clay Minerals*, *42*(2), 123–136.

Brandrup, J., Immergut, E. H., Grulke, E. A., Abe, A., & Bloch, D. R. (n.d.). Polymer Handbook (4th Edition). John Wiley & Sons.

Brigatti, M. F., Galan, E., & Theng, B. K. G. (2006). Chapter 2 Structures and Mineralogy of Clay Minerals. In B. K. G. T. Faïza Bergaya & G. Lagaly (Eds.), *Handbook of Clay Science* (Vol. 1, pp. 19–86).

Buggy, M., Bradley, G., & Sullivan, A. (2005). Polymer–filler interactions in kaolin/nylon 6,6 composites containing a silane coupling agent. *Composites Part A: Applied Science and Manufacturing*, *36*(4), 437–442.

Buxbaum, L. H. (1968). The degradation of poly (ethylene terephthalate). *Angewandte Chemie International Edition in English*, *7*(3), 182–190.

Carli, L. N., Crespo, J. S., & Mauler, R. S. (2011). {PHBV} nanocomposites based on organomodified montmorillonite and halloysite: The effect of clay type on the morphology and thermal and mechanical properties. *Composites Part A: Applied Science and Manufacturing*, *42*(11), 1601–1608.

Chae, D. W., & Kim, B. C. (2007). Thermal and rheological properties of highly concentrated PET composites with ferrite nanoparticles. *Composites Science and Technology*, *67*(7-8), 1348–1352.

Cho, J. W., & Paul, D. R. (2001). Nylon 6 nanocomposites by melt compounding. *Polymer*, *42*(3), 1083–1094.

Choudalakis, G., & Gotsis, A. D. (2009). Permeability of polymer/clay nanocomposites: A review. *European Polymer Journal*, *45*(4), 967–984.

Costache, M. C., Heidecker, M. J., Manias, E., & Wilkie, C. A. (2006). Preparation and characterization of poly(ethylene terephthalate)/clay nanocomposites by melt blending using thermally stable surfactants. *Polymers for Advanced Technologies*, *17*(9-10), 764–771.

Dealy, J. M., & Wissbrun, K. F. (1999). *Melt Rheology and Its Role in Plastics Processing: Theory and Applications*. Springer.

Dini, M., Mousavand, T., Carreau, P. J., Kamal, M. R., & Ton-That, M.-T. (2013). Effect of water-assisted extrusion and solid-state polymerization on the microstructure of PET/Clay nanocomposites. *Polymer Engineering & Science*. doi: 10.1002/pen.23685

Domka, L., Foltynowicz, Z., Jurga, S., & Kozak, M. (2003). Influence of silane modification of kaolins on physico-mechanical and structural properties of filled PVC composites. *Polymers & Polymer Composites*, *11*(5), 397–406.

Domka, L., Krysztafkiewicz, A., & Kozak, M. (2002). Silane modified fillers for reinforcing polymers. *Polymers & Polymer Composites*, *10*(7), 541–552.

Du, F., Scogna, R. C., Zhou, W., Brand, S., Fischer, J. E., & Winey, K. I. (2004). Nanotube Networks in Polymer Nanocomposites: Rheology and Electrical Conductivity. *Macromolecules*, *37*(24), 9048–9055.

Edge, M., Wiles, R., Allen, N. S., McDonald, W. A., & Mortlock, S. V. (1996). Characterisation of the species responsible for yellowing in melt degraded aromatic polyesters—I: Yellowing of poly (ethylene terephthalate). *Polymer Degradation and Stability*, *53*(2), 141–151.

Elbokl, T. A., & Detellier, C. (2006). Aluminosilicate nanohybrid materials. Intercalation of polystyrene in kaolinite. *Journal of Physics and Chemistry of Solids*, *67*(5-6), 950–955.

Fetters, L. J., Lohse, D. J., Richter, D., Witten, T. A., & Zirkel, A. (1994). Connection between Polymer Molecular Weight, Density, Chain Dimensions, and Melt Viscoelastic Properties. *Macromolecules*, *27*(17), 4639–4647.

Fischer, B., Ziadeh, M., Pfaff, A., Breu, J., & Altstädt, V. (2012). Impact of large aspect ratio, shear-stiff, mica-like clay on mechanical behaviour of PMMA/clay nanocomposites. *Polymer*, *53*(15), 3230–3237.

Fischer, H. (2003). Polymer nanocomposites: from fundamental research to specific applications. *Materials Science and Engineering: C*, *23*(6–8), 763–772.

Fornes, T. D., Hunter, D. L., & Paul, D. R. (2004). Nylon-6 Nanocomposites from Alkylammonium-Modified Clay: The Role of Alkyl Tails on Exfoliation. *Macromolecules*, *37*(5), 1793–1798.

Frances, C., Laguérie, C., Mazzarotta, B., & Veccia, T. (1996). On the analysis of fine wet grinding in a batch ball mill. *The Chemical Engineering Journal and the Biochemical Engineering Journal*, *63*(3),

Franco, F., & Ruiz Cruz, M. (2003). Thermal behaviour of dickite-dimethylsulfoxide intercalation complex. *Journal of Thermal Analysis and Calorimetry*, *73*(1), 151–165.

Frost, R. L., Horváth, E., Makó, É., & Kristóf, J. (2004). Modification of low- and high-defect kaolinite surfaces: implications for kaolinite mineral processing. *Journal of Colloid and Interface Science*, *270*(2), 337–346.

Frost, R. L., Kristof, J., Horvath, E., & Kloprogge, J. T. (1999). Modification of Kaolinite Surfaces through Intercalation with Potassium Acetate, II. *Journal of Colloid and Interface Science*, *214*(1), 109–117.

Frost, R. L., Kristof, J., Mako, E., & Kloprogge, J. T. (2000). Modification of the Hydroxyl Surface in Potassium-Acetate-Intercalated Kaolinite between 25 and 300° C. *Langmuir*, *16*(19), 7421–7428.

Frost, R. L., Kristof, J., Paroz, G. N., Kloprogge, J. T., & Frost J.; Paroz, G. N.; Kloprogge, J. T., R. L. . K. (1999). Intercalation of kaolinite with acetamide. *Physics and Chemistry of Minerals*, *26*(3), 257–263.

Frost, R. L., Mako, E., Kristof, J., Horváth, E., & Kloprogge, J. T. (2001). Mechanochemical treatment of kaolinite. *Journal of Colloid and Interface Science*, *239*(2), 458–466.

Frost, R. L., Makó, É., Kristóf, J., Horváth, E., & Kloprogge, J. T. (2001). Modification of Kaolinite Surfaces by Mechanochemical Treatment. *Langmuir*, *17*(16), 4731–4738.

Fu, S.-Y., Feng, X.-Q., Lauke, B., & Mai, Y.-W. (2008). Effects of particle size, particle/matrix interface adhesion and particle loading on mechanical properties of particulate–polymer composites. *Composites Part B: Engineering*, *39*(6), 933–961.

Gabor, M., Toth, M., Kristof, J., & Komaromi-Hiller, G. (1995). Thermal behavior and decomposition of intercalated kaolinite. *Clays and Clay Minerals*, *43*(2), 223–228.

Gain, O., Espuche, E., Pollet, E., Alexandre, M., & Dubois, P. (2005). Gas barrier properties of poly(ε-caprolactone)/clay nanocomposites: Influence of the morphology and polymer/clay interactions. *Journal of Polymer Science Part B: Polymer Physics*, *43*(2), 205–214.

Gardolinski L. C. M.; Cantão, M. P.; Wypych, F., J. E. . C. (2000). Layered polymer-kaolinite nanocomposites. *Journal of Materials Science*, *35*(12), 3113–3119.

Gardolinski Luiz Pereira; de Souza, Gabriel Pinto; Wypych, Fernando, J. E. R., Gardolinski, J. E., Ramos, L. P., de Souza, G. P., & Wypych, F. (2000). Intercalation of benzamide into kaolinite. *Journal of Colloid and Interface Science*, *221*(2), 284–290.

George, T. S., Krishnan, A., Anjana, R., & George, K. E. (2013). Studies on Nano Kaolin Clay Reinforced PS-HDPE Nanocomposites. *Indian Journal of Advances in Chemical Science*, *1*(4), 201–206.

Ghanbari, A., Heuzey, M. C., Carreau, P. J., & Ton-That, M. T. (2013). A novel approach to control thermal degradation of PET/organoclay nanocomposites and improve clay exfoliation. *Polymer*, *54*(4), 1361–1369.

Ghanbari, A., Heuzey, M.-C., Carreau, P. J., & Ton-That, M.-T. (2013a). Morphology and properties of polymer/organoclay nanocomposites based on poly(ethylene terephthalate) and sulfopolyester blends. *Polymer International*, *62*(3), 439–448.

Ghanbari, A., Heuzey, M.-C., Carreau, P., & Ton-That, M.-T. (2013b). Morphological and rheological properties of PET/clay nanocomposites. *Rheologica Acta*, *52*(1), 59–74.

Ghasemi, H., Carreau, P. J., & Kamal, M. R. (2012). Isothermal and non-isothermal crystallization behavior of PET nanocomposites. *Polymer Engineering & Science*, *52*(2), 372–384.

Ghasemi, H., Carreau, P. J., Kamal, M. R., & Chapleau, N. (2011). Effect of Processing Conditions on Properties of PET/Clay Nanocomposite Films. *International Polymer Processing*, *26*(2), 219–228.

Ghasemi, H., Carreau, P. J., Kamal, M. R., & Tabatabaei, S. H. (2012). Properties of PET/clay nanocomposite films. *Polymer Engineering & Science*, *52*(2), 420–430.

Ghasemi, H., Carreau, P. J., Kamal, M. R., & Uribe-Calderon, J. (2011). Preparation and Characterization of PET/Clay Nanocomposites by Melt Compounding. *Polymer Engineering and Science*, *51*, 1178–1187.

Giese, R. F. (1978). The Electrostatic Interlayer Forces of Layer Structure Minerals. *Clays and Clay Minerals*, *26*(1), 51–57.

Godet-Morand, L., Chamayou, A., & Dodds, J. (2002). Talc grinding in an opposed air jet mill: start-up, product quality and production rate optimization. *Powder Technology*, *128*(2–3), 306–313.

Gu, A., Kuo, S.-W., & Chang, F.-C. (2001). Syntheses and properties of PI/clay hybrids. *Journal of Applied Polymer Science*, *79*(10), 1902–1910.

Hoffmann, B., Kressler, J., Stöppelmann, G., Friedrich, C., & Kim, G.-M. (2000). Rheology of nanocomposites based on layered silicates and polyamide-12. *Colloid and Polymer Science*, *278*(7), 629–636.

Huertas, F. J., Fiore, S., Huertas, F., & Linares, J. (1999). Experimental study of the hydrothermal formation of kaolinite. *Chemical Geology*, *156*(1-4), 171–190.

Hyun, K., Chong, W., Koo, M., & Chung, I. J. (2003). Physical properties of polyethylene/silicate nanocomposite blown films. *Journal of Applied Polymer Science*, *89*(8), 2131–2136.

Iguchi, Y., & Senna, M. (1985). Mechanochemical polymorphic transformation and its stationary state between aragonite and calcite I. Effects of preliminary annealing. *Powder Technology*, *43*(2), 155–162.

Imai Satoshi; Abe, Eiichi; Tateyama, Hiroshi; Abiko, Akimasa; Yamaguchi, Akira; Aoyama, Tomohiro; Taguchi, Hiroaki, Y. N., Imai, Y., Nishimura, S., Abe, E., Tateyama, H., Abiko, A., … Taguchi, H. (2002). High-modulus poly (ethylene terephthalate)/expandable fluorine mica nanocomposites with a novel reactive compatibilizer. *Chemistry of Materials*, *14*(2), 477–479.

Itagaki, T., Komori, Y., Sugahara, Y., Kuroda, K., & Itagaki Yoshihiko; Sugahara, Yoshiyuki; Kuroda, Kazuyuki, T. K. (2001). Synthesis of a kaolinite--poly (β-alanine) intercalation compound. *Journal of Materials Chemistry*, *11*(12), 3291–3295.

Itagaki, T., Matsumura, A., Kato, M., Usuki, A., Kuroda, K., & Itagaki A.; Kato, M.; Usuki, A.; Kuroda, K., T. . M. (2001). Preparation of kaolinite--nylon6 composites by blending nylon6 and a kaolinite--nylon6 intercalation compound. *Journal of Materials Science Letters*, *20*(16), 1483–1484.

Jasmund, K., & Lagaly, G. (1993). *Tonminerale Und Tone: Struktur, Eigenschaften, Anwendungen Und Einsatz in Industrie Und Umwelt*. Dietrich Steinkopff.

Jéol, S., Fenouillot, F., Rousseau, A., Masenelli-Varlot, K., Gauthier, C., & Briois, J.-F. (2007). Drastic Modification of the Dispersion State of Submicron Silica during Biaxial Deformation of Poly(ethylene terephthalate). *Macromolecules*, *40*(9), 3229–3237.

Jeziorny, A. (1978). Parameters characterizing the kinetics of the non-isothermal crystallization of poly(ethylene terephthalate) determined by d.s.c. *Polymer*, *19*(10), 1142–1144.

Joost, B., & Schwedes, J. (1996). Comminution of white fused alumina and wear of grinding beads in stirred media mills. Pt. 1. The effect of the grinding chamber geometry and the hardness of the grinding beads on the grinding result. In *Ceramic Forum International* (Vol. 73, pp. 365–371).

Juhász, A. Z., Juhász, Z., & Opoczky, L. (1990). *Mechanical Activation of Minerals by Grinding: Pulverizing and Morphology of Particles*. Ellis Horwood.

KAO, S. V, & MASON, S. G. (1975). Dispersion of particles by shear. *Nature*, *253*(5493), 619–621.

Kakali, G., Perraki, T., Tsivilis, S., & Badogiannis, E. (2001). Thermal treatment of kaolin: the effect of mineralogy on the pozzolanic activity. *Applied Clay Science*, *20*(1–2), 73–80.

Kim Yun Hyuk; Choi, Soo Myung; Yoon, Kwan Han, H.-U. B., Kim, H.-U., Bang, Y. H., Choi, S. M., & Yoon, K. H. (2008). Morphology and mechanical properties of PET by incorporation of amine-polyhedral oligomeric silsesquioxane. *Composites Science and Technology*, *68*(13), 2739–2747.

Kim, E. S., Shim, J. H., Woo, J. Y., Yoo, K. S., & Yoon, J. S. (2010). Effect of the silane modification of clay on the tensile properties of nylon 6/clay nanocomposites. *Journal of Applied Polymer Science*, *117*(2), 809–816.

Kim, J. Y., Park, H. S., & Kim, S. H. (2006). Unique nucleation of multi-walled carbon nanotube and poly(ethylene 2,6-naphthalate) nanocomposites during non-isothermal crystallization. *Polymer*, *47*(4), 1379–1389.

Klaus Friedrich, Stoyko Fakirov, Zhong Zhang, Friedrich, K., Fakirov, S., & Zhang, Z. (2005). *Polymer Composites: From Nano- to Macro-Scale* (p. 367). New York: Springer.

Kohn, S. C., Brooker, R. A., Frost, D. J., Slesinger, A. E., & Wood, B. J. (2002). Ordering of hydroxyl defects in hydrous wadsleyite (β-Mg2SiO4). *American Mineralogist*, *87*(2-3), 293–301.

Komori, Y., Enoto, H., Takenawa, R., Hayashi, S., Sugahara, Y., Kuroda, K., & Komori Hiroyuki; Takenawa, Ryoji; Hayashi, Shigenobu; Sugahara, Yoshiyuki; Kuroda, Kazuyuki, Y. E. (2000). Modification of the Interlayer Surface of Kaolinite with Methoxy Groups. *Langmuir*, *16*(12), 5506–5508.

Komori, Y., Sugahara, Y., & Kuroda, K. (1998). Direct intercalation of poly (vinylpyrrolidone) into kaolinite by a refined guest displacement method. *Chemistry of Materials*, *11*(1), 3–6.

Kristóf, J., Frost, R. L., Horváth, E., Kocsis, L., & Inczédy, J. (1998). Thermoanalytical Investigations on Intercalated Kaolinites. *Journal of Thermal Analysis and Calorimetry*, *53*(2), 467–475.

Kukharskaya, E. V, & Fedoseev, A. D. (1963). ORGANIC DERIVATIVES OF LAMINAR SILICATES. *Russian Chemical Reviews*, *32*(9), 490.

Kumar, P., & Dr. E. Allen Foegeding Dr. Van Den Truong (Co-chair of Advisory Committee), Dr. K.P. Sandeep (Chair of Advisory Committee), D. R. E. G. (2009). *Development of Bio-nanocomposite Films with Enhanced Mechanical and Barrier Properties Using Extrusion Processing*. North Carolina State University, Raleigh, North Carolina.

Lai, M., & Kim, J.-K. (2005). Effects of epoxy treatment of organoclay on structure, thermo-mechanical and transport properties of poly(ethylene terephthalate-co-ethylene naphthalate)/organoclay nanocomposites. *Polymer*, *46*(13), 4722–4734.

Lee, B., Shin, T. J., Lee, S. W., Yoon, J., Kim, J., & Ree, M. (2004). Secondary Crystallization Behavior of Poly(ethylene isophthalate-co-terephthalate): Time-Resolved Small-Angle X-ray Scattering and Calorimetry Studies. *Macromolecules*, *37*(11), 4174–4184.

Lee, N. C., & of Plastics Engineers. Blow Molding Division, S. (1990). *Plastic blow molding handbook*. Van Nostrand Reinhold.

Letaief, S., & Detellier, C. (2005). Reactivity of kaolinite in ionic liquids: preparation and characterization of a 1-ethyl pyridinium chloride–kaolinite intercalate. *Journal of Materials Chemistry*, *15*(44).

Letaief, S., & Detellier, C. (2007). Nanohybrid materials from the intercalation of imidazolium ionic liquids in kaolinite. *Journal of Materials Chemistry*, *17*(15), 1476–1484. Retrieved from

Letaief, S., & Detellier, C. (2009). Clay-Polymer Nanocomposite Material from the Delamination of Kaolinite in the Presence of Sodium Polyacrylate. *Langmuir*, *25*(18), 10975–10979.

Letaief, S., & Detellier, C. (2011). Application of thermal analysis for the characterisation of intercalated and grafted organo-kaolinite nanohybrid materials. *Journal of Thermal Analysis and Calorimetry*, *104*(3), 831–839.

Letaief, S., Detellier, C., & S. Letaief. (2008). Interlayer grafting of glycidol (2,3-epoxy-1-propanol) on kaolinite. *Canadian Journal of Chemistry*, *86*(1), 1–6.

Letaief, S., Elbokl, T. A., & Detellier, C. (2006). Reactivity of ionic liquids with kaolinite: Melt intersalation of ethyl pyridinium chloride in an urea-kaolinite pre-intercalate. *Journal of Colloid and Interface Science*, *302*(1), 254–258.

Litchfield, D. W., & Baird, D. G. (2008). The role of nanoclay in the generation of poly(ethylene terephthalate) fibers with improved modulus and tenacity. *Polymer*, *49*(23), 5027–5036.

Liu W. J.; Clearfield, A.; Sue, H. J., J. . B. (2006). Intercalation and Exfoliation: A Review on Morphology of Polymer Nanocomposites Reinforced by Inorganic Layer Structures. *Materials and Manufacturing Processes*, *21*(2), 143–151.

Liu, Q., De Wijn, J. R., Van Blitterswijk, C. A., & Qing Liu Blitterswijk van C.A., A. W. de J. R. (1997). Nano-apatite/polymer composites: mechanical and physicochemical characteristics. *Biomaterials*, *18*(19), 1263–1270.

Liu, Q., Zhang, Y., & Xu, H. (2008). Properties of vulcanized rubber nanocomposites filled with nanokaolin and precipitated silica. *Applied Clay Science*, *42*(1–2), 232–237.

Liu, X., Zhang, H., Yang, Z., Ha, C., & Liu Hongtao; Yang, Zhizhong; Ha, Chengyong, X. Z. (2005). Preparation and characterization of poly (styrene/maleic anhydride)/kaolin nanocomposites. *Chinese Science Bulletin*, *50*(13), 1320–1325.

Ma, J., Qi, Z., & Hu, Y. (2001). Synthesis and characterization of polypropylene/clay nanocomposites. *Journal of Applied Polymer Science*, *82*(14), 3611–3617.

MacKenzie, K. J. D., Temuujin, J., & Okada, K. (1999). Thermal decomposition of mechanically activated gibbsite. *Thermochimica Acta*, *327*(1–2), 103–108.

Macosko, C. W. (1994). *Rheology: Principles, Measurements, and Applications*. Wiley.

Manas-Zloczower, I. (2009). *Mixing and Compounding of Polymers: Theory and Practice*. Hanser.

Maria Pilar Cabedo; José Maria, Lagarón; Enrique, Giménez, V. L. (2009). Comparative study of nanocomposites of polyolefin compatibilizers containing kaolinite and montmorillonite organoclays. *Journal of Applied Polymer Science*, *115*(3), 1325–1335.

Martens, W. N., Frost, R. L., Kristof, J., Horvath, E., & Martens Ray L.; Kristof, Janos; Horvath, Erzsebet, W. N. . F. (2002). Modification of Kaolinite Surfaces through Intercalation with Deuterated Dimethylsulfoxide. *The Journal of Physical Chemistry B*, *106*(16), 4162–4171.

Masoud, F., & Alireza, D. (2009). Oxygen Barrier Properties of Poly(ethylene terephthalate) Nanocomposite Films. *Macromolecular Materials and Engineering*, *294*(1), 68–74. Retrieved from

Meeten, G. H. (1986). *Optical properties of polymers*. Elsevier Applied Science Publishers.

Mende, S., Stenger, F., Peukert, W., & Schwedes, J. (2003). Mechanical production and stabilization of submicron particles in stirred media mills. *Powder Technology*, *132*(1), 64–73.

Miranda-Trevino, J. C., & Coles, C. A. (2003). Kaolinite properties, structure and influence of metal retention on pH. *Applied Clay Science*, *23*(1-4), 133–139.

Montaudo, G., Puglisi, C., & Samperi, F. (1993). Primary thermal degradation mechanisms of PET and PBT. *Polymer Degradation and Stability*, *42*(1), 13–28.

Murakami, J., Itagaki, T., & Kuroda, K. (2004). Synthesis of kaolinite-organic nanohybrids with butanediols. *Solid State Ionics*, *172*(1-4), 279–282.

Nair, P. B. R., & Paramasivam, R. (1999). Effect of grinding aids on the time-flow characteristics of the ground product from a batch ball mill. *Powder Technology*, *101*(1), 31–42.

Najafi, N., Heuzey, M. C., & Carreau, P. J. (2012). Polylactide (PLA)-clay nanocomposites prepared by melt compounding in the presence of a chain extender. *Composites Science and Technology*, *72*(5), 608–615.

Najafi, N., Heuzey, M. C., Carreau, P. J., & Wood-Adams, P. M. (2012). Control of thermal degradation of polylactide (PLA)-clay nanocomposites using chain extenders. *Polymer Degradation and Stability*, *97*(4), 554–565.

Nunes, R. A. X., Costa, V. C., Calado, V. M. de A., & Branco, J. R. T. (2009). Wear, friction, and microhardness of a thermal sprayed PET: poly (ethylene terephthalate) coating. *Materials Research*, *12*, 121–125.

Oya, A., Kurokawa, Y., & Yasuda, H. (2000). Factors controlling mechanical properties of clay mineral/polypropylene nanocomposites. *Journal of Materials Science*, *35*(5), 1045–1050.

Ozawa, T. (1971). Kinetics of non-isothermal crystallization. *Polymer*, *12*(3), 150–158. doi:10.1016/0032-3861(71)90041-3

P., D., Alexandre, M., & Dubois, P. (2000). Polymer-layered silicate nanocomposites: preparation, properties and uses of a new class of materials. *Mater. Sci. Eng. R.*, *28*(1-2), 1–63.

Palaniandy, S., & Azizli, K. A. M. (2009). Mechanochemical effects on talc during fine grinding process in a jet mill. *International Journal of Mineral Processing*, *92*(1–2), 22–33.

Papageorgiou, G. Z., & Karayannidis, G. P. (2001). Crystallization and melting behaviour of poly(butylene naphthalene-2,6-dicarboxylate). *Polymer*, *42*(6), 2637–2645.

Paul, D. R., & Robeson, L. M. (2008). Polymer nanotechnology: Nanocomposites. *Polymer*, *49*(15), 3187–3204.

Pegoretti, A., Kolarik, J., Peroni, C., & Migliaresi, C. (2004). Recycled poly(ethylene terephthalate)/layered silicate nanocomposites: morphology and tensile mechanical properties. *Polymer*, *45*(8), 2751–2759.

Phang, I. Y., Pramoda, K. P., Liu, T., & He, C. (2004). Crystallization and melting behavior of polyester/clay nanocomposites. *Polymer International*, *53*(9), 1282–1289.

Prasher, C. L. (1987). *Crushing and grinding process handbook*. Wiley.

Premalal, H. G. B., Ismail, H., & Baharin, A. (2002). Comparison of the mechanical properties of rice husk powder filled polypropylene composites with talc filled polypropylene composites. *Polymer Testing*, *21*(7), 833–839.

Priya, L., & Jog, J. P. (2002). Poly(vinylidene fluoride)/clay nanocomposites prepared by melt intercalation: Crystallization and dynamic mechanical behavior studies. *Journal of Polymer Science Part B: Polymer Physics*, *40*(15), 1682–1689.

Qin, H., Zhang, S., Liu, H., Xie, S., Yang, M., & Shen, D. (2005). Photo-oxidative degradation of polypropylene/montmorillonite nanocomposites. *Polymer*, *46*(9), 3149–3156.

Ram, A. (1997). *Fundamentals of Polymer Engineering*. Springer.

Rausell-Colom, J. A., Serratosa, J. M., & others. (1987). Reactions of clays with organic substances. *Monograph, Mineralogical Society*, (6), 371–422.

Ray, S., Quek, S. Y., Easteal, A., & Chen, X. D. (2006). The Potential Use of Polymer-Clay Nanocomposites in Food Packaging. *International Journal of Food Engineering*, *2*(4).

Rieckmann, T., & Völker, S. (2004). Poly(Ethylene Terephthalate) Polymerization – Mechanism, Catalysis, Kinetics, Mass Transfer and Reactor Design. In *Modern Polyesters: Chemistry and Technology of Polyesters and Copolyesters* (pp. 29–115). John Wiley & Sons, Ltd.

Ruan, H. D., Frost, R. L., Kloprogge, J. T., & Duong, L. (2002). Infrared spectroscopy of goethite dehydroxylation. II. Effect of aluminium substitution on the behaviour of hydroxyl units. *Spectrochimica Acta Part A: Molecular and Biomolecular Spectroscopy*, *58*(3), 479–491.

Russo, G. M., Simon, G. P., & Incarnato, L. (2006). Correlation between Rheological, Mechanical, and Barrier Properties in New Copolyamide-Based Nanocomposite Films. *Macromolecules*, *39*(11), 3855–3864.

S., I., Chang Sung Jong; Joo, Yong Lak; Im, Seungsoon, J.-H. K., Chang, J.-H., Kim, S. J., Joo, Y. L., & Im, S. (2004). Poly (ethylene terephthalate) nanocomposites by in situ interlayer polymerization: the thermo-mechanical properties and morphology of the hybrid fibers. *Polymer*, *45*(3), 919–926.

Sakthivel, S., & Pitchumani, B. (2011). Production of Nano Talc Material and Its Applicability as Filler in Polymeric Nanocomposites. *Particulate Science and Technology*, *29*(5), 441–449.

Sánchez, E. C., M, E. T., Diaz, C., & Saito, F. (2004). Effects of grinding of the feldspar in the sintering using a planetary ball mill. *Journal of Materials Processing Technology*, *152*(3), 284–290.

Sanchez-Solis, A., Garcia-Rejon, A., & Manero, O. (2003). Production of nanocomposites of PET-montmorillonite clay by an extrusion process. *Macromolecular Symposia*, *192*(1), 281–292.

Sánchez-Soto, P. J., del Carmen Jiménez de Haro, M., Pérez-Maqueda, L. A., Varona, I., & Pérez-Rodríguez, J. L. (2000). Effects of Dry Grinding on the Structural Changes of Kaolinite Powders. *Journal of the American Ceramic Society*, *83*(7), 1649–1657.

Santos, P. de S. (1989). *Ciência e Tecnologia de Argilas* (2nd ed.). São Paulo: Edgard Blücher.

Saujanya, C., Imai, Y., & Tateyama, H. (2002). Structure and thermal properties of compatibilized PET/expandable fluorine mica nanocomposites. *Polymer Bulletin*, *49*(1), 69–76. Retrieved from

Shao, W., Wang, Q., & Li, K. (2005). Intercalation and exfoliation of talc by solid-state shear compounding (S3C) using pan-mill equipment. *Polymer Engineering & Science*, *45*(4), 451–457.

Shelley, J. S., Mather, P. T., & DeVries, K. L. (2001). Reinforcement and environmental degradation of nylon-6/clay nanocomposites. *Polymer*, *42*(13), 5849–5858.

Shen, Y., Harkin-Jones, E., Hornsby, P., McNally, T., & Abu-Zurayk, R. (2011). The effect of temperature and strain rate on the deformation behaviour, structure development and properties of biaxially stretched PET–clay nanocomposites. *Composites Science and Technology*, *71*(5), 758–764.

Solomon, M. J., Almusallam, A. S., Seefeldt, K. F., Somwangthanaroj, A., & Varadan, P. (2001). Rheology of Polypropylene/Clay Hybrid Materials. *Macromolecules*, *34*(6), 1864–1872.

Soon, K., Harkin-Jones, E., Rajeev, R. S., Menary, G., Martin, P. J., & Armstrong, C. G. (2012). Morphology, barrier, and mechanical properties of biaxially deformed poly(ethylene terephthalate)-mica nanocomposites. *Polymer Engineering & Science*, *52*(3), 532–548. doi:10.1002/pen.22114

Spencer, M. W., Hunter, D. L., Knesek, B. W., & Paul, D. R. (2011). Morphology and properties of polypropylene nanocomposites based on a silanized organoclay. *Polymer*, *52*(23), 5369–5377.

Sperinck, S., Raiteri, P., Marks, N., & Wright, K. (2011). Dehydroxylation of kaolinite to metakaolin-a molecular dynamics study. *J. Mater. Chem.*, *21*(7), 2118–2125.

Stenger, F., Götzinger, M., Jakob, P., & Peukert, W. (2004). Mechano-Chemical Changes of Nano Sized α-Al2O3 During Wet Dispersion in Stirred Ball Mills. *Particle & Particle Systems Characterization*, *21*(1), 31–38.

Stenger, F., Mende, S., Schwedes, J., & Peukert, W. (2005). Nanomilling in stirred media mills. *Chemical Engineering Science*, *60*(16), 4557–4565.

Sukumar, R., & Menon, A. R. R. (2008). Organomodified kaolin as a reinforcing filler for natural rubber. *Journal of Applied Polymer Science*, *107*(6), 3476–3483. doi:10.1002/app.27469

Suraj, G., Iyer, C. S. P., Rugmini, S., & Lalithambika, M. (1997). The effect of micronization on kaolinites and their sorption behaviour. *Applied Clay Science*, *12*(1-2), 111–130.

Tekkanat, B. (2002). In PET Packaging Technology; Brooks, DW; Giles, GA, Eds. Sheffield Academic Press Ltd: Sheffield.

Thompson, J. G., Gabbitas, N., & Uwins, P. J. R. (1993). The intercalation of kaolinite by alkali halides in the solid state: A systematic study of the intercalates and their derivatives. *Clays and Clay Minerals*, *41*, 73.

Tkáčová, K. (1989). *Mechanical Activation of Minerals*. Butterworth-Heinemann Limited.

Tkáčová, K., Heegn, H., & Števulová, N. (1993). Energy transfer and conversion during comminution and mechanical activation. *International Journal of Mineral Processing*, *40*(1–2), 17–31.

Tsai, T.-Y., Li, C.-H., Chang, C.-H., Cheng, W.-H., Hwang, C.-L., Wu, R.-J., & R.J., W. (2005). Preparation of Exfoliated Polyester/Clay Nanocomposites. *Advanced Materials*, *17*(14), 1769–1773.

Tsunematsu, K., & Tateyama, H. (1999). Delamination of Urea-Kaolinite Complex by Using Intercalation Procedures. *Journal of the American Ceramic Society*, *82*(6), 1589–1591.

Tunney, J. J., & Detellier, C. (1996). Aluminosilicate Nanocomposite Materials. Poly(ethylene glycol)-Kaolinite Intercalates. *Chemistry of Materials*, *8*(4), 927–935.

Turhan, Y., Doğan, M., & Alkan, M. (2010). Poly(vinyl chloride)/Kaolinite Nanocomposites: Characterization and Thermal and Optical Properties. *Industrial & Engineering Chemistry Research*, *49*(4), 1503–1513.

Vaia, R. A., & Giannelis, E. P. (1997). Polymer Melt Intercalation in Organically-Modified Layered Silicates: Model Predictions and Experiment. *Macromolecules*, *30*(25), 8000–8009.

Vaia, R. A., Ishii, H., & Giannelis, E. P. (1993). Synthesis and properties of two-dimensional nanostructures by direct intercalation of polymer melts in layered silicates. *Chemistry of Materials*, *5*(12), 1694–1696. doi:10.1021/cm00036a004

Vempati, R. K., Mollah, M. Y. A., Reddy, G. R., Cocke, D. L., & Lauer, H. V. (1996). Intercalation of kaolinite under hydrothermal conditions. *Journal of Materials Science*, *31*(5), 1255–1259.

Vijayakumar, C. T., Ponnusamy, E., Balakrishnan, T., & Kothandaraman, H. (1982). Thermal and pyrolysis studies of copolyesters. *Journal of Polymer Science: Polymer Chemistry Edition*, *20*(9), 2715–2725.

Wang, Y., Gao, J., Ma, Y., & Agarwal, U. S. (2006). Study on mechanical properties, thermal stability and crystallization behavior of PET/MMT nanocomposites. *Composites Part B: Engineering*, *37*(6), 399–407.

Weit, H., & Schwedes, J. (1987). Scale-up of power consumption in agitated ball mills. *Chemical Engineering & Technology*, *10*(1), 398–404.

Welham, N. J., & Llewellyn, D. J. (1998). Mechanical enhancement of the dissolution of ilmenite. *Minerals Engineering*, *11*(9), 827–841.

Wen, B., Xu, X., Gao, X., Ding, Y., Wang, F., Zhang, S., & Yang, M. (2011). Highly Exfoliated Poly(Ethylene Terephthalate)/Clay Nanocomposites via Melt Compounding: Effects of Silane Grafting. *Polymer-Plastics Technology and Engineering*, *50*(4), 362–371.

Wieckowski, T., & Wiewióra, A. (1976). New approach to the problem of interlayer bonding in kaolinite. *Clays and Clay Minerals*, *24*, 219–223.

Wu, D., Wu, L., Wu, L., & Zhang, M. (2006). Rheology and thermal stability of polylactide/clay nanocomposites. *Polymer Degradation and Stability*, *91*(12), 3149–3155.

Wu, T., & Ke, Y. (2006). The absorption and thermal behaviors of PET SiO2 nanocomposite films. *Polymer Degradation and Stability*, *91*(9), 2205–2212.

Wu, T., & Ke, Y. (2007). Melting, crystallization and optical behaviors of poly (ethylene terephthalate)-silica/polystyrene nanocomposite films. *Thin Solid Films*, *515*(13), 5220–5226.

Xin, F., Li, L., Chan, S. H., & Zhao, J. (2012). Influences of carbon fillers on electrical conductivity and crystallinity of polyethylene terephthalate. *Journal of Composite Materials*, *46*(9), 1091–1099.

Xu, W., Ge, M., & He, P. (2002). Nonisothermal crystallization kinetics of polypropylene/montmorillonite nanocomposites. *Journal of Polymer Science Part B: Polymer Physics*, *40*(5), 408–414.

Xu, X., Ding, Y., Qian, Z., Wang, F., Wen, B., Zhou, H., … M.S., Y. (2009). Degradation of poly(ethylene terephthalate)/clay nanocomposites during melt extrusion: Effect of clay catalysis and chain extension. *Polymer Degradation and Stability*, *94*(1), 113–123.

Xu, X. F., Ghanbari, A., Leelapornpisit, W., Heuzey, M. C., & Carreau, P. (2011). Effect of Ionomer on Barrier and Mechanical Properties of PET/Organoclay Nanocomposites Prepared by Melt Compounding. *International Polymer Processing*, *26*(4), 444–455.

Yahaya, L. E., Adebowale, K. O., & Menon, A. R. R. (2009). Mechanical properties of organomodified kaolin/natural rubber vulcanizates. *Applied Clay Science*, *46*(3), 283–288.

Yangchuan, K., Chenfen, L., Zongneng, Q., Z.N., Q., Ke, Y., Long, C., & Qi, Z. (1999). Crystallization, properties, and crystal and nanoscale morphology of PET-clay nanocomposites. *Journal of Applied Polymer Science*, *71*(7), 1139–1146.

Yano, K., Usuki, A., Okada, A., Kurauchi, T., & Kamigaito, O. (1993). Synthesis and properties of polyimide–clay hybrid. *Journal of Polymer Science Part A: Polymer Chemistry*, *31*, 2493–2498.

Zhang, R., Gu, M., & Chen, G. (2011). Non-isothermal crystallization kinetics of kaolin modified polyester. *Journal of Wuhan University of Technology-Mater. Sci. Ed.*, *26*(5), 945–949.

Zhang, R. X., Xing, T. L., & Chen, G. Q. (2011). Preparation and Properties of Kaolin Modified Polyester Fibers. *Advanced Materials Research*, *332*, 227–230.

Zhang, X., & Xu, Z. (2007). The effect of microwave on preparation of kaolinite/dimethylsulfoxide composite during intercalation process. *Materials Letters*, *61*(7), 1478–1482.

Zhao, J., Milanova, M., Warmoeskerken, M. M. C. G., & Dutschk, V. (2012). Surface modification of TiO2 nanoparticles with silane coupling agents. *Colloids and Surfaces A: Physicochemical and Engineering Aspects*, *413*(0), 273–279.

Zhao, J., Morgan, A. B., & Harris, J. D. (2005). Rheological characterization of polystyrene–clay nanocomposites to compare the degree of exfoliation and dispersion. *Polymer*, *46*(20), 8641–8660.